



**DIEGO BEDIN MARIN**

**REMOTELY PILOTED AIRCRAFT IN SPATIAL  
MULTISPECTRAL MODELING OF STRESSORS IN COFFEE  
PLANTATIONS**

**LAVRAS – MG**

**2021**

**DIEGO BEDIN MARIN**

**REMOTELY PILOTED AIRCRAFT IN SPATIAL MULTISPECTRAL MODELING  
OF STRESSORS IN COFFEE PLANTATIONS**

Tese apresentada à Universidade Federal de Lavras, como parte das exigências do Programa de Pós-Graduação em Engenharia Agrícola para a obtenção do título de Doutor.

Prof. Dr. Gabriel Araújo e Silva Ferraz

Orientador

**LAVRAS – MG**

**2021**

**Ficha catalográfica elaborada pelo Sistema de Geração de Ficha Catalográfica da Biblioteca  
Universitária da UFLA, com dados informados pelo(a) próprio(a) autor(a).**

Marin, Diego Bedin.

Remotely Piloted Aircraft in Spatial Multispectral Modeling of  
Stressors in Coffee Plantations / Diego Bedin Marin. - 2021.  
106 p. : il.

Orientador(a): Gabriel Araújo e Silva Ferraz.

Tese (doutorado) - Universidade Federal de Lavras, 2021.  
Bibliografia.

1. Remote Sensing. 2. Precision Agriculture. 3. Unmanned  
Aerial Vehicle. I. Ferraz, Gabriel Araújo e Silva. II. Título.

**DIEGO BEDIN MARIN**

**REMOTELY PILOTED AIRCRAFT IN SPATIAL MULTISPECTRAL MODELING  
OF STRESSORS IN COFFEE PLANTATIONS**

Tese apresentada à Universidade Federal de Lavras, como parte das exigências do Programa de Pós-Graduação em Engenharia Agrícola para a obtenção do título de Doutor.

APROVADA em 23 de junho de 2021.

Prof. Dr. Gabriel Araújo e Silva Ferraz

Prof. Dr. Felipe Schwerz

Prof. Dr. Adão Felipe dos Santos

Pesquisador Dr. Marley Lamounier Machado

Prof. Dr. Giuseppe Rossi

Prof. Dr. Gabriel Araújo e Silva Ferraz

Orientador

**LAVRAS – MG**

**2021**

*Ao pai, ao Filho e Ao Espírito Santo*

*À Santa Terezinha*

*À Sant'Ana*

*A Santo Expedito*

*À minha família pelo amor incondicional, valores, incentivos, compreensão, respeito e confiança.*

*À minha esposa Andressa, por todo amor, carinho, companheirismo e por sempre acreditar em mim.*

**DEDICO.**

## **AGRADECIMENTOS**

A Deus por ter me iluminado e me guiado para conseguir trilhar este caminho. Agradeço a Ele todos os dias por ter me concedido esta oportunidade, e colocado as pessoas certas em minha jornada.

À minha esposa Andressa, aos meus pais, Airton e Rosângela, a meu irmão Rafael, à minha avó Ozaide, a meu sogro Milton e sogra Carmem, pelo amor incondicional, incentivos, compreensão e apoio durante esta realização profissional. Muito obrigado, sem vocês eu jamais teria conseguido, vocês sempre serão a base de tudo para mim.

Ao professor Dr. Gabriel Araújo e Silva Ferraz, pelos ensinamentos, pela orientação, pelo exemplo de profissional, e principalmente, pela credibilidade depositada em mim para o desenvolvimento deste estudo.

À Universidade Federal de Lavras (UFLA) e ao Programa de Pós-Graduação em Engenharia Agrícola pela oportunidade de realização do curso e pela contribuição à minha formação (humana e profissional).

À Coordenação de Aperfeiçoamento de Pessoal de Nível Superior – Brasil (CAPES) – Número do Processo 88882.446759/2019-1, pela concessão da bolsa de estudos durante o período do doutorado.

Aos membros da banca examinadora, por terem aceitado participar da avaliação deste trabalho.

Aos meus amigos do NESA que me ajudaram na coleta de dados.

Enfim, a todos que de alguma forma contribuíram para concretização deste doutorado, meus sinceros agradecimentos.

“Todas as vitórias ocultam uma abdicação” (Simone de Beauvoir).

## RESUMO GERAL

A utilização do Sensoriamento Remoto por meio de Aeronaves Remotamente Pilotadas, pode auxiliar o cafeicultor a identificar estratégias de manejo a serem adotadas, tornando a atividade mais competitiva, aumentando a produtividade e reduzindo o impacto ambiental. Nesse contexto, objetivou-se com esse estudo desenvolver uma metodologia para avaliar e monitorar a variabilidade espacial dos estressores bióticos e abióticos do cafeeiro (*Coffea arabica* L.), usando dados de Sensoriamento Remoto multiespectral obtidos a partir de Aeronave Remotamente Pilotada. No primeiro estudo, foram utilizados 09 índices de vegetação para avaliar os danos por geada em uma lavoura cafeeira. Os resultados obtidos demonstraram que os índices de vegetação têm forte relação e alta precisão com os danos da geada nos cafeeiros. Dentre os índices estudados, o *Índice de Vegetação por Diferença Normalizada* (NDVI) apresentou os melhores desempenhos ( $r = -0,89$ ,  $R^2 = 0,79$ , MAE = 10,87 e RMSE = 14,35). Além disso, a distribuição espacial dos índices de vegetação permitiu a constatação da influência da topografia na ocorrência de geadas na cafeicultura. No segundo estudo, foi avaliado o potencial do método de aprendizado de máquina Random Forest aplicado a índices de vegetação para mensurar o conteúdo de nitrogênio nas folhas dos cafeeiros. O modelo sugerido apresentou acurácia global e coeficiente *kappa* de até 0,91 e 0,86, respectivamente. Os melhores resultados foram alcançados com os índices *Green Normalized Difference Vegetation Index* (GNDVI) e *Green Optimal Soil Adjusted Vegetation Index* (GOSAVI). Além disso, esses índices permitiram verificar que apenas 22% de toda a área da lavoura apresentava plantas com sintomas de deficiência de nitrogênio (N), o que resultaria em uma redução de 78% na quantidade de N aplicada pelo produtor. E por fim, no terceiro estudo, 63 índices de vegetação foram combinados com diferentes métodos de aprendizado de máquina e árvores de decisão para detectar a severidade da ferrugem em cafeeiros. Concluiu-se que o método *Logistic Model Tree* (LMT) foi o que mais contribuiu para a previsão precisa da doença. Esse método alcançou *overall precision*, *recall* e *f-measure* de 0,672, 0,747 e 0,695, respectivamente. No entanto, para as classes 1 e 4, retornou valores de medida F de 0,915 e 0,875, sendo um bom indicador de *Coffee Leaf Rust* (CLR) precoce (entre 2 e 5%) e de estágios posteriores de CLR (entre 20 e 40%). Concluiu-se também que este modelo pode auxiliar nas práticas de agricultura de precisão, pois oferece o monitoramento eficiente não invasivo e espacialmente contínuo da doença.

**Palavras-chave:** Sensoriamento Remoto. Agricultura de Precisão. Veículo Aéreo Não Tripulado. Índices de Vegetação. Aprendizado de Máquina. Árvore de Decisão.



## GENERAL ABSTRACT

The use of Remotely Piloted Aircraft for remote sensing in coffee plantations can assist the producer to identify management strategies to be adopted, making the activity more competitive, increasing productivity, and reducing the environmental impact. Therefore, this study aimed to develop a methodology to evaluate and monitor the spatial variability of biotic and abiotic stress in coffee (*Coffea arabica* L.), using multispectral Remote Sensing data obtained from Remotely Piloted Aircraft. In the first study, 09 vegetation indices were applied to evaluate the damage caused by frost in coffee plants. The results show that the vegetation indices have a strong relation and great precision to the frost damage identified in the coffee plants. In between the indices assessed, the Normalized Difference Vegetation Index (NDVI) has shown the best performances ( $r = -0.89$ ,  $R^2 = 0.79$ ,  $MAE = 10.87$ , and  $RMSE = 14.35$ ). Additionally, the spatial distribution of the vegetation indices allowed the verification of topography's influence on the frost occurrence in coffee plantations. The second study evaluated the potential of the Random Forest machine learning method applied to vegetation indices to measure the nitrogen content in coffee leaves. The proposed model presented global accuracy and kappa coefficient of up to 0.91 and 0.86, respectively. The best results were achieved with the indices Green Normalized Difference Vegetation Index (GNDVI) and Green Optimal Soil Adjusted Vegetation Index (GOSAVI). Furthermore, the indices made it possible to verify that only 22% of the entire crop area had symptoms of nitrogen (N) deficiency in the plants, which would result in a 78% reduction in the amount of N applied by the producer. Finally, in the third study, 63 vegetation indices were combined to different machine learning methods, and decision trees to detect the severity of rust disease in coffee plants. The study concluded that the method Logistic Model Tree (LMT) was the one that most contributed to the accurate prediction of the disease. This method achieved overall precision, recall, and f-measure of 0.672, 0.747, and 0.695, respectively. Still, for classes 1 and 4, it returned F values of 0.915 and 0.875, being a good indicator of early Coffee Leaf Rust (CLR) between 2 and 5%, and at later stages of CLR, between 20 and 40 %. It also concluded that this model could help in precision farming practices, as it offers efficient, non-invasive, and spatially continuous monitoring of the disease.

**Keywords:** Remote Sensing. Precision Agriculture. Unmanned Aerial Vehicle. Vegetation Indices. Machine Learning. Decision Tree.

## LIST OF FIGURES

### CHAPTER II

- Figure 1. Geographical location of the study area. The sampling points are highlighted in red points and the climatic favorability zones were separated in yellow lines, where a: High risk, b: Medium Risk, and c: Low Risk. ....34
- Figure 2. (a) UAV 3DR Solo; (b) Multispectral Parrot Sequoia camera; (c) Sunshine sensor; (d) Calibrated reflectance panel. ....38
- Figure 3. Spatial distribution of vegetation indices in the study área.....45

### CHAPTER III

- Figure 1. Workflow used in the methodology of this study. ....58
- Figure 2. The geographic location of the study area. MG is the State of Minas Gerais, Brazil. .... 59
- Figure 3. Description of the classes of nitrogen level in the coffee leaves identified through RGB (red, green, and blue) composition in the orthomosaic images, to select sampling points in each level. ....61
- Figure 4. Overall accuracy and kappa coefficient for image classification through Random Forest (RF) from vegetation indices. ....65
- Figure 5. Receiver operating characteristic (ROC) curve and area under the curve (AUC) for image classification through RF from vegetation indices. ....68
- Figure 6. Predictive maps of the N content spatial distribution in coffee leaves, obtained from the classification of images using RF from vegetation indices Green Normalized Difference Vegetation (GNDVI), Green Optimized Soil Adjusted Vegetation Index (GOSAVI), Normalized Difference Vegetation Index (NDVI), Soil Adjusted Difference Vegetation Index (SAVI), Medium Resolution Imaging Spectrometer (MERIS) Terrestrial Chlorophyll Index (MTCI), and Normalized Difference Red Edge (NDRE). .... 70
- Figure 7. Predictive maps of the N content spatial distribution in coffee leaves, obtained from the classification of images using RF from vegetation indices Excessive Red (EXR), Green–Red Ratio Index (GRRI), Modified Photochemical Reflectance Index (MPRI), and Normalized Different Index (NDI). ....71

## CHAPTER IV

Figure 1.	The geographic location of the studied area and illustration of the defined sampling points. ....	85
Figure 2.	Examples of collected coffee leaves with different degrees of CLR disease severity. ....	86
Figure 3.	Box-plot indicating the F-measure results from the training analysis performed by 10 runs and 100 validation-sets. The same letters above the boxes indicate no statistical difference by the Mann-Whitney test at 95% probability. ....	93
Figure 4.	Receiver Operating Characteristic (ROC) of the prediction returned by the Logistic Model Tree (LMT) algorithm. F-measure value highlighted at the point with the best TP-FP ratio. ....	95
Figure 5.	Logistic Model Tree (LMT) representation with the vegetation indices formula for each class prediction. ....	96
Figure 6.	The individual contribution of the vegetation indices for the Logistic Model Tree (LMT). ....	97
Figure 7.	Predicted map of Coffee Leaf Rust (CLR) for the non-sampled portion of the area. The remaining plants were considered healthy since they were not classified in any of the predicted classes. ....	99

## LIST OF TABLES

### CHAPTER II

Table 1.	Classification index and description for assessing frost damage in coffee plants.....	36
Table 2.	Vegetation indices of multispectral images obtained using UAV. ....	40
Table 3.	Frost damage (FD) and standard deviation (SD) in different coffee canopy strata and whole plant at different climatic favorability zones in the studied area.....	42
Table 4.	Chlorophyll index (a, b, and total) and standard deviation (SD) in different coffee canopy strata and whole plant at different climatic favorability zones in the studied area. ....	44
Table 5.	Statistics indexes between frost damage and vegetation indices.....	47

### CHAPTER III

Table 1.	Climatic data of the region on 10 December 2018. City of Santo Antônio do Amparo, MG, Brazil. ....	59
Table 2.	Vegetation indices of multispectral images obtained using Remotely Piloted Aircraft (RPA). ....	62
Table 3.	Results of the descriptive statistics of the chemical analysis of N content in plants located in the sampling points, considered as N-sufficient, -critical and -deficient. ....	64
Table 4.	Percentage (%) of areas in the coffee plantation that had N content sufficient, critical, and deficient, according to the appraisal maps of the N content spatial distribution in coffee leaves presented from the best performance to the worst performance. ....	72

### CHAPTER IV

Table 1.	Vegetation indices of multispectral images obtained using UAV. ....	88
----------	---	----

Table 2.	Averaged classification metrics values with the testing-set for the decision tree-based models used. ....	94
Table 3.	Averaged performance of the LMT learner when reducing the number of vegetation indices as input variables. ....	98

## CONTENTS

	<b>CHAPTER I: INTRODUCTION AND LITERATURE REVIEW.....</b>	<b>14</b>
<b>1</b>	<b>GENERAL INTRODUCTION .....</b>	<b>14</b>
<b>2</b>	<b>LITERATURE REVIEW .....</b>	<b>15</b>
<b>2.1</b>	<b>Remote Sensing applied in Precision Agriculture .....</b>	<b>15</b>
<b>2.2</b>	<b>Main biotic and abiotic stressors in coffee production .....</b>	<b>17</b>
<b>2.2.1</b>	<b>Nitrogen deficiency .....</b>	<b>17</b>
<b>2.2.2</b>	<b>Coffee rust (<i>Hemileia vastatrix</i> Berkeley and Broome) .....</b>	<b>17</b>
<b>2.2.3</b>	<b>Frost occurrence .....</b>	<b>18</b>
<b>2.3</b>	<b>Remote Sensing for monitoring and evaluation of coffee plants conditions .....</b>	<b>19</b>
<b>2.4</b>	<b>Remotely Piloted Aircraft in coffee crops management .....</b>	<b>20</b>
	<b>REFERENCES .....</b>	<b>23</b>
	<b>CHAPTER II: UNMANNED AERIAL VEHICLE TO EVALUATE FROST DAMAGE IN COFFEE PLANTS.....</b>	<b>31</b>
	<b>CHAPTER III: REMOTELY PILOTED AIRCRAFT AND RANDOM FOREST IN THE EVALUATION OF THE SPATIAL VARIABILITY OF FOLIAR NITROGEN IN COFFEE CROP.....</b>	<b>55</b>
	<b>CHAPTER IV: DETECTING COFFEE LEAF RUST WITH UAV-BASED VEGETATION INDICES AND DECISION TREE MACHINE LEARNING MODELS.....</b>	<b>81</b>
	<b>CHAPTER V: FINAL CONSIDERATIONS.....</b>	<b>106</b>

## **CHAPTER I: INTRODUCTION AND LITERATURE REVIEW**

### **1 GENERAL INTRODUCTION**

Coffee is a very important commodity in international agricultural commerce, especially for countries that produce and depend on it to offset balance of payments, local taxes, and subsistence. However, biotic and abiotic stressors are increasingly affecting the coffee sector, being a critical factor of fluctuations in world coffee supply and market prices. Evidence shows that the challenges in coffee production are becoming increasingly complex, mostly due to climate change, increased disease occurrence, and limited soil nutrient supply. Due to those challenges and to meet the growing demand and export commitments, it is necessary to increase the productivity and quality of coffee without negatively affecting the environment, which is the foundation of productivity.

Given the importance of coffee in developing economies, consuming countries, and ecosystems, coffee-growing requires accurate, reliable, and cost-effective monitoring strategies for the conditions of coffee trees. These monitoring mechanisms are needed to support agricultural decisions, especially for large farms, insurance, and risk services, and national planning in the coffee sector. Additionally, monitoring coffee conditions is important in Precision Agriculture, whereas pesticides are efficiently applied with cost reduction and lower environmental impacts, that are associated with an excessive application.

Yet, current methods of monitoring coffee conditions depend largely on inspections and spontaneous field sampling, which are not only labor-intensive but also subjective, since in most cases the results are confirmed when the conditions of stress are already fully established. From this, Remote Sensing methodologies provide valuable opportunities for an objective, reliable, timely, and spatially precise assessment of coffee plants' condition during the phenological cycle. In addition, remote sensing can be used repeatedly to collect samples in a non-destructive and non-invasive way.

Among the remote sensing tools, Remotely Piloted Aircraft (RPA) is an emerging technology that has been gaining popularity in recent years in the remote sensing community, especially in the agriculture context. Unlike remote sensing based on orbital or aerial sensors, RPA's are operated at low altitudes, less limited by weather conditions, involve less cost and complexity in operations, and enjoy higher deployment flexibility for missions. Besides, when coupled to image sensors, they provide phenotypic information suitable for various purposes, such as supporting Precision Agriculture in different crops.

However, coffee production has specific factors that make it more difficult to apply the concepts and technologies of remote sensing. The physiological characteristics of the plants, the dense spacing, the lack of distinct phenological cycles, and the interrelationship of environmental variables limiting coffee yield, hamper the knowing of exactly which environmental variable is influencing the spectral reflectance. These factors justify the limited application of remote sensing data in perennial crops, such as coffee. So, there is a high potential to be explored for this gap to be filled. The possibility of carrying out continuous flights with the RPAs offers a great contribution to disseminate the use of remote sensing in coffee planting, making the coffee activity increasingly efficient and more sustainable.

Accordingly, the objective of this study was to develop a methodology to evaluate and monitor the spatial variability of biotic and abiotic stressors in coffee (*Coffea arabica* L.), using multispectral remote sensing data obtained from Remotely Piloted Aircraft. To achieve this objective, it was proposed: I) to evaluate the potential use of multispectral images obtained by RPA to analyze and identify damage caused by frosts on coffee trees in different climate favorable zones; II) evaluate the potential of the Random Forest (RF) machine learning method applied to vegetation indices obtained by RPA to measure the nitrogen (N) content in plants; III) detect coffee rust disease (CLR) using RPA-based vegetation indices and decision tree machine learning models.

This thesis is presented in four independent chapters, which can be read separately, without losing the general context of the subject. Chapter I presents a general introduction and a literature review on the application of remote sensing through RPAs, in coffee production. Chapter II provides a quick, continuous, and accessible method to identify and assess frost damage to coffee plants. Chapter III proposes a model to estimate the spatial distribution of nitrogen in coffee leaves. Chapter IV presents a framework for detecting coffee leaf rust (CLR). Finally, chapter V presents a summary of main conclusions of this study and recommendations for future research in assessing coffee crops conditions.

## **2 LITERATURE REVIEW**

### **2.1 Remote Sensing applied in Precision Agriculture**

In current and future climate perspectives the resilience and productivity of agriculture systems will be increasingly compromised (SEGARRA et al., 2020). Crop production around the world is under threat from pests, water stress, soil and water salinity, fire, inadequate



management, and other factors that are responsible for environmental degradation (MULLA, 2013). Therefore, monitoring, including the analysis of the plant's composition, structure, and functional properties, is essential for sustainability and agriculture productivity (MELESSE et al., 2007).

Thus, Precision Agriculture has been grown and established as a core technology in agricultural management to predict yield, monitor plant stress, optimize fertilization, irrigate, and soil tillage activities that promote more sustainable management and improvement of agricultural practices and productivity (SEGARRA et al., 2020). Moreover, in recent years, precision agriculture techniques aimed at observing and analyzing vegetation have found in Remote Sensing an emerging possibility for the analysis and support of crop monitoring (MELESSE et al., 2007). Remote sensing provides coverage of vast areas with high accuracy and can be a highly efficient technology for improved large-scale management (SEGARRA et al., 2020).

Remote sensing application in agriculture is based on the interaction of electromagnetic radiation with the soil and the plant. Usually, remote sensing involves reflectance radiation measurement rather than measuring transmitted or absorbed radiation. The basis for the application of remote sensing techniques in Precision Agriculture is the possibility of evaluating the variation amount of energy reflected by plants along the electromagnetic spectrum. Healthy plants present characteristic spectral reflectance in the visible (0.4 to 0.7 $\mu\text{m}$ ), near-infrared (0.7 to 1.3 $\mu\text{m}$ ), mid-infrared (1.3 to 2.6 $\mu\text{m}$ ), and thermal (3, 0 to 5.0 $\mu\text{m}$ ) (MAHAJAN et al., 2014; BARTON, 2012).

Previous studies have shown that the employment of remote sensing in agriculture is significant, especially under the broader scope of Precision Agriculture. The variation of energy reflected by the leaves of vegetation along the electromagnetic spectrum, has a higher correlation with the biophysical properties of crops, enabling the identification of areas that present water deficit, pest occurrence, nutrient deficiency, or even the existence of different productivity levels in the same crop (AHAMED et al., 2011; COLTRI et al., 2013; MULLA, 2013; VOLPATO et al., 2013; BERNARDES et al., 2012; CHEMURA et al., 2017; CHEMURA et al., 2013; CHEMURA et al., 2017; CHEMURA et al., 2017; al., 2018; MARIN et al., 2018; MARIN et al., 2019).

From this prospect, the ability of Remote Sensing to increase agricultural productivity has since gone from potential to reality, with evidence of practical applications around the world. For coffee production this is not different. The use of Remote Sensing combined with Precision Agriculture is useful and applicable since the monitoring of biotic and abiotic

variables is essential to estimate conditions of coffee plants and therefore apply the proper management of the crop in a localized, targeted, and timely manner.

## **2.2 Main biotic and abiotic stressors in coffee production**

Coffee cultivars have a narrow genetic base, making them susceptible to stressors that limit productivity and selection of genetically improved plants (VAN DER VOSSEN; WALYARO, 2009). Among the many stressors for the coffee plants in the south-central region of the state of Minas Gerais, nitrogen deficiency, frost damage, and rust diseases (*Hemileia vastatrix*) are considered the most critical.

### **2.2.1 Nitrogen deficiency**

Coffee plants require a high fertility level and an intensive fertilizer program, which are a requirement for successful coffee production (CHEMURA, 2017). Without proper soil fertility management, nutritional deficiencies and imbalances will affect the survival and productivity of the coffee plants (BOTE et al., 2018; MARTINEZ et al., 2003; NAZARENO et al., 2003). Among the essential nutrients for the coffee crop, nitrogen (N) is considered the most limiting in the development and productivity of the coffee (COSTE, 1992), playing several interconnected roles in the expansion and productivity of the plant. N determines plant establishment and root growth, that influences other aspects of plant health (CHEMURA et al., 2018). Additionally, it takes part in increasing productivity, ensuring the generation of new branches, which will be the basis for productivity in subsequent years (LOGAN; BISCOE, 1987). Furthermore, N plays a significant role in the resilience of plants to biotic and abiotic stressors (CHEMURA et al., 2018). Deficiency of N in coffee, on the other hand, promotes reduced leaf production and reduced plant growth, damage to fruit formation, decreased leaf area, reduced photosynthesis, resulting in gradual chlorosis of the leaves (initiating symptoms in older leaves) and greater susceptibility to diseases (MENGEL; KIRKBY, 2001).

### **2.2.2 Coffe rust (*Hemileia vastatrix* Berkeley and Broome)**

Coffee rust is considered the most severe of all coffee diseases, especially for the species *Coffea arabica* L. (DINESH; SHIVANNA; SANTA RAM, 2011; CACEFO; ARAÚJO; PACHECO, 2016). The basidiomycete *Hemileia vastatrix* is an obligate biotrophic fungus

found in almost all coffee producer countries (BROWN; HOVMØLLER, 2002). The plant tissue colonization results in small chlorotic spots that rapidly increase in number and diameter, resulting in the formation of orange-colored uredospore pustules (SILVA et al., 2006; HADDAD et al., 2009; AVELINO et al., 2012). The infection caused by this fungus affects both younger and older leaves of the coffee plants (SCHIEBER; ZENTMYER, 1984). The consequences of this infection reflect in the premature fall of leaves, a decrease in the rate of photosynthesis, and a reduction in productivity (AGRIOS, 2005; SILVA et al., 2006). Besides, it is also known that the severity of rust is positively correlated to productivity, which influences the nutritional status of plants (MULLER et al., 2004). In this context, according to Garçon et al. 2004 and Pozza, 2010, in the absence of early detection and adequate management, coffee rust can result in losses of up to 50% of the leaves, and a reduction of up to 70% in the productivity of the plant.

One challenge in identifying coffee rust using Remote Sensing is that the characteristics of the signs of infection occur only on the inferior side of the leaf, with little or no sign of infection on the upper side (CHEMURA, 2017). Furthermore, rust infection affects the distribution of nutrients in coffee leaves (BELAN et al., 2014) and, consequently, the characteristic reflectance associated with N deficiency can also be described in leaves infected by rust (CHEMURA, 2017).

### **2.2.3 Frost occurrence**

According to Caramori et al. (2001), frost is any drop in temperature that causes harmful effects on a plant, to its growth or development. Frost damage to coffee plants can cause plant tissue to die by a physicochemical process. In this process, there is cell dehydration, loss of turgor potential, increase in solute concentration, cell volume reduction, and plasma membrane rupture. Therefore, the leaves appear dark brown, with a burning aspect (LARCHER, 1981). The result of this is a reduction in the income by production of the year of frost occurrence, with impacts in the following years (RAMALHO et al. 2014).

In this context, the identification of areas with susceptibility to frost occurrence becomes crucial for the management of the crop (PEZZOPANE et al. 2010; ALVARES et al. 2017; GOBBETT; NIDUMOLU; CRIMP, 2018; NÓIA JÚNIOR et al. 2019). Based on this information, coffee producers can properly choose the location and planting orientation, as well as the most appropriate management for the crops installed in these areas of greater susceptibility. Further, for areas with greater climatic risk, especially in lowland areas, where

cold air accumulates, the producer can apply preventive practices to reduce the impact of frost on coffee plants, for example: maintain lines and between lines weed-free and administer fertilizer to raise the plant's solutes and increase the plant's resistance to low temperatures (CAMARGO, 2010).

### **2.3 Remote sensing for monitoring and evaluation of coffee plants conditions**

Although biotic to abiotic stressors are productivity-limiting factors and, consequently, cause financial losses, current methods of assessing and monitoring the conditions of coffee plants depend on surveys in occasional fields carried out by a qualified workforce, looking for signs of disease and nutritional imbalance of plants through observations (MARIN et al., 2019a). However, these methods are difficult to be implemented in larger areas of cultivation. And they are also subjective since in most cases the results are confirmed when the disease or imbalance is already fully established (MARIN et al., 2019b), with the compromise of plant growth and productivity. Thus, there is a growing interest in using Remote Sensing data for an early stage, efficient, objective, and non-destructive assessment of plant responses to different environmental stressors (LI et al., 2010).

Plants react to biotic and abiotic stressors through biophysical and biochemical changes, such as reductions in biomass, chlorophyll content, and changes in internal leaf structures, which are easily detected through differences in energy reflectance in the visible and near-infrared spectral regions (MAHAJAN et al., 2014; BARTON, 2012; BAJWA; RUPE; MASON, 2017; MULLA et al., 2013).

From this knowledge, Marin et al. (2019a) evaluated the potential of the Landsat 8 OLI/TIRS satellite for spatial and temporal monitoring of coffee plants affected by bacterial blight. The results showed correlations of vegetation indices with disease incidence and severity of  $r = 0.76$  and  $r = 0.52$ , respectively. In addition, the brightness temperature helped in mapping areas with optimal temperature conditions for the occurrence of the disease.

Similarly, Marin et al. (2019b) used vegetation indices obtained from Landsat 5/TM multispectral images to identify and map the physical, chemical, and biological characteristics of the soil and the macro and micronutrients in the leaves of coffee trees. The authors stated that the study results can contribute to more efficient management of coffee crops, as well as to the sustainability of the activity through the more rational use of fertilizers and phytosanitary products.

Chemura et al. (2018), evaluated the value of the Sentinel-2 satellite spectral bands and the vegetation indices in the empirical estimate of leaf nitrogen content in coffee plants. Leaf nitrogen content modeling using vegetation indices produced better accuracy ( $R^2 = 0.71$ ) when compared to spectral bands ( $R^2 = 0.57$ ). Hence, the authors concluded that Sentinel-2 data, particularly for vegetation indices, can be used accurately in landscape scale modeling of leaf nitrogen content.

Rafaelli et al. (2006) detected the coverage of the area affected by frost in the state of Paraná, as a function of the spectral response of coffee before and after the frost. For this, the NDVI derived from the MODIS satellite was used. Although MODIS data have been efficient for monitoring the effect of frost at the state level, soon after its occurrence, it was found that to qualitatively assess the impact of the frost and to quantify the coffee area, images from medium spatial resolution, such as TM/Landsat or CCD/CBERS.

In addition to the studies mentioned above, it is still possible to find other studies applying Remote Sensing in the assessment of coffee plants conditions (BERNARDES et al., 2012; COLTRI et al., 2013; VOLPATO et al., 2013; MARTINS et al., 2017; CORTEZ et al., 2020; MIRANDA et al.; 2020; PIRES; ALVES; POZZA, 2020). However, these studies used multispectral images obtained through low and medium spatial resolution orbital sensors. These sensors, due to their spatial resolution, may be influenced by other spectral targets such as soil, weeds, and even the presence of clouds. Furthermore, the revisit period makes it difficult to continuously monitor and assess the stress conditions of coffee crops. Thus, it is necessary to take advantage of other sensors and technologies that Remote Sensing offers, for example, Remotely Piloted Aircraft that can provide multispectral images of high spatial resolution and with low interference from targets other than coffee plants. And most importantly, it allows for continuous monitoring of coffee plantations, allowing for actions by growers promptly.

#### **2.4 Remotely Piloted Aircraft in coffee crops management**

RPA is an emerging technology that has gained increasing popularity in recent years in the Remote Sensing community, mainly due to its ability to continuously obtain images with a high spatial resolution (RANGO et al., 2006). Unlike Remote Sensing based on orbital or aerial sensors, RPAs are operated at low altitudes and, therefore, are less limited by weather conditions. The operation involves lower cost and complexity and possesses high deployment flexibility for repeated missions (HUNT et al., 2010; LALIBERTE et al., 2011). Furthermore,

they can be applied in smaller areas and in specific locations with the ease of obtaining data in less time, such as monitoring the growth of crops.

A proper sensor is a fundamental component of an RPA imaging system. Early RPA imaging systems typically used commercial video cameras or still cameras operating in the spectral regions of blue, green, red, and near-infrared (HUNT et al., 2010; ZHOU et al., 2009). Recent developments in tailor-made sensors for RPAs operation offer improved possibilities for Remote Sensing applications in terms of better image quality, multispectral, hyperspectral, and thermal images (BERNI et al., 2009; LALIBERTE et al., 2011; HRUSKA et al., 2012). Thus, RPAs coupled to image sensors can provide phenotypic information suitable for various purposes, such as supporting Precision Agriculture in different crops (PRIMICERIO et al., 2012; TATTARIS; REYNOLDS; CHAPMAN, 2016; AKHTMAN et al., 2017).

Due to these advances, research on the use of RPAs in Precision Farming has been increasing considerably in recent years. It is possible to find in the literature applications of RPAs in several crops, for wheat crops (HONKAVAARA et al., 2013; TORRES-SÁNCHEZ et al., 2013), grape (PRIMICERIO et al., 2014), canola (SEVERTSON et al., 2014). al., 2016) and corn (CASTALDI et al., 2017), to perennial crops such as apple (GÓMEZ-CANDÓN et al., 2016), palm (ROMERO et al., 2015), and citrus (OSCO et al., 2019), using various platforms, including fixed-wing (LALIBERTE et al., 2010) and rotary (XIANG; TIAN, 2011); containing RGB (Red, Green, Blue) (CARRIJO et al., 2017), multispectral (PEÑA et al., 2013) and thermal (BERNI et al., 2009) cameras, and performing various forms of image processing for each purpose.

However, for the coffee crop, research is limited to the evaluation of fruit maturation, the evaluation of biophysical parameters, and the identification of plant failures. For example, Johnson et al. (2004), Furfaro et al. (2005), Furfaro et al. (2007), and Carrijo et al. (2017), used RGB images, obtained from RPAs, and Neural Network and Machine Learning algorithms to evaluate the maturation of coffee fruits. The results of these studies suggest that Remote Sensing technologies applied to RPAs can provide an alternative method, more comprehensive from a spatial point of view, to monitor fruit maturation and assess the best time to harvest this high-value agricultural commodity. Martins et al. (2021), proposed a vegetation index based on RGB images, obtained from RPAs, to estimate coffee maturation. The proposed vegetation index showed high sensitivity to discriminate ready-to-harvest and non-ready to harvest coffee plants. Oliveira et al. (2018), developed a methodology to detect planting failures in coffee plantations from RGB images of high spatial resolution, obtained using an RPA. According to the authors, the results of the study show that the proposed method is reliable to accurately

identify gaps in the rows of planted coffee crops. And finally, Santos et al. (2020), evaluated the accuracy of the photogrammetry technique using a Structure from Motion (SfM) point cloud to estimate the height and diameter of the coffee canopy from aerial images obtained by RPA equipped with an RGB camera and compared the results with data measured in situ for 12 months. The authors obtained a correlation of 87% and 95% between the values of height in the field and diameter of the crown, respectively, and the values obtained employing RPA.

Thus, studies using RPAs in coffee production are still scarce. The studies cited above did not explore the potential of multispectral cameras. These cameras, together with RGB cameras and other Remote Sensing tools, can contribute to the proper management of coffee crops, reducing production costs, increasing productivity, and protecting ecosystem services in coffee production areas.

## REFERENCES

AGRIOS, G. N. **Plant Pathology**. Amsterdam: Elsevier, 2005. 922 p.

ALVARES, C. A. et al. Climatic favourability zones for Eucalyptus rust in Brazil. **Forest Pathology**, Malden, v. 47, n. 1, p. 1-17, jul. 2017.

AKHTMAN, Y. et al. Application of hyperspectral images and ground data for precision farming. **Geography, Environment, Sustainability**, Moscou, v. 10, n. 4, p. 117-128, 2017.

AHAMED, T. et al. A review of remote sensing methods for biomass feedstock production. **Biomass and Bioenergy**, Oxford, v. 35, n. 7, p. 2455-2469, jul. 2011.

AVELINO, J. et al. Landscape context and scale differentially impact coffee leaf rust, coffee berry borer, and coffee root-knot nematodes. **Ecological applications**, Washington, v. 22, n. 2, p. 584-596, mar. 2012.

BAJWA, S. G.; RUPE, J. C.; MASON, J. Soybean disease monitoring with leaf reflectance. **Remote Sensing**, Basel, v. 9, n. 2, p. 127, fev. 2017.

BARTON, C. V. M. Advances in remote sensing of plant stress. **Plant and Soil**, Dordrecht, v. 354, n. 1-2, p. 41-44, nov. 2012.

BELAN, L. L. et al. Diagrammatic scale for assessment of bacterial blight in coffee leaves. **Journal of Phytopathology**, Malden, v. 162, n. 11-12, p. 801-810, maio. 2014.

BERNARDES, T. et al. Monitoring biennial bearing effect on coffee yield using MODIS remote sensing imagery. **Remote Sensing**, Basel, v. 4, n. 9, ago. p. 2492-2509, 2012.

BERNI, J. A. et al. Thermal and narrowband multispectral remote sensing for vegetation monitoring from an unmanned aerial vehicle. **IEEE Transactions on Geoscience and Remote Sensing**, Piscataway, v. 47, n. 3, p. 722-738, mar. 2009.

BOTE, A. D. et al. Analysis of coffee (*Coffea arabica* L.) performance in relation to radiation levels and rates of nitrogen supply I. Vegetative growth, production and distribution of



biomass and radiation use efficiency. **European Journal of Agronomy**, Amsterdã, v. 92, p. 115-122, jan. 2018.

BROWN, J. K. M; HOVMØLLER, M. S. Aerial dispersal of pathogens on the global and continental scales and its impact on plant disease. **Science**, Washington, v. 297, n. 55-81, p. 537-541, jul. 2002.

CACEFO, V.; ARAÚJO, F. F.; PACHECO, A. C. Biological control of *Hemileia vastatrix* Berk. & Broome with *Bacillus subtilis* Cohn and biochemical changes in the coffee. **Coffee Science**, Lavras, v. 11, n. 4, p. 567-574, out/dez. 2016.

CAMARGO, M. B. P. D. The impact of climatic variability and climate change on Arabic coffee crop in Brazil **Bragantia**, Campinas, v. 69, n. 1, p. 239-247, 2010.

CARAMORI, P. H. et al. Zoneamento de riscos climáticos para a cultura de café (*Coffea arábica* L.) no estado do Paraná. **Revista Brasileira de Agrometeorologia**, Passo Fundo, v.9, n.3, p.486-494, 2001.

CARRIJO, G. L. A. et al. **Automatic detection of fruits in coffee crops from aerial images**. In: 2017 Latin American Robotics Symposium (LARS) and 2017 Brazilian Symposium on Robotics (SBR). IEEE, 2017. p. 1-6.

CASTALDI, F. et al. Assessing the potential of images from unmanned aerial vehicles (UAV) to support herbicide patch spraying in maize. **Precision Agriculture**, Dordrecht, v. 18, n. 1, p. 76-94, ago. 2017.

COLTRI, P. P. et al. Biomass and carbon stock estimation with usage of high resolution satellites images. **IEEE Journal of Selected Topics in Applied Earth Observations and Remote Sensing**, Piscataway, v. 6, n. 3, p. 1786-1795, 2013.

COSTE, R. **Coffee - The Plant and the Product**. Londres: MacMillan Press, 1992. 336 p.

CORTEZ, M. L. J. et al. Relationship between Sentinel-2 orbital data and in situ monitoring of coffee rust. **SN Applied Sciences**, v. 2, n. 8, p. 1-13, jul. 2020.

CHEMURA, A. et al. Mapping spatial variability of foliar nitrogen in coffee (*Coffea arabica* L.) plantations with multispectral Sentinel-2 MSI data. **ISPRS Journal of Photogrammetry and Remote Sensing**, Londres, v. 138, p. 1-11, abr. 2018.

CHEMURA, A.; MUTANGA, O.; DUBE, T. Integrating age in the detection and mapping of incongruous patches in coffee (*Coffea arabica*) plantations using multi-temporal Landsat 8 NDVI anomalies. *International Journal of Applied Earth Observation and Geoinformation*, **Enschede**, v. 57, p. 1-13, maio. 2017.

CHEMURA, A. **Modelling spatial variability of coffee (*Coffea Arabica* L.) Crop condition with multispectral remote sensing data**. 2017. 220 p. Tese (Doutorado Filosofia e Ciências Ambientais) - University of KwaZulu-Natal, Pietermaritzburg, 2017.

DINESH, K. P.; SHIVANNA, M. B.; SANTA RAM, A. Identification of RAPD (random amplified polymorphic DNA) markers for Ethiopian wild *Coffea arabica* L. genetic resources conserved in India. **The IIOAB Journal**, Purba Medinipur, v. 2, n. 4, p. 1-7, maio. 2011.

FURFARO, R. et al. Neural network algorithm for coffee ripeness evaluation using airborne images. **Applied Engineering in Agriculture**, v. 23, n. 3, p. 379-387, 2007.

FURFARO, R. et al. **Model-based neural network algorithm for coffee ripeness prediction using Helios UAV aerial images**. *In: Remote Sensing for Agriculture, Ecosystems, and Hydrology VII*. International Society for Optics and Photonics, 2005. p. 59760X.

GARÇON, C. L. P. et al. Controle da ferrugem do cafeeiro com base no valor de severidade. **Fitopatologia Brasileira**, Brasília, v. 29, p. 486-491, set/out. 2004.

GOBBETT, D. L.; NIDUMOLU, U.; CRIMP, S. Modelling frost generates insights for managing risk of minimum temperature extremes. **Weather and Climate Extremes**, v. 27, p. 1-9, mar. 2020.

GÓMEZ-CANDÓN, D. et al. Field phenotyping of water stress at tree scale by UAV-sensed imagery: new insights for thermal acquisition and calibration. **Precision agriculture**, Dordrecht, v. 17, n. 6, p. 786-800, abr. 2016.

HADDAD, F. et al. Biological control of coffee rust by antagonistic bacteria under field conditions in Brazil. **Biological Control**, Amsterdã, v. 49, n. 2, p. 114-119, maio. 2009.

HONKAVAARA, E. et al. Processing and assessment of spectrometric, stereoscopic imagery collected using a lightweight UAV spectral camera for precision agriculture. **Remote Sensing**, Basel, v. 5, n. 10, p. 5006-5039, out. 2013.

HUNT, E.R. et al. Raymond et al. Acquisition of NIR-green-blue digital photographs from unmanned aircraft for crop monitoring. **Remote Sensing**, Piscataway, v. 2, n. 1, p. 290-305, jan. 2010.

HRUSKA, R. et al. Radiometric and geometric analysis of hyperspectral imagery acquired from an unmanned aerial vehicle. **Remote Sensing**, Piscataway, v. 4, n. 9, p. 2736-2752, set. 2012.

JOHNSON, L. F. et al. Feasibility of monitoring coffee field ripeness with airborne multispectral imagery. **Applied Engineering in Agriculture**, v. 20, n. 6, p. 845-849, 2004.

LALIBERTE, A. et al. Multispectral remote sensing from unmanned aircraft: Image processing workflows and applications for rangeland environments. **Remote Sensing**, Piscataway, v. 3, n. 11, p. 2529-2551, nov. 2011.

LARCHER, W. Effects of low temperature stress and frost injury on plant productivity. *In*: JOHNSON C. B. **Physiological Processes Limiting Plant Productivity**. London: Butterworths, 1981, p. 253-269.

LI, G. et al. Leaf chlorophyll fluorescence, hyperspectral reflectance, pigments content, malondialdehyde and proline accumulation responses of castor bean (*Ricinus communis* L.) seedlings to salt stress levels. **Industrial crops and products**, Amsterdã, v. 31, n. 1, p. 13-19, jan. 2010.

LOGAN, W. J. C.; BISCOE, J. **Coffee handbook**, 1987. 182 p.

- MAHAJAN, G.R. et al. Using hyperspectral remote sensing techniques to monitor nitrogen, phosphorus, sulphur and potassium in wheat (*Triticum aestivum* L.). **Precision Agriculture**, Dordrecht, v. 15, n. 5, p. 499-522, fev. 2014.
- MARIN, D. B. et al. Multispectral radiometric monitoring of bacterial blight of coffee. **Precision Agriculture**, Dordrecht, p. 1-24, dez. 2019a.
- MARIN, D. B. et al. Multispectral remote sensing in the identification and mapping of biotic and abiotic coffee tree variables. **Revista Ceres**, Viçosa, v. 66, n. 2, p. 142-153, mar/abr. 2019b.
- MARTINEZ, H. E. P. et al. Faixas críticas de nutrientes e avaliação do estado nutricional de cafeeiros em quatro regiões de Minas Gerais. **Pesquisa Agropecuária Brasileira**, Brasília, v. 38, n. 6, p. 703-713, jun. 2003.
- MARTINS, G. D.; GALO, M. D. L. B. T.; VIEIRA, B. S. Detecting and mapping root-knot nematode infection in coffee crop using remote sensing measurements. **IEEE Journal of Selected Topics in Applied Earth Observations and Remote Sensing**, Piscataway, v. 10, n. 12, p. 5395-5403, ago. 2017.
- MARTINS, N. R.; PINTO, F. A. C.; QUEIROZ, D. M.; VALENTE, D. S. M.; ROSAS, J. T. F. A Novel Vegetation Index for Coffee Ripeness Monitoring Using Aerial Imagery. **Remote Sensing**, Piscataway, v. 13, n. 2, p. 263, 2021.
- MELESSE, A. M. et al. Remote sensing sensors and applications in environmental resources mapping and modelling. **Sensors**, Basel, v. 7, n. 12, p. 3209-3241, nov. 2007.
- MENGEL, K.; KIRKBY, E.A. **Princípios de nutrición vegetal**. Basel: International Potash Institute, 2001. 692 p.
- MIRANDA, J. et al. Detection of coffee berry necrosis by digital image processing of landsat 8 oli satellite imagery. **International Journal of Applied Earth Observation and Geoinformation**, Amsterdã, v. 85, p. 1-10, mar. 2020.

MULLA, D. J. Twenty five years of remote sensing in precision agriculture: Key advances and remaining knowledge gaps. **Biosystems engineering**, New York, v. 114, n. 4, p. 358-371, abr. 2013.

NAZARENO, R. B. et al. Crescimento inicial do cafeeiro Rubi em resposta a doses de nitrogênio, fósforo e potássio e a regimes hídricos. **Pesquisa Agropecuária Brasileira**, Brasília, v. 38, n. 8, p. 903-910, ago. 2003.

NÓIA JÚNIOR, R. S et al. Eucalyptus rust climatic risk as affected by topography and ENSO phenomenon. **Australasian Plant Pathology**, Collingwood, v. 48, n. 2, p. 131-141, nov. 2019.

OLIVEIRA, H. C. et al. Failure detection in row crops from UAV images using morphological operators. **IEEE Geoscience and Remote Sensing Letters**, Piscataway v. 15, n. 7, p. 991-995, jul. 2018.

OSCO, L. P. et al. Predicting canopy nitrogen content in citrus-trees using random forest algorithm associated to spectral vegetation indices from UAV-Imagery. **Remote Sensing**, Basel, v. 11, n. 24, p. 2925, dez. 2019.

PEÑA, J. M. et al. Weed mapping in early-season maize fields using object-based analysis of unmanned aerial vehicle (UAV) images. **PloS one**, São Francisco, v. 8, n. 10, p. e77151, out. 2013.

PEZZOPANE, J. R. M. et al. Climatic risk zoning for Conilon coffee in Espírito Santo, Brazil. **Revista Ciência Agronômica**, Fortaleza, v. 41, n. 3, p. 341, jul/set. 2010.

PIRES, M. S. et al. Multispectral radiometric characterization of coffee rust epidemic in different irrigation management systems. **International Journal of Applied Earth Observation and Geoinformation**, Amsterdã, v. 86, p. 102016, abril. 2020.

POZZA, E. A.; CARVALHO, V. L.; CHALFOUN, S. M. **Sintomas de injurias causadas por doenças do cafeeiro**. In: GUIMARÃES, R. J., MENDES, A. N. G., BALIZA, D. P. (Eds.), *Semiologia do Cafeeiro*. Brasil: Editora UFLA, 2010, p. 67-106.

PRIMICERIO, J. et al. A flexible unmanned aerial vehicle for precision agriculture. **Precision Agriculture**, Dordrecht v. 13, n. 4, p. 517-523, jan. 2012.

PRIMICERIO, J. et al. Individual plant definition and missing plant characterization in vineyards from high-resolution UAV imagery. **European Journal of Remote Sensing**, Florença, v. 50, n. 1, p. 179-186, abr. 2017.

RAMALHO, J. C. et al. Cold impact and acclimation response of Coffea spp. plants. **Theoretical and Experimental Plant Physiology**, Amsterdã, v. 26, n. 1, p. 5-18, fev. 2014.

RAFAELLI, D. R.; MOREIRA, M. A.; FARIA, R. T. Análise do potencial de dados MODIS para monitorar o impacto de geada em nível estadual em lavouras de café. **Agricultura em São Paulo**, São Paulo, v. 53, n. 1, jan/jun. p. 5-15, 2006.

RANGO, A. et al. Using unmanned aerial vehicles for rangelands: current applications and future potentials. **Environmental Practice**, Abingdon, v. 8, n. 3, p. 159-168, jul. 2006.

ROMERO, V. R. et al. Perspectivas de la tecnología VANT en el cultivo de palma de aceite: monitorización del cultivo mediante imágenes aéreas de alta resolución. **Revista Palmas**, Bogotá, v. 36, n. 3, p. 25-41, jul/set. 2015.

SANTOS, L. M. et al. Biophysical parameters of coffee crop estimated by UAV RGB images. **Precision Agriculture**, Dordrecht, p. 1-15, abril. 2020.

SEGARRA, J. et al. Remote Sensing for Precision Agriculture: Sentinel-2 Improved Features and Applications. **Agronomy**, Basel, v. 10, n. 5, p. 1-18, maio. 2020.

SEVERTSON, D. et al. Unmanned aerial vehicle canopy reflectance data detects potassium deficiency and green peach aphid susceptibility in canola. **Precision agriculture**, Dordrecht v. 17, n. 6, p. 659-677, mar. 2016.

SILVA, M. C. et al. Coffee resistance to the main diseases: leaf rust and coffee berry disease. **Brazilian Journal of Plant Physiology**, Londrina, v. 18, n. 1, p. 119-147, jan/mar. 2006.

SCHIEBER, E.; ZENTMYER, G.A. Coffee rust in the Western Hemisphere. **Plant Disease**, St. Paul, v. 68, n. 2, p. 89-90, fev. 1984.

TATTARIS, M.; REYNOLDS, M. P.; CHAPMAN, S. C. A direct comparison of remote sensing approaches for high-throughput phenotyping in plant breeding. **Frontiers in Plant Science**, Lausana, v. 7, p. 1-9, ago. 2016.

TORRES-SÁNCHEZ, J. et al. Configuration and specifications of an unmanned aerial vehicle (UAV) for early site specific weed management. **PloS one**, São Francisco, v. 8, n. 3, p. 58210, mar. 2013.

VAN DER VOSSSEN, H. A. M.; WALYARO, D. J. Additional evidence for oligogenic inheritance of durable host resistance to coffee berry disease (*Colletotrichum kahawae*) in arabica coffee (*Coffea arabica* L.). **Euphytica**, Basel, v. 165, n. 1, p. 105-111, jul. 2009.

VOLPATO, M. M. L. et al. MODIS images for agrometeorological monitoring of coffee areas. **Coffee Science**, Lavras, v. 8, n. 2, p. 168-175, abr/jun. 2013.

UNITED STATES DEPARTMENT OF AGRICULTURE - USDA. **Coffee: world markets and trade Foreign Agricultural Service/USDA**. Washington, 2018. Disponível em <<https://apps.fas.usda.gov/psdonline/circulars/coffee.pdf>>. Acesso em: 04 maio. 2019.

XIANG, H.; TIAN, L. Method for automatic georeferencing aerial remote sensing (RS) images from an unmanned aerial vehicle (UAV) platform. **Biosystems Engineering**, São Diego, v. 108, n. 2, p. 104-113, fev. 2011.

ZHOU, G. Near real-time orthorectification and mosaic of small UAV video flow for time-critical event response. **IEEE Transactions on Geoscience and Remote Sensing**, Piscataway, v. 47, n. 3, p. 739-747, mar. 2009.

## CHAPTER II: UNMANNED AERIAL VEHICLE TO EVALUATE FROST DAMAGE IN COFFEE PLANTS

### This chapter is based on:

**Marin, D. B.**, Ferraz, G. A. S., Schwerz, F., Barata, R. A. P., de Oliveira Faria, R., and Dias, J. E. L. (2021). Unmanned aerial vehicle to evaluate frost damage in coffee plants. *Precision Agriculture*, 1-16. <https://doi.org/10.1007/s11119-021-09815-w>.

### Abstract

Damage caused by frost on coffee plants can impact significantly in the reduction of crop quality and productivity. Remote sensing can be used to evaluate the damage caused by frost, providing precise and timely agricultural information to producers, assisting in decision making, and consequently minimizing production losses. In this context, this study aimed to evaluate the potential use of multispectral images obtained by unmanned aerial vehicle (UAV) to analyze and identify damage caused by frost in coffee plants in different climatic favorability zones. Visual evaluations of frost damage and chlorophyll content quantification were carried out in a commercial coffee plantation in Southern Minas Gerais, Brazil. The images were obtained from a multispectral camera coupled to a UAV with rotating wings. The results obtained demonstrated that the vegetation indices had a strong relationship and high accuracy with the frost damage. Among the indices studied the normalized difference vegetation index (NDVI) was the one that had better performances ( $r = -0.89$ ,  $R^2 = 0.79$ ,  $MAE = 10.87$  e  $RMSE = 14.35$ ). In a simple way, this study demonstrated that multispectral images, obtained from UAV, can provide a fast, continuous, and accessible method to identify and evaluate frost damage in coffee plants. This information is essential for the coffee producer for decision-making and adequate crop management.

**Keywords** Remote Sensing · Vegetation indices · Multispectral images · UAV



## Introduction

Coffee is a tropical crop that is currently grown in about 80 countries, being one of the most traded agricultural commodities worldwide. The coffee crop has great importance economically and socially in Brazil which is the world's largest producer and exporter of coffee, but still, a wide number of factors strongly limit agricultural yields and quality of this commodity, including drought and extreme temperatures (Martins et al. 2019).

The coffee crop cultivated in regions where air temperature reaches below 18°C shows a substantially reduced growth index. Besides that, the occurrence of frosting in those regions can limit the economic viability of coffee production (Camargo 2010). The damage caused by frosting on the coffee plants can cause severe limitations, directly reducing the yield of the year, and impacting in the following years (Ramalho et al. 2014). One of the main effects of frosting in plants is the reduction of the leaf area which can be observed by the reduction of chlorophyll a and b, as well as by the processes of necrosis and senescence of leaves, decreasing the solar radiation absorption and photosynthesis. In this sense, the awareness of the damage caused by frosting is essential for the producer mainly to assist in the decision making to perform, for example, pruning and fertilizing to maintain leaves that were not damaged.

A large part of the national production comes from the southern region of Minas Gerais, an area that has a strong feature on its topography, where high slope and lowlands characterize the geographical relief. In varying terrain, the topography is a known factor that influences the frosting patterns (Kotikot & Onywere 2014). Therefore, the identification of areas of climate favorability for frost occurrence becomes essential for crop management (Gobbett et al. 2018; Nóia Júnior et al. 2019). Possessing that information, coffee producers could adequately choose the location, orientation, and low-temperature resistant cultivars to be used. Also, for areas showing higher climate risk, especially lowland areas where cold air accumulates, the producer may use preventive measures to reduce the impact of frost on the coffee plants, for example, keep cultivation lines clean from weeds and apply calcium sulphate to increase solute of the plant as well as low-temperature resistance (Camargo 2010).

To establish a risk zone for frost occurrence is an important step to integrated management and protection of coffee production. Considering the diversity of the geographical reliefs found in coffee-producing areas in Brazil, it is essential to understand how frost formation occurs and how topography influences frost occurrence in coffee plantations. Knowledge of climatic variability affected by topography can help producers identify high and low-risk areas, even when macroclimatic conditions are not favorable.

However, despite the importance of coffee plantations and the occurrence of frost in the producing regions, there are still few studies in the literature evaluating the impact of frost on the coffee crop. Moreover, monitoring damage due to frost requires intensive field survey work (Wei et al. 2017). These procedures, besides being expensive and subjective, are time-consuming and lead to market speculation for coffee, due to the lack of real knowledge of the impact of frost in the region combined with the time to obtain the information (Rafaelli et al. 2006). Thus, it is necessary to develop a more effective approach to define and monitor frost damage for the coffee crop.

Remote sensing can be used to evaluate the damage caused by frost, providing precise and timely agricultural information to producers, assisting in decision making, and consequently minimizing production losses (Marin et al. 2019). The use of remote sensing in agriculture is based on the reflectance characteristics of the leaves in the visible and near-infrared spectral regions, obtained mainly by variations in the photosynthetic pigment content, cell structure, and moisture content (Feng et al. 2018). In the case of frost damage, the reflectance characteristic in the spectral region is modified according to the damage of the cell structure of the leaves (Wang et al. 2015; Wei et al. 2017). Based on that, remote sensing may successfully assess the damage caused by frosting in the coffee crop.

Previous studies have shown potential in orbital remote sensing to monitor damage by plant frosting in different cultures, such as wheat (Feng et al. 2009; Wang et al. 2015), oilseed rape (She et al. 2017; Wei et al. 2017), sugarcane (Tan et al. 2008) and tea (Lou et al. 2013). For the coffee crop, Rafaelli et al. (2006) reported that normalized difference vegetation index (NDVI), obtained with MODIS images, was enough to monitor the effect of frost in the coffee plantation locally and regionally. However, these studies did not investigate suborbital remote sensing using unmanned aerial vehicle (UAVs) that offers advantages in evaluating injury by frosting when compared to images obtained from satellites. The application of satellite images for evaluation of agricultural cultures might be limited due to the low spatial and temporal resolution, cloudiness, and high operating costs that may not be suitable, especially for smaller farms (Zhang et al. 2016; Zhou et al. 2016). On the other hand, UAVs can collect images with high spatial resolution, down to centimeters, and temporal frequency based on the producer's needs (Zhang et al. 2016). Additionally, it can be used for evaluation in small areas (Santos et al. 2019) with the low-cost advantage in these areas (Zhou et al. 2016).

The lack of information about frost damage in coffee crops grown under different relief conditions limits the ability to understand related plant responses and the economic impacts of this extreme event at a local and regional scale. Therefore, the authors hypothesized that the use

of UAVs may contribute to decision-making and adequate management of coffee crops affected by frosting. For this reason, the objective of this study was to evaluate the potential usage of multispectral images obtained by UAV to analyze and identify damage caused by frost in coffee plants in different climatic favorability zones.

## Materials and methods

### Description of the experimental area

The study was carried out in the coffee farm Bom Jardim, located in the city of Santo Antonio do Amparo, State of Minas Gerais, Brazil, geographical co-ordinates 21°01'11.93" S, 44°55'24.46" W and altitude 927 m (Fig. 1). The plantation area represents a total of 3.5 ha cultivating coffee (*Coffea arabica* L.), cultivar Catucaí red IAC 144, aging 6 years old, spaced by 3.5 m between lines and 0.5 m between plants, resulting in 5,700 plants ha<sup>-1</sup>.

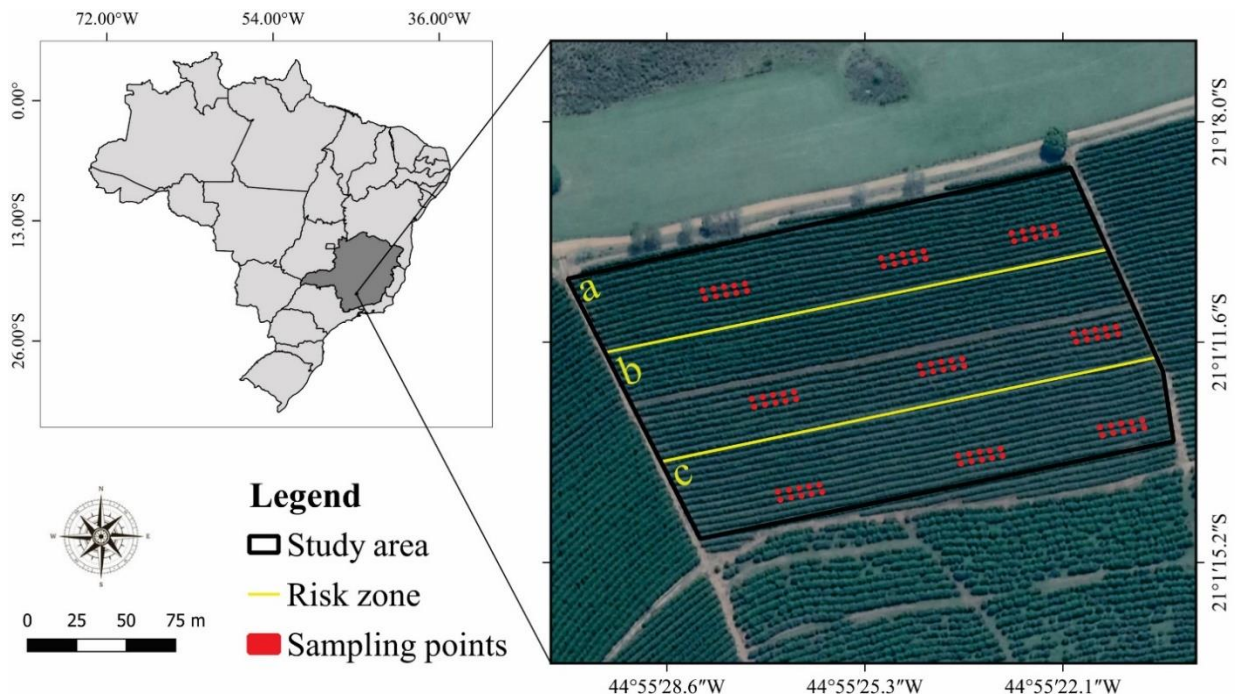


**Fig. 1** Geographical location of the study area. The sampling points are highlighted in red points and the climatic favorability zones were separated in yellow lines, where a: High risk, b: Medium Risk, and c: Low Risk

Frost occurrence was observed on July 8th and 9th of 2019. The minimum temperatures on those days were 1.8 and 0.3 °C, respectively. Temperature data were collected from an

automatic weather station, located within the coffee farm Bom Jardim. During the winter, the occurrence of extremely low temperatures is a considerable limitation for agriculture, especially for coffee, in the southern region of Minas Gerais. Temperatures there often reach 0 °C, and sometimes, below zero, enabling frost formation and consequently damage to the coffee plants. Furthermore, due to the topographic conditions, frost formation is favored because this region has places with high altitudes and lower flat terrain (lowlands).

### **Frost risk area classification**

To evaluate the effects of frosting in coffee plants, the study area was divided into three distinct areas of climate risk from frost damage. The criteria used were altitude variability and geographical configuration of the terrain. The areas were classified as low, medium, and high climate risk for frost occurrence (Fig. 1). The classification of the study area into three different risk zones was due to the need to understand factors related to climate favorability and to help the coffee producers in decision-making for reducing frost damage before it occurs.

Also, the classification in different risk zones was carried out before the data analysis because the authors aimed to understand and recommend alternatives to reduce possible frost damage. If the coffee producer knows possible plantation areas that present climatic favorability for frost occurrence, he can use strategies to minimize the damage, which would not be possible with the classification of the area after the analysis of the results.

### **Canopy stratification**

The determination of frost damage and chlorophyll content was carried out for each coffee canopy strata. The sampled plants were divided into three canopy sections of similar size to individually analyze the contribution of each canopy strata, according to the location of their vegetative and reproductive structures. The criterion used for sectioning the plant canopy was that to constitute the lower stratum, the plant structures should be located from 0 % to 33 % of the height of the plants, the middle stratum of 33.34 % to 66.66 %, and the upper stratum of 66.67 % to 100 %, respectively.

To analyze the hypothesis that the most significant damage occurred in the upper stratum of the coffee plants, the evaluation of different strata was carried out using vegetation indices obtained by the UAV.

### Visual frost damage evaluation

Using a standard scale described in Table 1, based on the percentage of the plant showing frost damage, a visual evaluation was conducted in the coffee plants, including leaves, branches, stem, and fruits on July 11, 2019. The authors considered as frost damage the plant parts that presented brown color and necrosis since that is the aspect caused by cell death by freezing.

**Table 1** Classification index and description for assessing frost damage in coffee plants

Damage index	Description
0	No visible damage, %
1	10*
2	20
3	30
4	40
5	50
6	60
7	70
8	80
9	90
10	100

\*% of the plant with visible damage; frost damage in this study was characterized as damage (cell death by necrosis) caused by the effect of frost on the plant parts (leaf, branch, stem, and fruit).

The visual evaluation was carried out in the three different climatic favorability areas and in the different plant strata. To perform the evaluation, three blocks were separated in each climatic favorability area. For each block, 10 plants were selected for evaluation, considering 5 plants of each line. In this context, 30 plants in each risk area were evaluated, resulting in 90 plants data for analysis. The sampling site was chosen, aiming to achieve greater possible representation and homogeneity of the plants in each plot. The location of the selected plants is indicated in Figure 1.

In this system of evaluation, grades from 0 to 10 were assigned to the different strata of the plant (Table 1). Three experienced observers performed the visual assessment of the frost damage. The end value attributed to the data analysis was the average of the three observer's values.

## Evaluation of chlorophyll content

Measurements were made with the atLEAF+ chlorophyll meter (FT Green LLC, Wilmington, DE, USA) by clipping the sensor onto the coffee leaf. The measurement area of the sensor atLEAF+ was 6 mm<sup>2</sup>. All of the measurements were conducted in the morning period, from 9 to 10 am on July 11, 2019, to avoid sunlight interference. In each plant, 15 measurements were conducted, divided into 5 for each stratum. The measurements were conducted in representative leaves of each stratum. To perform the measurement, leaves positioned on the third and fourth pair from the top of the plant were selected. Once the measurement was read, the equations developed and described by Padilha et. al. (2018) were used to estimate the chlorophyll a and chlorophyll b content in mg cm<sup>-2</sup>.

$$\text{Total Chlorophyll} = 0.078 \times \text{atLEAF}^{1.63} \quad (1)$$

$$\text{Chlorophyll a} = -5.774 + 0.430 \times \text{atLEAF} + 0.0045 \times \text{atLEAF}^2 \quad (2)$$

$$\text{Chlorophyll b} = 0.040 \times \text{atLEAF}^{1.57} \quad (3)$$

where atLEAF is the value measured by the sensor.

## Acquisition of multispectral images

The commercial UAV 3DR Solo (3D Robotics, Berkeley, CA, USA) was used to collect the multispectral images on July 11, 2019, 2 days after the frost occurrence. The UAV had rotating wings and four motors (quadcopter), driven by the automatic pilot system 3DR Pixhawk 2, and flight controller APM: Copter (Duffy et al. 2018) (Fig. 2a). The UAV was equipped with a multispectral camera Parrot Sequoia (MicaSense, Seattle, WA, USA) (Fig. 2b), comprising four spectral sensors, 1.5 megapixels resolution (1280 x 960), spectral bands of green (530–570 nm), red (640–680 nm), red-edge (730–740 nm) and near-infrared (770–810 nm). This camera was used to map and monitor vegetation. It includes a sunshine sensor (Fig. 2c) pointing upwards, that allowed radiometric calibration during image collection (MicaSense Sequoia, 2018). Additionally, to transform digital numbers (gray levels) from sensors to reflectance values, a calibrated reflectance panel (MicaSense, Seattle, WA, USA) (Fig. 2d) was used before and after the flight (Freitas et al. 2019).

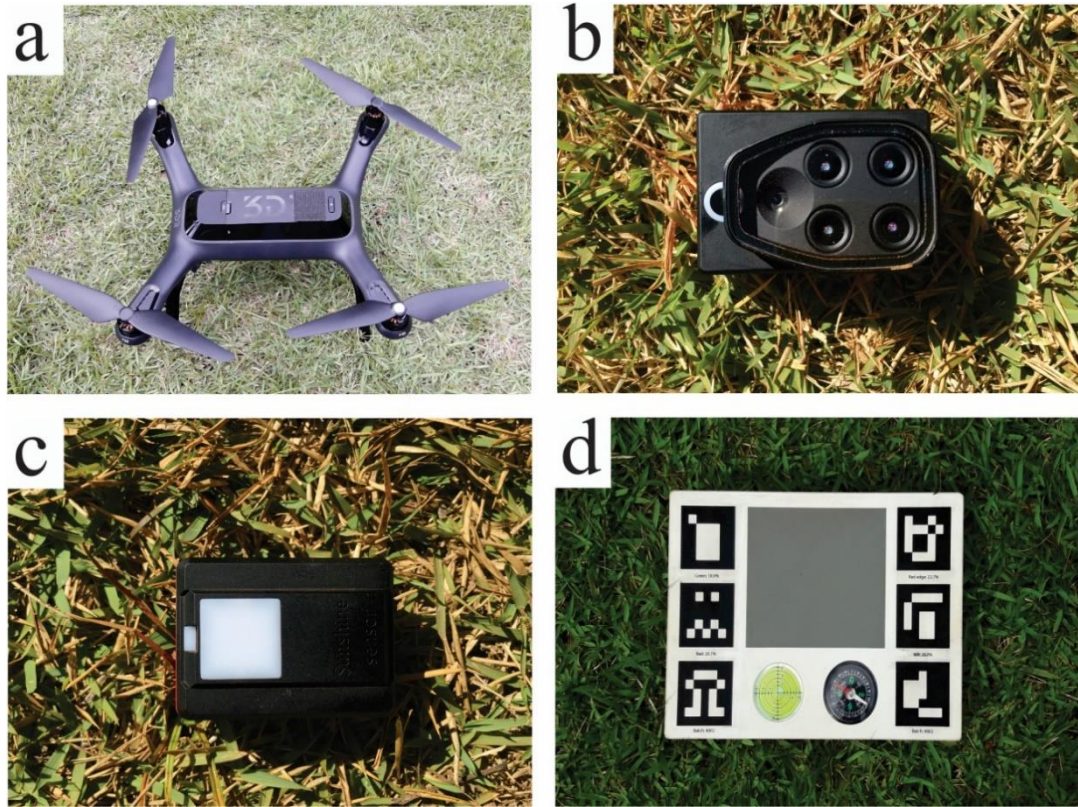


**Fig. 2** (a) UAV 3DR Solo; (b) Multispectral Parrot Sequoia camera; (c) Sunshine sensor; (d) Calibrated reflectance panel

The 3DR Solo is capable of performing flights being remotely controlled or autonomously while using a global navigation satellite system (GNSS) and a navigation system by waypoint. For this study, the flights were operated autonomously. The flight missions were planned using the Mission Planner (Osborne, 2018), a complete and open source ground station software for UAV autopilot systems (Lu et al. 2016), running on a portable computer. The flight altitude was fixed at 60 m from the ground, and the speed was  $3 \text{ m}\cdot\text{s}^{-1}$ . The images were captured at every 1 s, with a frontal and lateral overlap of 80%, resulting in a total of 150 images with a spatial resolution of 64.4 mm.

### Image processing

The image processing was performed by the software Pix4Dmapper, version 4.4.12 (Pix4D, Lausanne, Switzerland). This software contains computational vision technics that allow photogrammetry algorithms that obtain high precision processing in aerial images (Ruzgienė et al. 2015). The standard template "Ag Multispectral" from Pix4Dmapper was used to generate the orthomosaics from individual spectral bands (green, red, red-edge, and near-

infrared). To improve the precision and the accuracy of the orthomosaics, the images were georeferenced using control points collected previously in the field area by a differential GNSS (Trimble Navigation Limited, Sunnyvale, California, USA) spectra precision model SP 60 with a horizontal and vertical accuracy of 0.07 m. Additionally, the calibrated reflectance panel corrected the reflectance of the images. After generating the orthomosaics, the vegetation indices were calculated using the Pix4D and exported to the TIFF extension for later analysis. For that, the average value extracted from the pixels in a 0.20 m radius was calculated from the center of each plant sampled, using the Zonal Statistics resource available on the QGIS 2.18.13 (QGIS Development Team, 2017).

### **Vegetation indices**

Based on the literature, there are no studies applying vegetation indices to evaluate the damage caused by frost in coffee plants. However, for choosing vegetation indices, a literature revision was made to identify the indices capable of differentiating characteristics from stress conditions in coffee plants, and with the capacity to evaluate the spectral response of the plants due to frost damage. After this revision, the vegetation indices chosen were the ones that had two characteristics at the same time, that is the capacity to assess the stress conditions of the coffee plants and the spectral response of the plants after frost damage (Table 2).



**Table 2** Vegetation indices of multispectral images obtained using UAV.

Vegetation indices	Calculation	Reference
NDVI (normalized difference vegetation index)	$\frac{\rho_{nir} - \rho_{red}}{\rho_{nir} + \rho_{red}}$	Rouse et al. (1974)
MSR (modified simple ratio)	$\frac{\left(\frac{\rho_{nir}}{\rho_{red}}\right) - 1}{\sqrt{\left(\frac{\rho_{nir}}{\rho_{red}}\right) + 1}}$	Chen (1996)
SAVI (soil adjusted difference vegetation index)	$\frac{(1+L)\rho_{nir} - \rho_{red}}{\rho_{nir} + \rho_{red} + L}$	Huete (1988)
GNDVI (green normalized difference vegetation index)	$\frac{\rho_{nir} - \rho_{green}}{\rho_{nir} + \rho_{green}}$	Gitelson et al. (1996)
MTCI (terrestrial chlorophyll index)	$\frac{\rho_{nir} - \rho_{edge}}{\rho_{edge} + \rho_{red}}$	Dash and Curran (2004)
NDRE (normalized difference red edge)	$\frac{\rho_{nir} - \rho_{edge}}{\rho_{nir} + \rho_{edge}}$	Gitelson and Merzlyak (1994)
NDI (normalized different index)	$\frac{\rho_{green} - \rho_{red}}{\rho_{green} + \rho_{red} + 0.01}$	Mao et al. (2003)
MPRI (modified photochemical reflectance index)	$\frac{\rho_{green} - \rho_{red}}{\rho_{green} + \rho_{red}}$	Yang et al. (2008)
MCARI1 (first modified chlorophyll absorption ratio index)	$1.2[2.5(\rho_{nir} - \rho_{red}) - 1.3((\rho_{nir} - \rho_{green}))]$	Haboudane et al. (2004)

$\rho_{green}$ : green band reflectance;  $\rho_{red}$ : red band reflectance;  $\rho_{edge}$ : red-edge band reflectance;  $\rho_{nir}$ : near-infrared band reflectance.

### Statistics analysis

The statistical analysis was performed on the software R version 3.4 (R Core Team 2017). The significant differences in the frost damage analysis and the chlorophyll content in the climatic favorability zones were measured by the Tukey test ( $p < 0.05$ ). To evaluate the linear relation between the vegetation indices and the occurrence of frost in the upper stratum of the plants, and in the whole plant, the respective data sets were subjected to Pearson's correlation ( $r$ ) analysis ( $p < 0.01$ ) and coefficient of determination ( $R^2$ ). The average values for vegetation indices were obtained from the present pixels in a 0.20 m radius from the center of each plant.

To value the performance of the vegetation indices on the estimation of the damage caused by frost in coffee plants, the following statistical indices were applied: mean absolute error (MAE) (Eq. 4), root mean square error (RMSE) (Eq. 5), and index of agreement (d) (Eq. 6).

$$MAE = \frac{1}{n} \sum_{i=1}^n |P_i - O_i|$$

(4)

$$RMSE = \sqrt{\frac{1}{n} \sum_{i=1}^n (P_i - O_i)^2}$$

(5)

$$d = 1 - \left[ \frac{\sum_{i=1}^n (P_i - O_i)^2}{\sum_{i=1}^n (|P_i| + |O_i|)^2} \right]$$

(6)

Where, n is the number of observations,  $P_i$  the predicted observation based on the linear regression model,  $O_i$  is a measured observation,  $P'_i = P_i - M$  and  $O'_i = O_i - M$  (M is the mean of the observed variable).

## Results and discussion

### Frost damage in different coffee canopy strata

The coffee plants evaluated in the low climate risk areas did not show frost damage for any stratum of the plant (Table 3). This indicates a significant interference of the topography in the favorability for frost occurrence since, in the other evaluated areas, the effect of frost was observed, mainly in the upper stratum of the plants.

**Table 3** Frost damage (FD) and standard deviation (SD) in different coffee canopy strata and whole plant at different climatic favorability zones in the studied area.

Coffee canopy	Climatic favorability zones					
	Low		Average		High	
	FD (%)	SD	FD (%)	SD	FD (%)	SD
Lower	0 b*	± 0	3 b	± 0.29	14 a	± 2.25
Middle	0 c	± 0	11 b	± 1.74	43 a	± 4.92
Upper	0 c	± 0	30 b	± 5.8	78 a	± 8.45
Whole plant	0 c	-	15 b	-	45 a	-

\*Different small letters indicate significant differences ( $p < 0.05$ ) by Tukey test among climatic favorability zones for each coffee canopy strata and whole plant.

Significant differences for frost damage in coffee plants were observed among the climatic risk zones. The higher frost damage value was observed in the upper canopy stratum that was located in the high climate risk zone for frost occurrence. The coffee evaluated in the average climate risk zone showed higher values than the low climatic risk for the middle and upper canopy stratum. When combined with the whole plant, the average damage caused by frost in the areas of high, medium, and lower climatic favorability was 45, 15, and 0% respectively.

The frost damage in the upper stratum of the plant can have a significant effect on the coffee production, reducing the leaf area and, consequently, the photosynthetic activity, compromising the accumulation of dry matter, decreasing productivity in the current harvest and during the next cycles of the crop (DaMatta & Ramalho 2006).

Being aware of the damage caused by frost is essential for coffee producers to assist in decision-making and agricultural planning. For example, in the high climatic risk areas, plants have shown 45% of the leaf area damaged. In this case, the producer could decide to perform a drastic pruning on the plants. Also, according to the results of this study, the most damaged area in the plant was the upper stratum. In this case, the producer could perform the pruning only in that region of the plant, exposing the less damaged leaves.

The establishment of risk zones for frost occurrence and coffee leaf damage is an important step towards an integrated management plan for these events. The identification and classification of zones of greater or lesser climatic favorability are important for the coffee

producers, for them to perform appropriate management in the production area, considering, for example, the topography and the areas where cold air accumulates. Because of the effects of land surface heterogeneity on spatial variation of near-surface temperatures, the spatial occurrence of frost can be linked to land surface characteristics (Kotikot et al. 2020). Of most importance is the concept of cold air pooling where cold dense air flows downslope and settles beneath warmer air (Kotikot et al. 2020). For this reason, low temperatures and therefore frost zones tend to accumulate in low regions of the landscape (Bigg et al. 2014; Chung et al. 2006). In this context, the information generated in this study can help coffee producers to avoid the use of susceptible cultivars in those zones where frost occurrence poses the greatest risk, and to optimize strategies for reducing the damage by frost in coffee plants.

When analyzing the chlorophyll content in the different canopy strata and climatic risk zones (Table 4), it is possible to observe a little variation in the chlorophyll a, b, and total content for middle and lower strata, regardless of the climate risk zone. However, for the upper stratum of the coffee plants, the content of chlorophyll a, b, and total were higher for the area of lower climate risk. Considering the total value of chlorophyll (a + b), a significant reduction in the medium and high-risk zones was observed when comparing it to the low-risk zone of climate favorability.

**Table 4** Chlorophyll index (a, b, and total) and standard deviation (SD) in different coffee canopy strata and whole plant at different climatic favorability zones in the studied area.

Coffee canopy	Climatic favorability zones					
	Low		Average		High	
	Chlorophyll a					
	CA ( $\mu\text{g cm}^{-2}$ )	SD	CA ( $\mu\text{g cm}^{-2}$ )	SD	CA ( $\mu\text{g cm}^{-2}$ )	SD
Lower	39.48 a*	$\pm 1.4$	36.69 a	$\pm 1.9$	40.21 a	$\pm 0.6$
Middle	40.16 a	$\pm 2.4$	37.73 a	$\pm 3.3$	36.17 b	$\pm 0.5$
Upper	46.41 a	$\pm 2.7$	32.8 b	$\pm 5.1$	21.39 c	$\pm 1.4$
Whole plant	42.02 a	$\pm 1.5$	35.74 b	$\pm 3.4$	32.59 b	$\pm 0.5$
Coffee canopy	Chlorophyll b					
	CB ( $\mu\text{g cm}^{-2}$ )		CB ( $\mu\text{g cm}^{-2}$ )		CB ( $\mu\text{g cm}^{-2}$ )	
	SD	SD	SD	SD	SD	SD
Lower	26.93 a	$\pm 0.9$	25.07 a	$\pm 1.3$	27.42 a	$\pm 0.4$
Middle	27.39 a	$\pm 1.8$	25.77 a	$\pm 2.2$	24.72 a	$\pm 0.3$
Upper	31.56 a	$\pm 1.6$	22.48 b	$\pm 3.4$	14.91 c	$\pm 0.9$
Whole plant	28.63 a	$\pm 1.1$	24.44 ab	$\pm 2.3$	22.35 b	$\pm 0.3$
Coffee canopy	Total Chlorophyll					
	CT ( $\mu\text{g cm}^{-2}$ )		CT ( $\mu\text{g cm}^{-2}$ )		CT ( $\mu\text{g cm}^{-2}$ )	
	SD	SD	SD	SD	SD	SD
Lower	66.41 a	$\pm 2.3$	61.76 a	$\pm 2.2$	67.63 a	$\pm 1.0$
Middle	67.55 a	$\pm 4.0$	63.5 ab	$\pm 5.5$	60.89 b	$\pm 0.8$
Upper	77.98 a	$\pm 4.3$	55.28 b	$\pm 8.5$	36.3 c	$\pm 2.3$
Whole plant	70.65 a	$\pm 2.7$	60.18 b	$\pm 5.7$	54.94 c	$\pm 0.8$

\*Different small letters indicate significant differences ( $p < 0.05$ ) by Tukey test among climatic favorability zones for each coffee canopy strata and whole plant.

The response observed in the chlorophyll content follows the same pattern seen in the results reported on frost damage, shown in Table 3, where the upper stratum has presented greater frost damage and lower chlorophyll content. It is important to highlight that the reduction in the chlorophyll content of coffee leaves is due to the damage caused by frosting. In cases of extreme temperatures, such as frost occurrence, the degradation of chlorophyll is associated with the structural changes that release cellular acids and various degradative enzymes (Hodges & Forney 2000). Therefore, the reduction of the chlorophyll content in coffee plants due to frosting, mainly in the upper stratum, significantly impacts the photosynthetic efficiency, and in the productivity of the plant. In this sense, the two variables are associated, being the visual damage observed and reduction of the chlorophyll content.

### Spatial distribution of vegetation indices

The spatial distribution of the vegetation indices in the study area can be seen in Figure 3. The maps of NDVI, MSR, NDI, and MPRI have shown the lower values in the high climatic favorability area of the crop, and the greater values in low-risk areas, evidencing the effect of relief in the frost occurrence. According to Caramori et al. (2001), the crops located in lowlands and terrains with concave configuration and small slopes have a higher probability of frost occurrence. As for the indices GNDVI, SAVI, MTCI, NDRE, and MCARI1, the spatial distribution made it difficult to identify and map the effect of frost in the coffee plants.

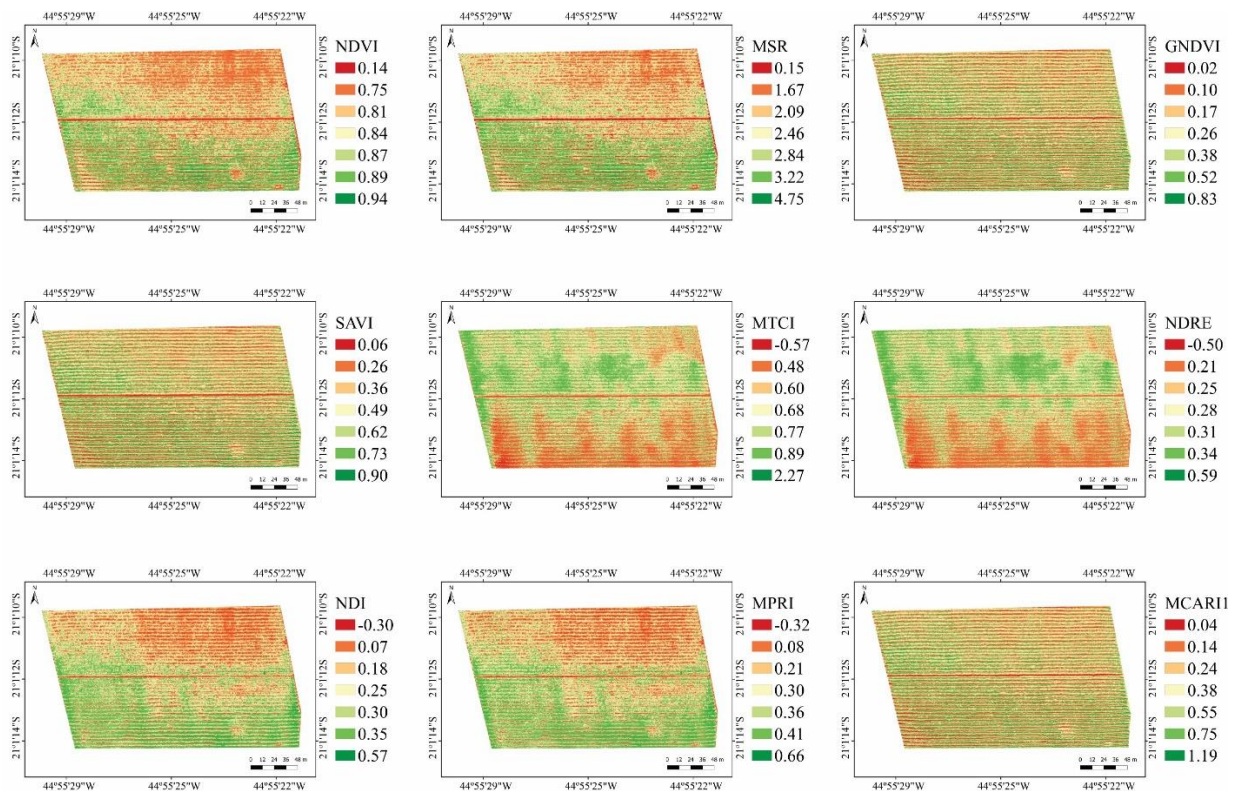


**Fig. 3** Spatial distribution of vegetation indices in the study area

Knowledge of the characteristics and spatial distribution of the frosting effect on the coffee crop is highly applicable in the orientation of extension workers in the field, governmental agencies, and agricultural producers to support decision-making regarding the management of the coffee crop. This is more emphasized by the fact that one of the effects of frosting in coffee plants is a reduction in the productivity of the crop (Carvalho et al. 2017). Therefore, the vegetation indices can quickly, precisely, and continuously indicate areas of the crop that need lighter or drastic pruning, or even dispense with pruning. Besides that, in severe

cases, it can be a useful tool to assist the application of agricultural insurance to compensate for losses. In this context, Rafaelli et al. (2006) have successfully demonstrated the potential of the NDVI index, obtained with MODIS sensor images, for monitoring coffee crops affected by frosting at a state scale, for the state of Paraná, in the South of Brazil.

However, orbital sensors like MODIS show limitations that make it difficult to monitor and evaluate the frosting effect continuously at local scales. Those limitations include low spatial resolution (250 to 500m) that can be influenced by other spectral targets compromising its accuracy (Ke et al. 2016; Feng et al. 2017). A potential solution for this problem is high spatial resolution satellites, even though, the acquisition of data from them is expensive and limited due to cloudiness (Hellweger et al. 2007; Müllerová et al. 2017), which is not ideal for analyzing the effect of frost in coffee plants. When working with vegetation indices obtained from UAVs, those limitations are reduced, since the images can be captured continuously and with high spatial resolution, decreasing the interference of other spectral targets present in the crop.

### **Evaluation of the estimative of frost damage generated by vegetation indexes**

The results of the performance evaluation of the vegetation indices on estimating the frost damage in the upper stratum of coffee plants are shown in Table 5. It was possible to observe that the occurrence of frost in the upper stratum and the whole plant presented similar correlation coefficients with the vegetation indices, validating the hypothesis that the evaluation of the upper stratum is enough to measure the frost damage when using images captured by UAVs.

**Table 5** Statistics indexes between frost damage and vegetation indices

Vegetation Indice	Whole plant				
	MAE*	RMSE	d	R <sup>2</sup>	r
NDVI	13.66	16.72	0.87	0.72	-0.85
MSR	14.01	16.99	0.86	0.69	-0.83
GNDVI	21.21	25.99	0.79	0.38	-0.62
SAVI	19.88	23.51	0.81	0.42	-0.65
MTCI	27.99	31.54	0.73	0.20	0.45
NDRE	28.09	32.11	0.73	0.19	0.44
NDI	14.13	17.08	0.85	0.66	-0.81
MPRI	14.14	17.10	0.85	0.66	-0.81
MCARI1	23.57	27.77	0.77	0.29	-0.54
Vegetation Indice	Upper stratum				
	MAE	RMSE	d	R <sup>2</sup>	r
NDVI	10.87	14.35	0.89	0.79	-0.89
MSR	11.01	14.70	0.88	0.77	-0.88
GNDVI	19.92	23.67	0.82	0.46	-0.68
SAVI	17.45	21.89	0.83	0.55	-0.74
MTCI	25.31	28.84	0.76	0.26	0.51
NDRE	27.93	31.50	0.73	0.20	0.45
NDI	13.95	16.92	0.86	0.69	-0.83
MPRI	13.88	16.82	0.87	0.70	-0.84
MCARI1	25.36	28.80	0.76	0.26	-0.51

\*Statistics indices: MAE (Mean absolute error), RMSE (Root mean square error), d (Index of Agreement), R<sup>2</sup> (determination coefficient), and r (correlation coefficient).

The correlation coefficients (r) and the determination coefficients (R<sup>2</sup>) have shown strong relationships to vegetation indices and frost damage. Regarding the accuracy, most of the vegetation indices have presented MAE and RMSE values between 10% to 20%, evidencing the potential of the vegetation indices in evaluating damage by frost. According to Jamieson et al. (1991), the model is considered excellent if the normalized RMSE is inferior to 10%, good if the normalized RMSE is between 10 and 20%, fair if the normalized RMSE is greater than 20 but inferior to 30%, and bad if the normalized RMSE is greater than 30%. Besides that, the values of the index of agreement (d) between 0.73 to 0.89 confirm the quality of the model, because the (d) represents the ratio between the squared average error and the potential error, where the concordance value equals 1 indicates the perfect combination (Willmott, 1981).

In general, the vegetation indices NDVI and MSR, which are indices that use the combination of near-infrared reflectance with the red reflectance, showed better performance in estimating the damage caused by frost in coffee plants. On the other hand, the indices



GNDVI, SAVI, MTCI, and NDRE, which combine the near-infrared reflectance with the green and red-edge reflectance, showed the worst performance. The NDI and MPRI indices that use reflectance of the green and red wavelengths, showed performance close to the best ones (NDVI and MSI), demonstrating that the visible spectral region is directly related to the frost damage in the coffee plants.

The best performance for indices that used the red wavelength can be associated with the color change in the leaves due to the frosting. According to Larcher (1981), frost causes the death of vegetation tissue by a physical-chemical process. The results of these processes are dehydration of the cell, loss of turgor potential, increase of solute concentration, reduction of cellular volume, and rupture of the plasmatic membrane. Thus, the leaves become dark brown colored, with a burning aspect.

Although these indices presented the best performance, better results were expected for indices that use green and red-edge wavelengths, since these wavelengths are directly related to the chlorophyll content in leaves damaged by frosting (Table 4). This relationship is in line with other studies that have shown that the chlorophyll content is significantly correlated to the green and red-edge wavelengths (Li et al. 2007; Devadas et al. 2009).

It is worth mentioning that the NDI and MPRI are indices that use only visible wavelengths, showed elevated performance and results, close to the vegetation indices with the best results (NDVI and MSR). Because of that, RGB cameras have become an interesting alternative for producers, being easier to operate and lower cost compared to multispectral cameras. They also require little data processing and present reliable results (Barbosa et al. 2019; Svensgaard et al. 2019). As in this study, Nuttall et al. (2019) also observed that RGB vegetation indices are reliable in evaluating the damage caused by frost. However, NDVI still stands as more efficient to map, monitor, and identify damage in plants provoked by frosting (Rafaelli et al. 2006; Feng et al. 2009; Wei et al. 2017).

## **Conclusion**

The multispectral images obtained using UAV can provide for the coffee producers a fast, continuous and accessible method to identify and evaluate frost damage in coffee plants, confirming the hypothesis of this study. Specifically, the NDVI and MSR (indices that use the combination of near-infrared and red spectral bands) have shown better results. Otherwise, the indices MTCI and NDRE which use the red-edge band showed the worst results. The spatial distribution of the vegetation indices indicated that the topography is directly related to the frost

occurrence in the coffee plantation. Greatest damage and lower chlorophyll a and b content were observed in areas with greater climatic risk (lowlands) for the upper strata of the plant.

Due to climate change and its consequences, extreme events are becoming more frequent, making it even more essential to comprehend the physiological response of coffee plants after frosting. Therefore, other research using UAVs with greater autonomy and other sensors can contribute even more to the understanding of this relationship, as well as assisting producers on how to manage their crops.

### **Acknowledgements**

This work was supported by the Embrapa Café—Consórcio Pesquisa Café, project approved in the call n° 20/2018, the National Council for Scientific and Technological Development (CNPq), the Coordination for the Improvement of Higher Education Personnel (CAPES), the Federal University of Lavras (UFLA) and farm Bom Jardim.

### **Conflict of interest**

The authors declare that they have no conflict of interest.

### **References**

- Barbosa, B. D. S., Ferraz, G. A. S., Santos, L. M., Marin, D. B., Maciel, D. T., Ferraz, P. F. P., et al. (2019). RGB vegetation indices applied to grass monitoring: a qualitative analysis. *Agronomy Research*, 17(2), 349–357. <https://doi.org/10.15159/ar.19.119>.
- Bigg, G. R., Wise, S. M., Hanna, E., Mansell, D., Bryant, R. G., & Howard, A. (2014). Synoptic climatology of cold air drainage in the Derwent Valley, Peak District, UK. *Meteorological Applications*, 21(2), 161–170. <https://doi.org/10.1002/met.1317>.
- Camargo, M. B. P. D. (2010). The impact of climatic variability and climate change on Arabic coffee crop in Brazil. *Bragantia*, 69(1), 239–247. <http://dx.doi.org/10.1590/S0006-87052010000100030>.
- Caramori, P. H., Caviglione, J. H., Wrege, M. S., Gonçalves, S. L., Faria, R. T., Filho, A. A., et al. (2001). Climatic risk zoning for coffee (*Coffea arabica* L.) in Paraná state, Brazil. *Revista Brasileira de Agrometeorologia*, 9(3), 486–494.

- Carvalho, L. C., Silva, F. M. D., Ferraz, G. A., Stracieri, J., Ferraz, P. F., & Ambrosano, L. (2017). Geostatistical analysis of Arabic coffee yield in two crop seasons. *Revista Brasileira de Engenharia Agrícola e Ambiental*, 21(6), 410–414. <http://dx.doi.org/10.1590/1807-1929/agriambi.v21n6p410-414>.
- Chen, J. M. (1996). Evaluation of vegetation indices and a modified simple ratio for boreal applications. *Canadian Journal of Remote Sensing*, 22(3), 229–242. <https://doi.org/10.1080/07038992.1996.10855178>.
- Chung, U., Seo, H. H., Hwang, K. H., Hwang, B. S., Choi, J., Lee, J. T., & Yun, J. I. (2006). Minimum temperature mapping over complex terrain by estimating cold air accumulation potential. *Agricultural and Forest Meteorology*, 137(1–2), 15–24. <https://doi.org/10.1016/j.agrformet.2005.12.011>.
- DaMatta, F. M., & Ramalho, J. D. C. (2006). Impacts of drought and temperature stress on coffee physiology and production: a review. *Brazilian Journal of Plant Physiology*, 18(1), 55–81. <http://dx.doi.org/10.1590/S1677-04202006000100006>.
- Dash, J., & Curran, P. J. (2004). The MERIS terrestrial chlorophyll index. *International Journal of Remote Sensing*, 25(23), 5403–5413. <https://doi.org/10.1080/0143116042000274015>.
- Devadas, R., Lamb, D. W., Simpfendorfer, S., & Backhouse, D. (2009). Evaluating ten spectral vegetation indices for identifying rust infection in individual wheat leaves. *Precision Agriculture*, 10(6), 459–470. <https://doi.org/10.1007/s11119-008-9100-2>.
- Duffy, J. P., Pratt, L., Anderson, K., Land, P. E., & Shutler, J. D. (2018). Spatial assessment of intertidal seagrass meadows using optical imaging systems and a lightweight drone. *Estuarine, Coastal and Shelf Science*, 200, 169–180. <https://doi.org/10.1016/j.ecss.2017.11.001>.
- Feng, G., Anderson, M. C., Zhang, X., Yang, Z., Alfieri, J. G., Kustas, W. P., et al. (2017). Toward mapping crop progress at field scales through fusion of Landsat and MODIS imagery. *Remote Sensing of Environment*, 188, 9–25. <https://doi.org/10.1016/j.rse.2016.11.004>.
- Feng, M. C., Yang, W. D., Cao, L. L., & Ding, G. W. (2009). Monitoring winter wheat freeze injury using multi-temporal MODIS data. *Agricultural Sciences in China*, 8(9), 1053–1062. [https://doi.org/10.1016/S1671-2927\(08\)60313-2](https://doi.org/10.1016/S1671-2927(08)60313-2).
- Feng, M., Guo, X., Wang, C., Yang, W., Shi, C., Ding, G., et al. (2018). Monitoring and evaluation in freeze stress of winter wheat (*Triticum aestivum* L.) through canopy hyperspectrum reflectance and multiple statistical analysis. *Ecological indicators*, 84, 290–297. <https://doi.org/10.1016/j.ecolind.2017.08.059>.

- Freitas, P., Vieira, G., Canário, J., Folhas, D., & Vincent, W. F. (2019). Identification of a threshold minimum area for reflectance retrieval from thermokarst lakes and ponds using full-pixel data from Sentinel-2. *Remote Sensing*, 11(6), 657. <https://doi.org/10.3390/rs11060657>.
- Gitelson, A. A., Kaufman, Y. J., & Merzlyak, M. N. (1996). Use of a green channel in remote sensing of global vegetation from EOS-MODIS. *Remote sensing of Environment*, 58(3), 289–298. [https://doi.org/10.1016/S0034-4257\(96\)00072-7](https://doi.org/10.1016/S0034-4257(96)00072-7).
- Gitelson, A., & Merzlyak, M. N. (1994). Quantitative estimation of chlorophyll-a using reflectance spectra: Experiments with autumn chestnut and maple leaves. *Journal of Photochemistry and Photobiology B: Biology*, 22(3), 247–252. [https://doi.org/10.1016/1011-1344\(93\)06963-4](https://doi.org/10.1016/1011-1344(93)06963-4).
- Gobbett, D. L., Nidumolu, U., & Crimp, S. (2018). Modelling frost generates insights for managing risk of minimum temperature extremes. *Weather and Climate Extremes*, 100176. <https://doi.org/10.1016/j.wace.2018.06.003>.
- Haboudane, D., Miller, J. R., Pattey, E., Zarco-Tejada, P. J., & Strachan, I. B. (2004). Hyperspectral vegetation indices and novel algorithms for predicting green LAI of crop canopies: Modeling and validation in the context of precision agriculture. *Remote Sensing of Environment*, 90(3), 337–352. <https://doi.org/10.1016/j.rse.2003.12.013>.
- Hellweger, F.L., Miller, W., & Oshodi, K.S. (2007). Mapping turbidity in the Charles River, Boston using a high-resolution satellite. *Environmental monitoring and assessment*, 132(1-3), 311–320. <https://doi.org/10.1007/s10661-006-9535-8>
- Hodges, D. M., & Forney, C. F. (2000). The effects of ethylene, depressed oxygen and elevated carbon dioxide on antioxidant profiles of senescing spinach leaves. *Journal of Experimental Botany*, 51(344), 645–655. <https://doi.org/10.1093/jexbot/51.344.645>.
- Huete, A. R. (1988). A soil-adjusted vegetation index (SAVI). *Remote Sensing of Environment*, 25(3), 295–309. [https://doi.org/10.1016/0034-4257\(88\)90106-X](https://doi.org/10.1016/0034-4257(88)90106-X).
- Jamieson, P. D., Porter, J. R., & Wilson, D. R. (1991). A test of the computer simulation model ARCWHEAT1 on wheat crops grown in New Zealand. *Field crops research*, 27(4), 337–350. [https://doi.org/10.1016/0378-4290\(91\)90040-3](https://doi.org/10.1016/0378-4290(91)90040-3).
- Ke, Y., Im, J., Park, S., & Gong, H. (2016). Downscaling of MODIS One kilometer evapotranspiration using Landsat-8 data and machine learning approaches. *Remote Sensing*, 8(3), 215. <https://doi.org/10.3390/rs8030215>.

- Kotikot, S. M., & Onywere, S. M. (2014). Application of GIS and remote sensing techniques in frost risk mapping for mitigating agricultural losses in the Aberdare ecosystem, Kenya. *Geocarto International*, 30, 104–121. <http://dx.doi.org/10.1080/10106049.2014.965758>.
- Kotikot, S. M., Flores, A., Griffin, R. E., Nyaga, J., Case, J. L., Mugo, R., et al. (2020). Statistical characterization of frost zones: Case of tea freeze damage in the Kenyan highlands. *International Journal of Applied Earth Observation and Geoinformation*, 84, 101971. <https://doi.org/10.1016/j.jag.2019.101971>.
- Larcher, W. (1981). Effects of low temperature stress and frost injury on plant productivity. In Johnson C. B. (Ed.), *Physiological Processes Limiting Plant Productivity*, (pp. 253-269). London, UK: Butterworths
- Li, X. Y., Liu, G. S., Yang, Y. F., Zhao, C. H., Yu, Q. W., & Song, S. X. (2007). Relationship between hyperspectral parameters and physiological and biochemical indexes of flue-cured tobacco leaves. *Agricultural Sciences in China*, 6(6), 665–672. [https://doi.org/10.1016/S1671-2927\(07\)60098-4](https://doi.org/10.1016/S1671-2927(07)60098-4).
- Lou, W., Ji, Z., Sun, K., & Zhou, J. (2013). Application of remote sensing and GIS for assessing economic loss caused by frost damage to tea plantations. *Precision agriculture*, 14(6), 606–620. <https://doi.org/10.1007/s11119-013-9318-5>.
- Lu, B., He, Y., & Liu, H. (2016). Investigating species composition in a temperate grassland using Unmanned Aerial Vehicle-acquired imagery. In 2016 4th International Workshop on Earth Observation and Remote Sensing Applications (EORSA). IEEE, (pp. 107–111). <https://doi.org/10.1109/EORSA.2016.7552776>.
- Mao, W., Wang, Y., & Wang, Y. (2003). Real-time detection of between-row weeds using machine vision. Paper No. 031004, St Joseph, MI, USA: ASAE. <http://dx.doi.org/10.13031/2013.15381>.
- Marin, D. B., Alves, M. C., Pozza, E. A., Gandia, R. M., Cortez, M. L. J., & Mattioli, M. C. (2019). Multispectral remote sensing in the identification and mapping of biotic and abiotic coffee tree variables. *Revista Ceres*, 66(2), 142–153. <http://dx.doi.org/10.1590/0034-737x201966020009>.
- Martins, M. Q., Partelli, F. L., Golynski, A., Sousa Pimentel, N., Ferreira, A., Oliveira Bernardes, C., et al. (2019). Adaptability and stability of *Coffea canephora* genotypes cultivated at high altitude and subjected to low temperature during the winter. *Scientia Horticulturae*, 252, 238–242. <https://doi.org/10.1016/j.scienta.2019.03.044>.
- MicaSense Sequoia (2018). Sequoia User Guide. Drones Parrot SAS, (pp. 4-13). Paris, France. ([www.micasense.com/sequoia](http://www.micasense.com/sequoia)). Accessed 30 March 2021.

- Müllerová, J., Brůna, J., Bartaloš, T., Dvořák, P., Vítková, M., & Pyšek, P. (2017). Timing is important: unmanned aircraft vs. satellite imagery in plant invasion monitoring. *Frontiers in plant science*, 8, 887. <https://doi.org/10.3389/fpls.2017.00887>
- Nóia Júnior, R. N., Schwerz, F., Safanelli, J. L., Rodrigues, J. C., & Sentelhas, P. C. (2019). Eucalyptus rust climatic risk as affected by topography and ENSO phenomenon. *Australasian Plant Pathology*, 48(2), 131–141. <https://doi.org/10.1007/s13313-018-0608-2>.
- Nuttall, J. G., Perry, E. M., Delahunty, A. J., O'Leary, G. J., Barlow, K. M., & Wallace, A. J. (2019). Frost response in wheat and early detection using proximal sensors. *Journal of Agronomy and Crop Science*, 205(2), 220–234. <https://doi.org/10.1111/jac.12319>.
- Padilla, F.M., Souza, R., Peña, T., Gallardo, M., Gimenez, C., & Thompson, R. (2018). Different responses of various chlorophyll meters to increasing nitrogen supply in sweet pepper. *Frontiers in plant science*, 9, 1752. <https://doi.org/10.3389/fpls.2018.01752>.
- Oborne, M. (2018). Mission Planner. Available in: <http://ardupilot.org/planner/index.html>. Accessed 30 March 2021.
- QGIS Development Team (2017). QGIS Geographic Information System. Open Source Geospatial Foundation Project. Available online: <http://www.qgis.org>. Accessed 30 March 2021.
- R Development Core Team (2017). R: A Language and Environment for Statistical Computing. R Foundation for Statistical Computing, Vienna, Austria.
- Rafaelli, D. R., Moreira, M. A., & Farias, R. (2006). Analysis of the MODIS data potential to monitor (state and local level) frost impact on coffee. *Agricultura em São Paulo*, 53(1), 5–15.
- Ramalho, J. C., DaMatta, F. M., Rodrigues, A. P., Scotti-Campos, P., Pais, I., Batista-Santos, P., et al. (2014). Cold impact and acclimation response of *Coffea* spp. plants. *Theoretical and Experimental Plant Physiology*, 26(1), 5–18. <https://doi.org/10.1007/s40626-014-0001-7>.
- Rouse, J. W., Haas, R. H., Deering, D. W., Schell, J. A., & Harlan, J. C. (1974). Monitoring the Vernal Advancement and Retrogradation (Green Wave Effect) of Natural Vegetation. *Greenbelt: NASA/GSFC, Type III, Final Report*, 371p.
- Ruzgienė, B., Berteška, T., Gečyte, S., Jakubauskienė, E., & Aksamitauskas, V. Č. (2015). The surface modelling based on UAV Photogrammetry and qualitative estimation. *Measurement*, 73, 619–627. <https://doi.org/10.1016/j.measurement.2015.04.018>.

- Santos, L. M. D., Andrade, M. T., Santana, L. S., Rossi, G., Maciel, D. T., Barbosa, B. D. S., et al. (2019). Analysis of flight parameters and georeferencing of images with different control points obtained by RPA. *Agronomy Research* 17(5), 2054–2063. <https://doi.org/10.15159/ar.19.173>.
- She, B., Huang, J.F., Zhang, D.Y., & Huang, L.S. (2017). Assessing and characterizing oilseed rape freezing injury based on MODIS and MERIS data. *International Journal of Agricultural and Biological Engineering*, 10(3), 143–157.
- Svensgaard, J., Jensen, S. M., Westergaard, J. C., Nielsen, J., Christensen, S., & Rasmussen, J. (2019). Can reproducible comparisons of cereal genotypes be generated in field experiments based on UAV imagery using RGB cameras? *European Journal of Agronomy*, 106, 49–57. <https://doi.org/10.1016/j.eja.2019.03.006>.
- Tan, Z., Ding, M., Wang, L., Yang, X., & Ou, Z. (2008). Monitoring freeze injury and evaluating losingto sugarcane using RS and GPS. In *International Conference on Computer and Computing Technologies in Agriculture*, (pp. 307–316). Boston, USA: Springer.
- Wang, H., Huo, Z., Zhou, G., Wu, L., & Feng, H. (2015). Monitoring and forecasting winter wheat freeze injury and yield from multi-temporal remotely sensed data. *Intelligent Automation & Soft Computing*, 22(2), 255–260. <https://doi.org/10.1080/10798587.2015.1095475>.
- Wei, C., Huang, J., Wang, X., Blackburn, G. A., Zhang, Y., Wang, S., et al. (2017). Hyperspectral characterization of freezing injury and its biochemical impacts in oilseed rape leaves. *Remote Sensing of Environment*, 195, 56–66. <https://doi.org/10.1016/j.rse.2017.03.042>.
- Willmott, C. J. (1981). On the validation of models. *Physical Geography*, 2(2), 184–194. <https://doi.org/10.1080/02723646.1981.10642213>.
- Yang, Z., Willis, P., & Mueller, R. (2008). Impact of band-ratio enhanced AWIFS image to crop classification accuracy. In *Proceedings of the 17th William Pecora Memorial Remote Sensing Symposium*, (pp. 1–11). Bethesda, MD, USA: American Society for Photogrammetry & Remote Sensing.
- Zhang, J., Hu, J., Lian, J., Fan, Z., Ouyang, X., & Ye, W. (2016). Seeing the forest from drones: Testing the potential of lightweight drones as a tool for long-term forest monitoring. *Biological Conservation*, 198, 60–69. <https://doi.org/10.1016/j.biocon.2016.03.027>.
- Zhou, J., Pavek, M. J., Shelton, S. C., Holden, Z. J., & Sankaran, S. (2016). Aerial multispectral imaging for crop hail damage assessment in potato. *Computers and Electronics in Agriculture*, 127, 406–412. <https://doi.org/10.1016/j.compag.2016.06.019>.

### **CHAPTER III: REMOTELY PILOTED AIRCRAFT AND RANDOM FOREST IN THE EVALUATION OF THE SPATIAL VARIABILITY OF FOLIAR NITROGEN IN COFFEE CROP**

#### **This chapter is based on:**

**Marin, D. B.**, Ferraz, G. A. S., Guimarães, P. H. S., Schwerz, F., Santana, L. S., Barbosa, B. D. S., Barata, R. A. P., Faria, R.O., Dias, J.E.L., Conti, L. and Rossi, G. (2021). Remotely Piloted Aircraft and Random Forest in the Evaluation of the Spatial Variability of Foliar Nitrogen in Coffee Crop. *Remote Sensing*, 13(8), 1471. <https://doi.org/10.3390/rs13081471>.

**Abstract:** The development of approaches to determine the spatial variability of nitrogen (N) into coffee leaves is essential to increase productivity and reduce production costs and environmental impacts associated with excessive N applications. Thus, this study aimed to assess the potential of the Random Forest (RF) machine learning method applied to vegetation indices (VI) obtained from Remotely Piloted Aircraft (RPA) images to measure the N content in coffee plants. A total of 10 VI were obtained from multispectral images by a camera attached to a rotary-wing RPA. The RGB orthomosaic was used to determine sampling points at the crop area, which were ranked by N levels in the plants as deficient, critical, or sufficient. The chemical analysis of N content in the coffee leaves, as well as the VI values in sample points, were used as input parameters for the image training and its classification by the RF. The suggested model has shown global accuracy and a kappa coefficient of up to 0.91 and 0.86, respectively. The best results were achieved using the Green Normalized Difference Vegetation (GNDVI) and Green Optimized Soil Adjusted Vegetation Index (GOSAVI). In addition, the model enabled the evaluation of the spatial distribution of N in the coffee trees, as well as quantification of N deficiency in the crop for the whole area. The GNDVI and GOSAVI allowed the verification that 22% of the entire crop area had plants with N deficiency symptoms, which would result in a reduction of 78% in the amount of N applied by the producer.

**Keywords:** Machine learning; Vegetation indices; Unmanned Aerial Vehicle; Nitrogen management; RGB Camera.



## 1 Introduction

To succeed in coffee production, good fertility of the soil, along with an intense fertility care program is necessary [1]. Without the proper assessment of soil fertility, nutritional deficiencies will affect the survival and productivity of coffee plants [2,3]. Among the essential nutrients that are necessary for coffee crops, nitrogen (N) is considered the one that limits the development and productivity of the coffee [4]. The adequate administration of N promotes an increase of pairs of leaves and branches per node in the plants, which is immediately related to coffee [3]. Additionally, the N determines the plant settlement and root development, influencing numerous aspects of the plant's health [5].

Meanwhile, the proper management of N in coffee crops is still a challenging task for most producers. Cases of both excessive and deficient N application are problems in coffee production [6]. Excessive application of nitrogen fertilizers is a common practice among small and big producers, being the main cause of low-efficiency fertilization, reducing the quality of the production and lowering the profit for farmers [7,8]. Furthermore, the excess of N can cause susceptibility for plague attacks on the plants [9,10]. Environmental damage has been reported in the literature caused by leaching and volatilization of excessive N. In contrast, N deficiency causes fall of leaves, fewer leafy plants, smaller sized fruits, and drying in branches [11,12].

Consequently, to achieve satisfactory levels of N in coffee plants, producers apply nitrogen fertilizers based on a calendar or samples occasionally collected from soil and leaves for laboratory analysis [5,6]. In extreme cases of nutrient deficiency, symptoms like the yellowing of leaves start to show and are used for reactive decision-making [5,13]. However, these methods are impractical in large areas, requiring a lot of human resources, materials, sample collection, laboratory testing, and data processing [14,15]. Additionally, only a few plants are randomly sampled, making it possible that it does not represent the spatial variability properly across the crops [16]. In the long term, these methods are not suitable for balancing the nitrogen need of the coffee plants, resulting in an unstable production with productiveness deficits [5].

As an alternative to those methods, remote sensing technologies have been used to estimate nitrogen content in coffee plants. For example, [5] used vegetation indices obtained from Sentinel-2 MultiSpectral Instrument (MSI) images and machine learning to model the leaf nitrogen content in coffee bushes. The results have shown precision up to  $R^2 = 0.78$ . The study performed by [8] obtained precision up to  $R^2 = 0.81$  while estimating nitrogen levels in coffee plants for different growing stages and field conditions. However, these studies have not

explored the potential of Remotely Piloted Aircraft combined with machine learning techniques.

In the past few years, remote sensing based on Remotely Piloted Aircraft (RPA) has rapidly developed, due to its low cost, operation facility, and wide field of view [17,18]. With a nondestructive approach, data from remote sensing obtained using multispectral images from RPAs is commonly used to monitor nitrogen content in vegetation [19,20,21,22]. Still, due to the amount of data that is generated, remote sensing combined with high-resolution images requires a robust technique, such as methods of machine learning [23]. These methodologies, when applied to agriculture, achieve advantages, like the ability to solve nonlinear problems using datasets from various sources [24,25,26] and discover information hidden on the data [27]. There are still few studies in the literature contemplating RPA, management of nitrogen fertilizers, and machine learning [23,28,29,30]. For coffee production, [31] study used RGB-based vegetation indices from RPA images with Random Forest to monitor the nitrogen status of the plants. However, the models developed in the study were not capable of explaining and predicting the spatial variability of the nitrogen in the coffee plants. Therefore, a solution to these unsatisfactory results is possibly to explore vegetation indices from multispectral images.

Thus, based on the hypothesis that the learning method Random Forest applied to vegetation indices obtained from RPAs can contribute to the more efficient management of the nitrogen content in coffee crops, the objectives of this study were (i) to map the spatial variability of the nitrogen content in the coffee plantations, (ii) quantify the deficiency of nitrogen in coffee plants, and (iii) determine the most efficient vegetation index to predict N content in coffee plants using the Random Forest (RF) machine learning method.

## **2. Material and Methods**

The methodology proposed in this study is briefly explained in Figure 1. In the first step, multispectral images of the study area were acquired by a multispectral camera coupled to an RPA. These images were processed, creating the orthomosaics, to then later calculate the vegetation indices. In the second step, the RGB mosaic composition was used to define sampling points in the study area, used for analyzing the chemical content of N in the coffee leaves. Finally, in the third step, values of the vegetation indices and chemical analysis of N in the leaves in each sample point were used as input parameters to calibrate the algorithm Random Forest and classify the images in three N content categories. The accuracy of the classification was measured by the overall accuracy metrics, kappa coefficient, receiver operating

characteristic (ROC) curve, and area under the curve (UAC). The methodology is further detailed in the following topics.

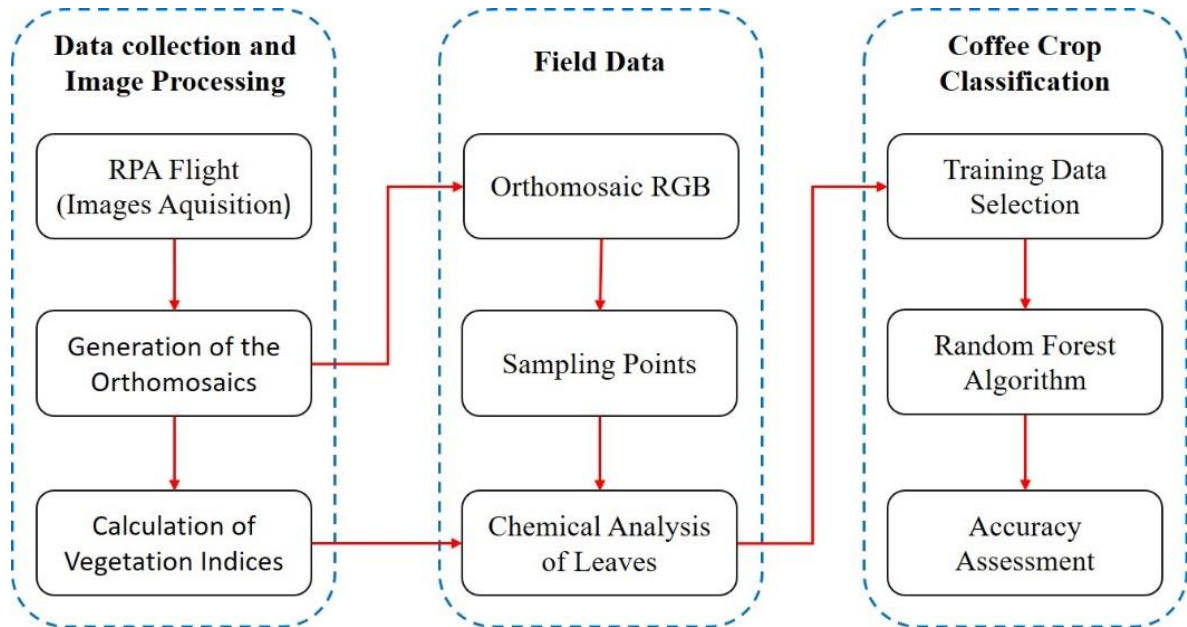


**Figure 1.** Workflow used in the methodology of this study.

## 2.1 Study Site

The study was carried out in a field located in the commercial farm Bom Jardim, in the city of Santo Antonio do Amparo, state of Minas Gerais, Brazil, geographic coordinates 21°01'09.69"S and 44°55'45.03"W, and the average altitude of 935 m. This plantation occupies an area of 1.5 ha cultivating coffee plants (*Coffea arabica* L.), Catucaí Amarelo 2SL cultivar aging 3 years old, spaced by 3.5 m from centerlines, and 0.5 m plant to plant, adding 5700 plants ha<sup>-1</sup> (Figure 2).

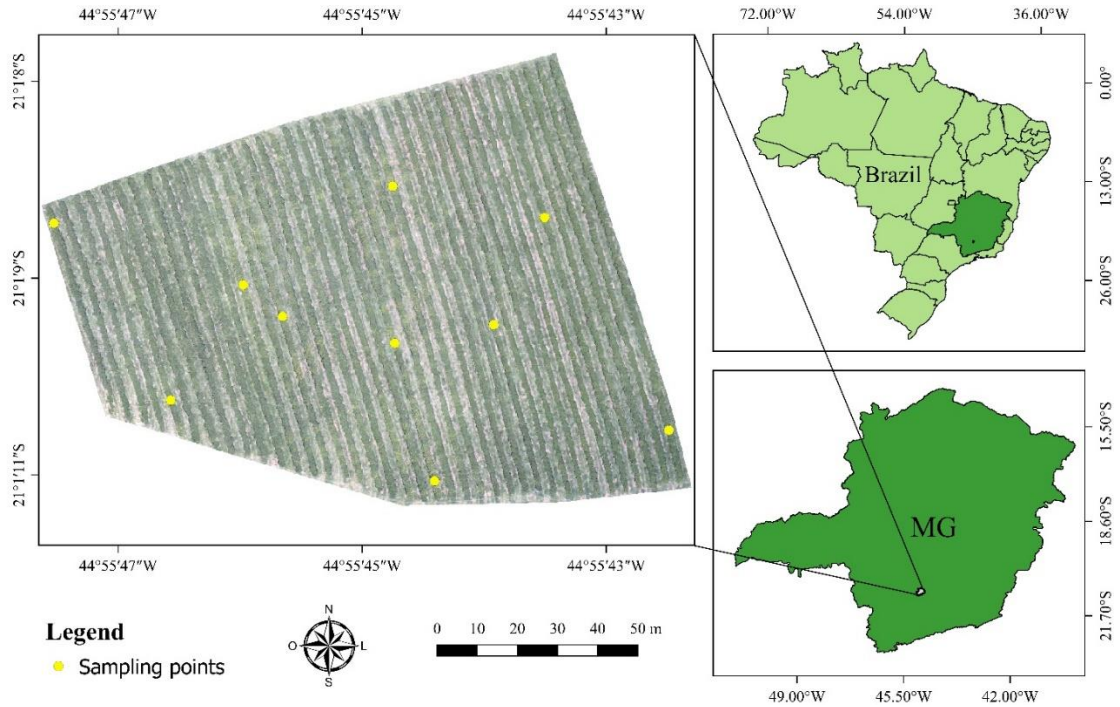


**Figure 2.** The geographic location of the study area. MG is the State of Minas Gerais, Brazil.

According to the Köppen-Geiser climate classification, the region has a Cwa climate, humid subtropical, with hot and humid summers and cold and dry winters, with an annual average air temperature of 19.8 °C and average annual total rainfall of 1670 mm [32]. The climatic data [33] of the study area from the period of the analysis is shown in Table 1.

**Table 1.** Climatic data of the region on 10 December 2018. City of Santo Antônio do Amparo, MG, Brazil.

Temp (°C)	RH (%)	Pressure (kPa)	WS (m.s <sup>-1</sup> )	Max Temp (°C)	Min Temp (°C)	RFE (mm)
19.73	73.31	91.6	1.51	25.6	13.28	0

Temp is temperature; RH is relative humidity; WS is wind speed; Max Temp is maximum temperature; Min Temp is minimum temperature; RFE is rainfall.

## 2.2 RPA Image Acquisition and pre-processing

The images were captured using a commercial RPA 3DR Solo (3D Robotics, Berkeley, CA, USA), with four engines (quadcopter), powered by the automatic pilot system 3DR Pixhawk 2 and flight controller APM:Copter. A multispectral camera Parrot Sequoia with a focal distance fixed at 4.0 mm was coupled to the RPA. This camera has an RGB sensor with 16 megapixels resolution (4608 × 3456) and four extra sensors with 1.5 megapixels resolution

(1280 × 960) in the spectral bands of green (550 nm BP 40), red (660 nm BP40), red-edge (735 nm BP 10), and near-infrared (790 nm BP 40). This camera is designed to map and monitor vegetation; it includes an upward-facing sunshine sensor, which allows the radiometric calibration of those 4 multispectral bands during image collection. The software Mission Planner from a complete ground station, open-source for RPA automatic piloting systems, was used to plan the flight mission. The flight altitude was fixed at 60 m above ground, and the flight speed was an average of 3 m s<sup>-1</sup>. The images were captured every 1 s with a spatial resolution of 2.07 cm and overlapping the frontal position of 80% and lateral position of 75%.







The image processing was made using the software Agisoft PhotoScan® Professional, version 1.2.4 (Agisoft LLC, St. Petersburg, Russia). This software works in a three-step workflow. The first step was the alignment of the images by identifying corresponding resources. For executing the alignment of the image, the software calculates the parameters that orient the internal and external camera, including the radial nonlinear distortion. For this study, this task was executed with a high precision set. The results of this step are positions of the camera matching each image, representing the parameters for internal calibration, and the 3D coordinates of the sparse cloud of points in the terrain. In the second step, the sparse cloud is georeferenced in a local coordinates system (WGS 84—UTM Zone 23S), and the densified cloud of points is obtained using the heightfield method, which is based on paired depth map computation, resulting in a detailed 3D model. The third step applies a texture to the mesh obtained previously, generating the orthomosaic. This way, orthomosaics were created for each spectral band (green, red, red-edge, and near-infrared).

To minimize the effects of other targets in the spectral response of the coffee plants, such as soil and weeds, the mosaics were differentiated in the software eCognition version 9.0.1 (eCognition Developer, Munich, Germany). Two distinct classes were visually defined: coffee plants and noncoffee plants. From that, the classes were manually sorted for the orthomosaics of each spectral band.

### **2.3 Determining leaf nitrogen**

Leaf nitrogen analyzes were performed on 10 December 2018. After obtaining the orthomosaics, the nitrogen level in the leaves of the coffee plants was visually evaluated, defining three distinct regions as deficient, critical, and sufficient N content (Figure 3). For that, we used the orthomosaic of the RGB composition (red, green, and blue) that allows a better perception than the human eye of vegetation. Thus, 10 targeted sampling points were chosen,

with 2 sampling points for regions with N content in the plants considered sufficient, 4 points for regions of critical level, and 4 points for deficient regions (Figure 2).

Nutritional status	RGB orthomosaic	Picture	Classes description
Sufficient (n=2)			Plants without yellow leaves
Critical (n=4)			Plants with some yellowish-green leaves
Deficient (n=4)			Plants with a great number of yellow leaves

**Figure 3.** Description of the classes of nitrogen level in the coffee leaves identified through RGB (red, green, and blue) composition in the orthomosaic images, to select sampling points in each level.

Each sample point was composed of 5 plants, 1 central plant and 2 plants oriented north-south from the central plant. From every plant, 3 leaves were collected from both sides of the planting line in three different canopy heights, totalizing 30 leaves collected for each sample point. After the collection, the leaves were sent to the laboratory of leaf analysis in the University of Lavras to quantify the nitrogen content using the Kjeldahl method. This method has been widely applied to determine nitrogen content, especially in the analysis of plant tissues. The Kjeldahl procedure involves three steps—destruction, distillation, and titration [8]. The leaf diagnosis for mature coffee plants proposed by [34] was used to classify the nitrogen content in the leaves as N-deficient (<2.5%), N-critical (2.5 to 3.0%), and N-sufficient (3.0 to 3.5%).

## 2.4 Vegetation Indices

The vegetation indices (Table 2) were chosen based on their capability to determine the nitrogen content in the coffee crops from remote sensing data [5,7,8].

**Table 2:** Vegetation indices of multispectral images obtained using Remotely Piloted Aircraft (RPA).

Vegetation indices	Formula	Reference
GNDVI (Green Normalized Difference Vegetation Index)	$\frac{\rho_{nir} - \rho_{green}}{\rho_{nir} + \rho_{green}}$	Gitelson et al. (1996)
GOSAVI (Green Optimal Soil Adjusted Vegetation Index)	$(1+0.16) \frac{\rho_{nir} - \rho_{green}}{\rho_{nir} + \rho_{green} + 0.16}$	Rondeaux et al. (1996)
NDVI (Normalized Difference Vegetation Index)	$\frac{\rho_{nir} - \rho_{red}}{\rho_{nir} + \rho_{red}}$	Rouse et al. (1974)
SAVI (Soil Adjusted Difference Vegetation Index)	$\frac{(1+L)\rho_{nir} - \rho_{red}}{\rho_{nir} + \rho_{red} + L}$	Huete (1988)
MTCI (MERIS Terrestrial Chlorophyll Index)	$\frac{\rho_{nir} - \rho_{edge}}{\rho_{edge} - \rho_{red}}$	Dash and Curran (2004)
NDRE (Normalized Difference Red Edge)	$\frac{\rho_{nir} - \rho_{edge}}{\rho_{nir} + \rho_{edge}}$	Gitelson and Merzlyak (1994)
EXR (Excessive Red)	$1.4 * \rho_{red} - \rho_{green}$	Meyer et al. (1998)
MPRI (Modified Photochemical Reflectance Index)	$\frac{\rho_{green} - \rho_{red}}{\rho_{green} + \rho_{red}}$	Yang et al. (2008)
GRR (Green-Red Ratio Index)	$\frac{\rho_{green}}{\rho_{red}}$	Gamon and Surfus (1999)
NDI (Normalized Different Index)	$\frac{\rho_{green} - \rho_{red}}{\rho_{green} + \rho_{red} + 0.01}$	Mao et al. (2003)

$\rho_{blue}$ : reflectance in the blue band;  $\rho_{green}$ : reflectance in the green band;  $\rho_{red}$ : reflectance in the red band;  $\rho_{nir}$ : reflectance in the near-infrared band;  $\rho_{edge}$ : reflectance in the red-edge band

## 2.5 Random Forest (RF) classification

The Random Forest (RF) algorithm was used for classifying the N content in the leaves of the coffee plants from the vegetation indices proposed in this study (Table 2). The modeling was created in R [45], using the R Random Forest package [46]. For the training of the algorithm, the values of the vegetation indexes in the pixels referring to each of the 5 plants of each sampling point were used with the results of the chemical analysis of the N content in the leaves of the coffee plants of these sampling points. RF is one of the most successful classifiers based on learning strategies. The algorithm consists of a collection of three-based classifiers  $\{h(x, \Theta_k), k = 1, \dots\}$ , where  $x$  is the input vector and  $\{\Theta_k\}$  are the random vectors distributed identically and independently [47]. Each decision tree was constructed using a bootstrap deterministic algorithm, allowing the remaining data points to validate and issue a unitary vote to the most popular class. The RF uses the procedure of initialization with replacement to increase the diversity of the classifying trees, which allocated pixels to one class, according to the maximum number of votes in the collection [48].

To execute the RF for classifying images, two parameters must be defined: the number of trees ( $n_{tree}$ ), and the number of predictors concerning the maximization of the model ( $m_{try}$ ) [49,50]. In this study, the  $n_{tree}$  was set to 1000 trees, while the  $m_{try}$  was set to equal to the square root of the total number of input resources.

## 2.6 Accuracy Assessment

To validate the results of the RF classification, a crossed validation approach was used 10 times [51]. This involved the random division of the reference objects in 10 joints of datasets, each one including around 15% of data from each class. In the steps of the assessment, the RF was tuned with 85% of the reference data and then applied to the other 15% left (that were the validation joint of data). This step was repeated ten times. In the end, the results were aggregated to one confusion matrix. The classification performance was assessed based on common statistical measures [52], derived from the confusion matrix. The select statistical measures included the overall accuracy (Equation (1)), kappa coefficient (Equation (2)), receiver operating characteristic (ROC curve), and area under the curve (UAC). The ROC curve was obtained by plotting a graph of sensitivity (true positive rate) versus specificity (false positive rate), and UAC was estimated using the method proposed by [53].



$$\text{Overall Accuracy} = \frac{\sum_{i=1}^q n_{ii}}{n} \times 100\% \quad (1)$$

$$\text{Kappa Coefficient} = \frac{n \sum_{i=1}^q n_{ii} - \sum_{i=1}^q n_{i+} n_{+i}}{n^2 - \sum_{i=1}^q n_{i+} n_{+i}} \times 100\% \quad (2)$$

where  $q$  is the number of classes,  $n$  represents the total number of considered pixels,  $n_{ii}$  are the diagonal elements of the confusion matrix,  $n_{i+}$  represents the marginal sum of the rows in the confusion matrix, and  $n_{+i}$  is the marginal sum of the columns in the confusion matrix.

### 3 Results and Discussion

#### 3.1. Nitrogen Content in Coffee Leaves

First, as described in the Material and Methods section, one flight was performed in the area; then, from the RGB images, the orthomosaic was generated, which allowed the identification and establishment of the leaves sampling points. The results of the statistical descriptive analyses of the chemical analysis of nitrogen content in coffee leaves are shown in Table 3. The areas in the crops with N levels considered sufficient, critical, and deficient are denoted with values within the nutritional scale established by [34]. However, as can be seen in Figure 2, regions with a critical level of N presented plants with a considerable amount of yellowish leaves, which is a symptom of nutritional deficiency. This may have occurred because the plants in this region had leaves with a medium nitrogen content (2.69%), with the content value close to the level considered nutritionally deficient (<2.5%).

**Table 3.** Results of the descriptive statistics of the chemical analysis of N content in plants located in the sampling points, considered as N-sufficient, -critical and -deficient.

Nitrogen Levels	%			
	Min	Max	Mean	SD
Sufficient	3.00	3.11	3.05	0.08
Critical	2.51	2.85	2.69	0.18
Deficient	2.13	2.44	2.31	0.13

Min is minimum; Max is maximum; SD is the standard deviation.

The high-resolution images captured using RPA showed great potential in differentiating samples to evaluate the nitrogen content in the coffee leaves. According to [13], changes in the nutritional status of the plants have a direct impact on the canopy color of the coffee plantation. The color of leaves deficient in nitrogen is lighter, causing the color of the canopy to be green–yellowish, whereas leaves with sufficient nitrogen content reflect energy more intensely in the green wavelength than in the red wavelength. In contrast, leaves with N deficiency reflect energy intensely both in the green and in the red wavelengths, resulting in leaves with a yellow coloration [8,13].

### 3.2. Overall Accuracy and Kappa Performance

The results of the overall accuracy and the kappa coefficient of the images classified by RF from vegetation indices are shown in Figure 4. In general, the classification has presented a high performance in assessing the nitrogen content of the leaves in coffee plants: values of accuracy and kappa coefficient were from 0.78 to 0.91 and 0.46 to 0.86, respectively.

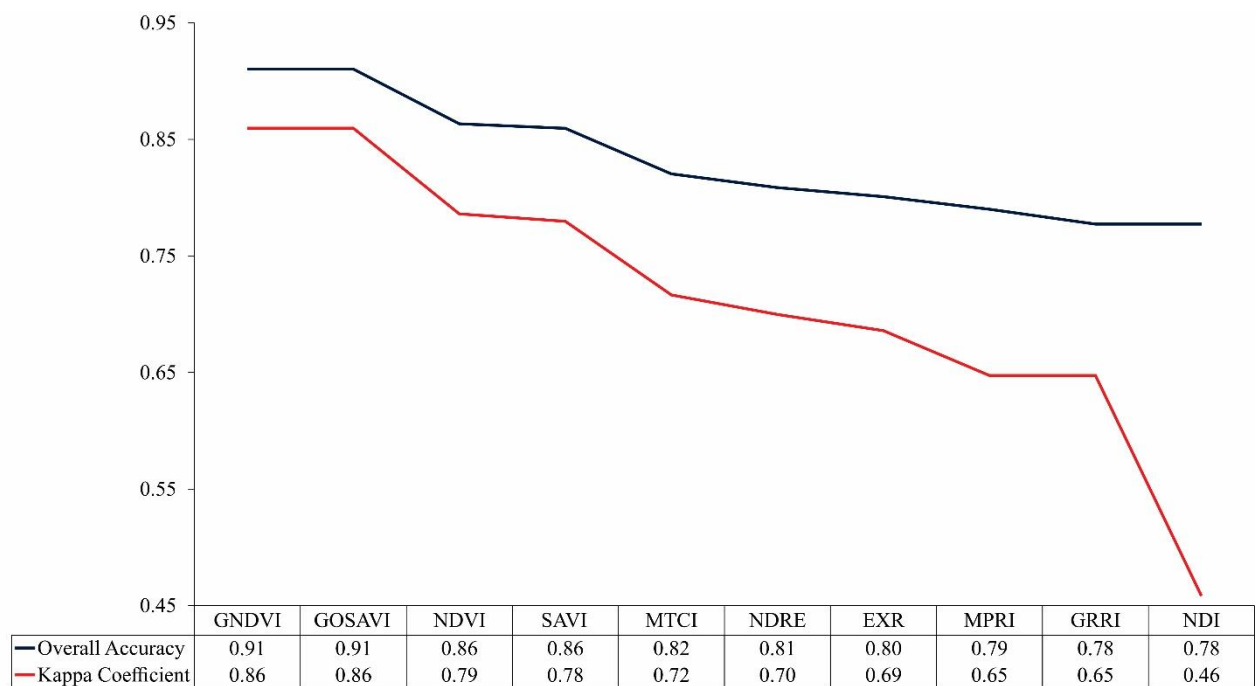


**Figure 4.** Overall accuracy and kappa coefficient for image classification through Random Forest (RF) from vegetation indices.

It was possible to notice that vegetation indices that use a combination of the near-infrared band with bands in the visible spectral region presented better results. Between those indices,

the Green Normalized Difference Vegetation (GNDVI) and the Green Optimized Soil Adjusted Vegetation Index (GOSAVI) obtained the greatest values. These results are associated with the larger predominance of plants with sufficient N content in the crops and, consequently, higher chlorophyll content in the leaves. According to [54,55], the reflectance in the green band is greatly affected by the variations in the chlorophyll content, when compared to the red band reflectance. Thus, the spectral indices based on the near-infrared and green bands have proved more sensitive to changes in chlorophyll content than the indices with near-infrared and red bands [56,57]. The GNDVI and GOSAVI have also been reported by other authors as more suitable indices to evaluate N status in vegetation. Similarly to this study, [29] used an approach based on RF and vegetation indices from RPA images to describe the variation of plant N uptake (PNU), and N nutrition index (NNI) for rice crops in the northwest lowlands of China. The results, resembling this study, presented GOSAVI and GNDVI indices as having better performances. In [22], they applied the RF model to vegetation indices obtained from three sensors (RGB, color infrared, and multispectral), coupled to an RPA, for determining the N status in the rice crops, finding the GNDVI to have the better results. Therefore, the results of this study align with the literature and recent research.

For the Medium Resolution Imaging Spectrometer (MERIS) Terrestrial Chlorophyll Index (MTCI) and Normalized Difference Red Edge (NDRE) indices, the bandwidth of the red-edge band that is 4 times smaller than the green and red bands may have contributed to the worst performances among the indices that use the combination of the near-infrared band with visible bands. As demonstrated by [5], the width of the red-edge band can make indices less sensitive to the vegetation characteristics. However, better results were expected from them, since the relation between near-infrared and red-edge spectral bands with the N content in the plants is well established in the literature [5,6,22].

For the indices Excessive Red (EXR), Modified Photochemical Reflectance Index (MPRI), Green–Red Ratio Index (GRRI), and Normalized Different Index (NDI) that use only visible spectral bands, the results had inferior performances. The possible explanation for that is the lack of radiometric correction for RGB images, letting fewer alterations in the lighting conditions influence the precision of the color reproduction [58,59]. However, even with those indices showing worse performances, when compared to indices that combine near-infrared bands to visible bands, their results still express the potential for the application of RGB cameras. These types of cameras can be a viable alternative to evaluate the N status in plants, especially for medium and smaller farmers. RGB cameras are easy to operate and accessible for most researchers. Furthermore, the RGB images can be used right after downloading from

the memory card, without preprocessing, for example, for band registry, and to process images, various sophisticated commercial platforms are now available, such as Agisoft Photoscan and Pix4D.

Regarding the RGB indices, the results obtained by this study diverge from the reported by [31]. The Random Forest models based on RGB indices from RPA that were developed by the authors did not succeed in evaluating and predicting the N content of the coffee plants. This may have occurred because the Parot Sequoia camera that was used in the present study presents superior techniques, compared to the RGB camera used by [31], for example, when calibrating the radiometric individual bands. Additionally, the focus of the sampling points in this study may have been crucial for more effective training samples and clearer results.

### **3.3. ROC curve and AUC**

Regarding the analysis of the image classification using the ROC curve and AUC, in general, all the vegetation indices presented excellent performances for assessing the nitrogen content in coffee plants (Figure 5).

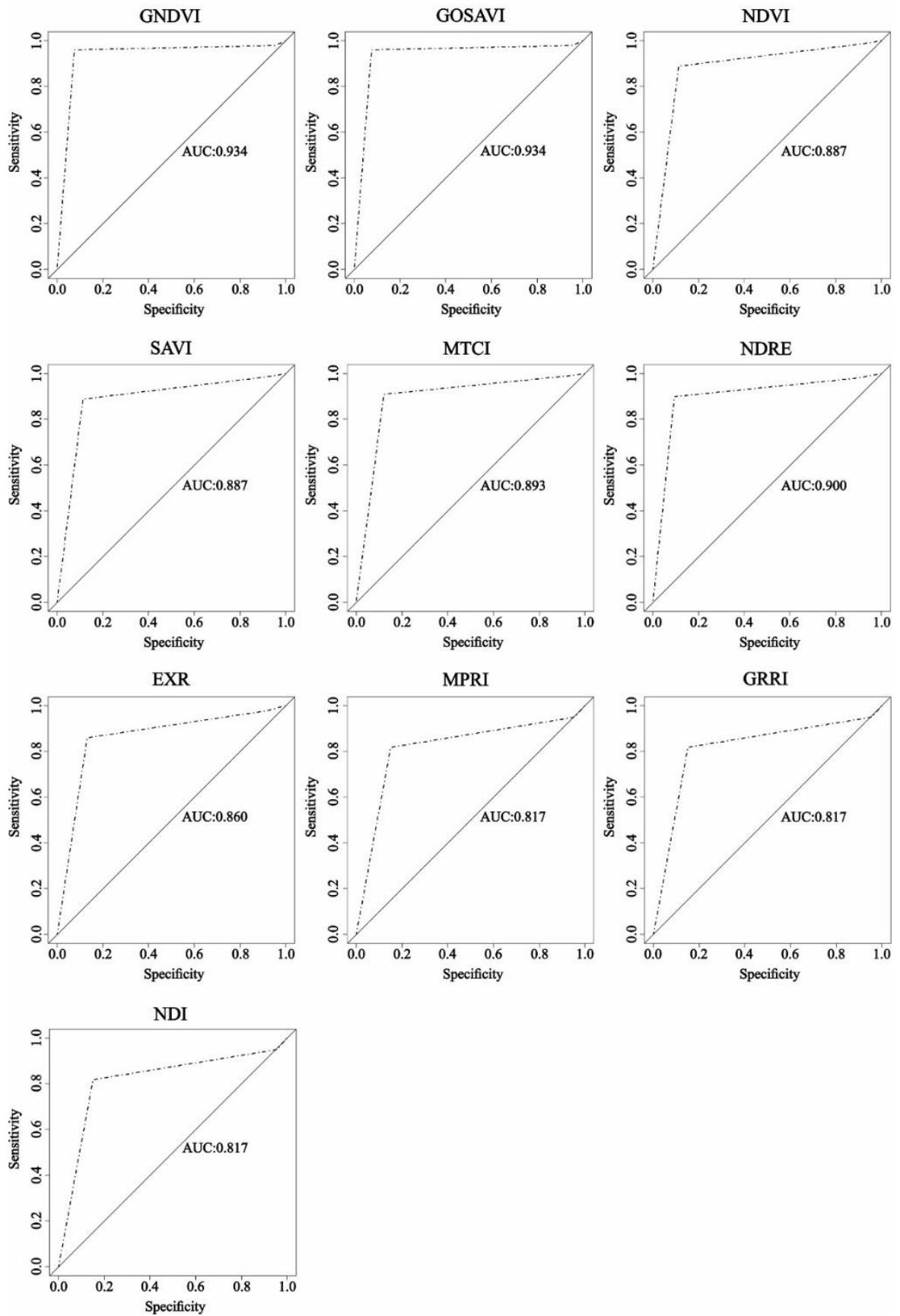


**Figure 5.** Receiver operating characteristic (ROC) curve and area under the curve (AUC) for image classification through RF from vegetation indices.

It was possible to observe all vegetation indices approximate to the point (0, 100%) in the ROC curve. According to [60], to rate a model as optimum, its analysis has to be as close as possible to the point (0, 100%). Moreover, [61] describes the ROC curve as a description of the relative compensation between benefits (true positives) and costs (false positives) of a classification. Thus, a point located in the upper left corner means a greater number of positive and negative examples were classified correctly, consequently creating a lower cost to the classification.

For the AUC, the values were from 0.817 to 0.934, where greater values came from the indices that combined near-infrared band to visible bands, matching what happened with overall accuracy and kappa coefficient. According to [62], the closer the AUC gets to 1, the better the overall test performance, meaning the AUC= 1 test is the perfectly accurate result. For the approach in this study, the indices GNDVI and GOSAVI had the greatest performances, while the indices MPRI, GRRRI, and NDI presented the worse performances.

### **3.3. Mapping and quantifying N spatial distribution in coffee leaves**

Predictive maps for nitrogen spatial distribution in coffee leaves and quantification in the percentage of those maps, obtained from the classification of images using RF from vegetation indices data, are shown in Figure 6, Figure 7 and Table 4, respectively.

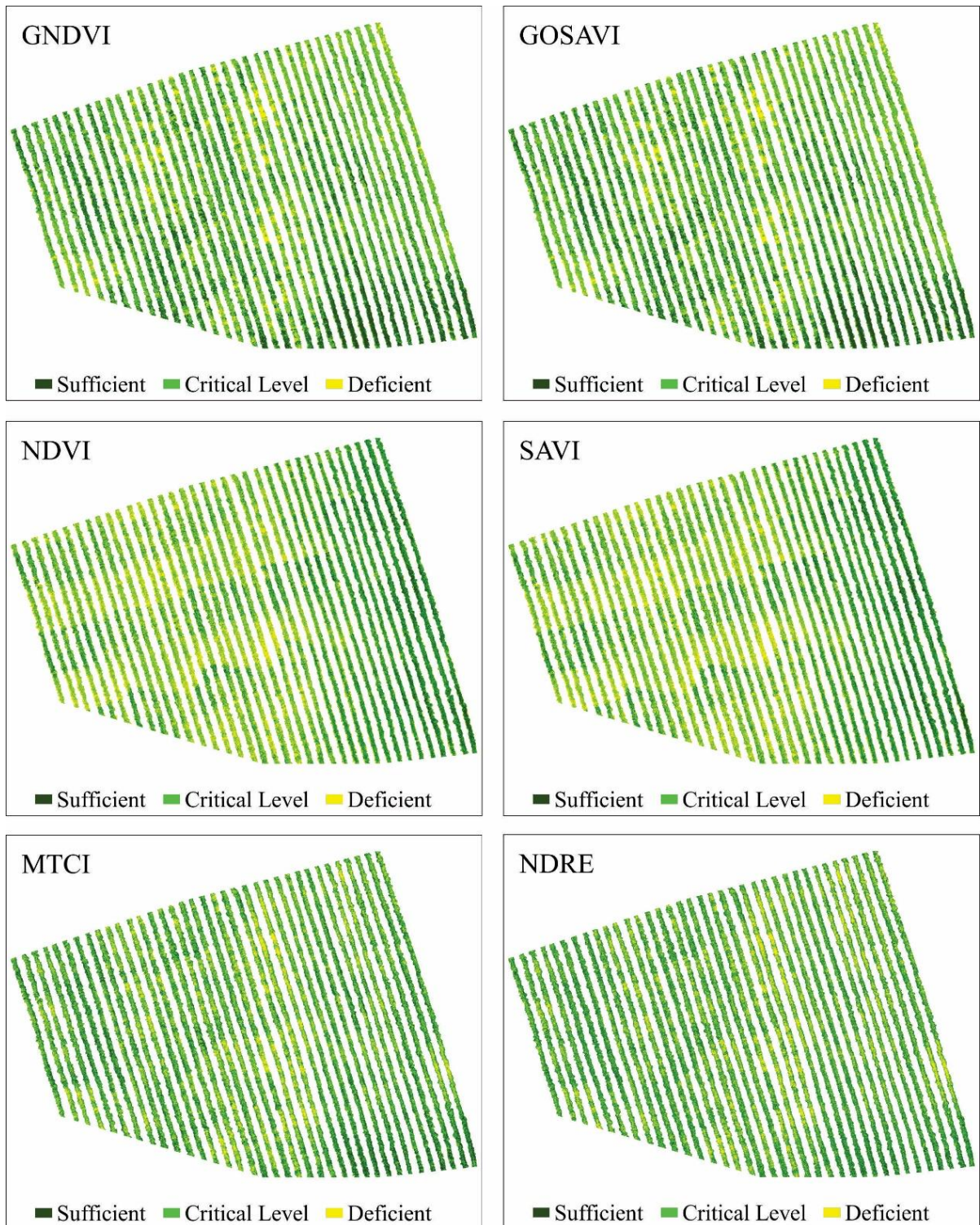


**Figure 6.** Predictive maps of the N content spatial distribution in coffee leaves, obtained from the classification of images using RF from vegetation indices Green Normalized Difference Vegetation (GNDVI), Green Optimized Soil Adjusted Vegetation Index (GOSAVI), Normalized Difference Vegetation Index (NDVI), Soil Adjusted Difference Vegetation Index (SAVI), Medium Resolution Imaging Spectrometer (MERIS) Terrestrial Chlorophyll Index (MTCI), and Normalized Difference Red Edge (NDRE).

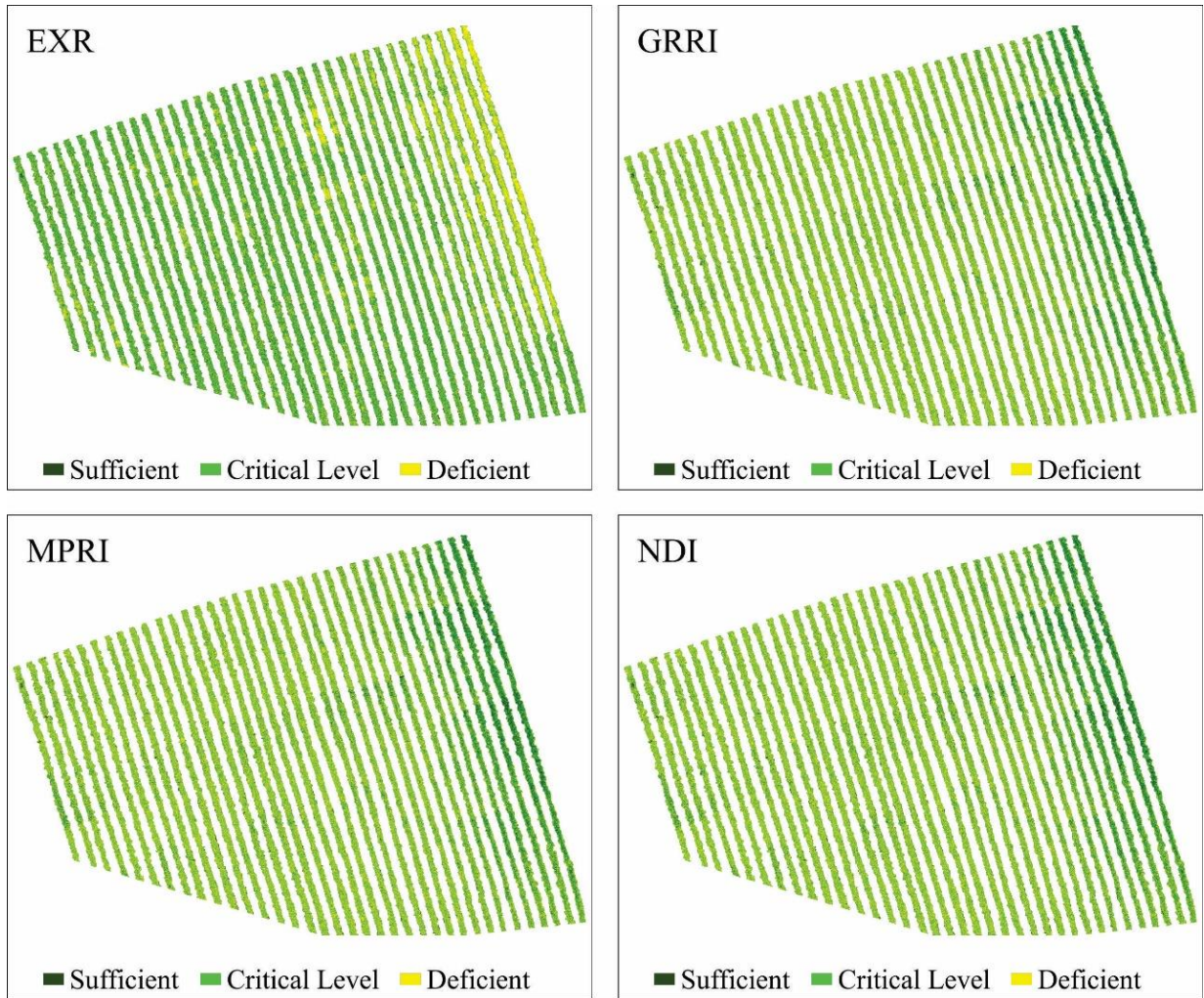


**Figure 7.** Predictive maps of the N content spatial distribution in coffee leaves, obtained from the classification of images using RF from vegetation indices Excessive Red (EXR), Green–Red Ratio Index (GRRI), Modified Photochemical Reflectance Index (MPRI), and Normalized Different Index (NDI).



**Table 4.** Percentage (%) of areas in the coffee plantation that had N content sufficient, critical, and deficient, according to the appraisal maps of the N content spatial distribution in coffee leaves, presented from the best performance to the worst performance.

Vegetation Indices	Area (%)			
	Sufficient	Critical	Deficient	Total
GNDVI	26	52	22	100
GOSAVI	26	52	22	100
NDVI	23	46	31	100
SAVI	23	46	31	100
MTCI	31	47	22	100
NDRE	31	46	22	100
EXR	25	45	31	100
MPRI	21	42	37	100
GRRI	21	41	38	100
NDI	21	41	38	100

GNDVI and GOSAVI indices had the best performances (Figure 6), presenting the best class definition. These maps had the largest area at the N-critical level (52%) and the smallest area for deficient N levels (22%). According to these maps, the plants in the central region of the crops showed a greater N deficiency. Similar to these indices, NDVI and SAVI maps indicated greater N deficiency in the central region of the crops, although they also indicated a large number of N-deficient plants in the western region, evinced by the 9% increase in the N-deficient areas, when compared to the GNDVI and GOSAVI maps. Regarding the MTCI and NDRE indices (Figure 6), they both presented the same percentage of N-deficient areas as the GNDVI and the GOSAVI, but they overestimated areas with sufficient N content (31%). Additionally, in these maps, the area with N deficiency extended from the central region to the eastern region of the plantation. The indices that had worse performances were MPRI, GRRI, and NDI (Figure 7). They overestimated the percentage of N-deficient areas and underestimated areas with sufficient N levels (21%) as well as areas with critical N levels (41%). The maps for these indices showed mixed classes, especially between critical and deficient levels of nitrogen, showing deficiency in practically all regions of the crops.

These results confirmed the possibility of managing nitrogen locally using images obtained from RPA. Knowing the spatial distribution of areas with N deficiency becomes essential for

managing nitrogen properly in the plantation. Overestimating or underestimating areas with N deficiency can increase production costs, reduce productivity, and cause environmental damage. In this context, the methodology proposed by this study, especially for GNDVI and GOSAVI indices, can promote a 78% reduction in nitrogen fertilizer treatments in the studied area, when compared to the conventional management and application methods. For this, applying fertilizers would be recommended only for plants showing N deficiency, which means 22% of the total area, unlike the conventional application of fertilizer, where producers apply it to the entire area of the plantation.

Based on information previously published by [34,63], it is possible to illustrate how the methodology proposed in this study could prove economically relevant to monitor the N status in coffee plantations. The data used in the simulation were as follows: study area: 1.5 ha; ammonium nitrate price for 50 Kg: \$15.00; average amount of N applied by coffee producers: 300 kg ha<sup>-1</sup> per year; N concentration in ammonium nitrate: 33%; total ammonium nitrate applied by coffee producers: 833 kg ha<sup>-1</sup> per year; and reduction of the demand for N observed in this study, considering results from the GNDVI and GOSAVI indices: 78%.

To that end, the calculation of the total price per hectare of N was 833 kg ha<sup>-1</sup> per year × \$15.00 (50 Kg) = \$249.90 kg ha<sup>-1</sup>. Considering the 1.5 ha plantation area, it would have a cost of \$374.85 per year for nitrogen fertilization. When considering the actual demand for N for this coffee field, which, in this study, would reduce by 78% of the total, the coffee producer cost could be reduced to  $\$374.85 \times 0.22 = \$82.47$  per year. In conclusion, the coffee producer could save \$292.38 during the year with nitrogen fertilization. This was possible, considering the use of N only for plants that showed deficiency. This example is hypothetical. However, it shows the application and importance of carrying out properly the monitoring of N status in coffee plantations, which is especially relevant to minimize the use of N and reduce the costs of nitrogen fertilization, as well as its impacts.

In this study, the learning method of the RF algorithm applied to the vegetation indices from images obtained using a multispectral camera coupled to an RPA was used to evaluate the N content in a coffee plantation. The results proved that this methodology could be used to diagnose the nitrogen status in coffee plants and also orient producers on how to do the application of nitrogen fertilizers at a variable rate. However, other local conditions, such as density, canopy cover, age, species of plant, and spacing can reduce the accuracy of the model suggested. From this, to deal with the problem complexity, a systemic approach that simulates and predicts the impact of applying N fertilizers over space and time, affecting the cultivation yield, is necessary. To validate this relation, more studies using different conditions and plants

are needed. In addition, the use of RPAs with greater flight autonomy and different multispectral cameras with better resolution can improve the model efficiency, as well as the size of the monitored area. To administer N fertilizers at a variable rate, the process used in the practical application needs to develop into management zones, pixel-based, and plant-based, to make easy the reduction and viable the application for producers.

#### **4 Conclusions**

The results of this study showed that the machine learning method Random Forest, applied to vegetation indices from multispectral images obtained by RPA, offers a very promising approach to map and quantify nitrogen status in a coffee plantation and also indicates the possibility to apply fertilizers in a localized manner. The proposed model allowed the assessment of the N spatial distribution in the coffee leaves and the quantification of area presenting N deficiency. The model also indicated that the most efficient vegetation indices to evaluate the nitrogen status in coffee plants were GNDVI and GOSAVI. Additionally, the application of the methodology proposed in this study can contribute to a more rational management of N in the crops.

#### **Funding**

This research was funded by the Embrapa Café—Consórcio Pesquisa Café, project approved in the call n° 20/2018, the National Council for Scientific and Technological Development (CNPq), the Coordination for the Improvement of Higher Education Personnel (CAPES) and the Federal University of Lavras (UFLA) and University of Firenze (UniFI).

#### **Acknowledgments**

The authors would like to thank farm Bom Jardim.

#### **Conflicts of Interest**

The authors declare that they have no conflict of interest.

## References

1. Chemura, A. Modelling Spatial Variability of Coffee (*Coffea Arabica* L.) Crop Condition with Multispectral Remote Sensing Data. Ph.D. Thesis, University of KwaZulu-Natal, Pietermaritzburg, South Africa, 2017.
2. Bote, A.D.; Ayalew, B.; Ocho, F.L.; Anten, N.P.R.; Vos, J. Analysis of coffee (*Coffea arabica* L.) performance in relation to radiation levels and rates of nitrogen supply I. Vegetative growth, production and distribution of biomass and radiation use efficiency. *Eur. J. Agron.* **2018**, *92*, 115–122, doi:10.1016/j.eja.2017.10.007.
3. Nazareno, R.B.; Da Silva Oliveira, C.A.; Sanzonowicz, C.; Ramos Sampaio, J.B.; Pereira Da Silva, J.C.; Guerra, A.F. Crescimento inicial do cafeeiro Rubi em resposta a doses de nitrogênio, fósforo e potássio e a regimes hídricos. *Pesqui. Agropecu. Bras.* **2003**, *38*, 903–910, doi:10.1590/s0100-204x2003000800002.
4. Coste, R. *Coffee—The Plant and The Product*; MacMillan Press: London, UK, 1992.
5. Chemura, A.; Mutanga, O.; Odindi, J.; Kutuywayo, D. Mapping spatial variability of foliar nitrogen in coffee (*Coffea arabica* L.) plantations with multispectral Sentinel-2 MSI data. *ISPRS J. Photogramm. Remote Sens.* **2018**, *138*, 1–11, doi:10.1016/j.isprsjprs.2018.02.004.
6. Putra, B.T.W.; Soni, P.; Morimoto, E.; Pujiyanto, P. Estimating biophysical properties of coffee (*Coffea canephora*) plants with above-canopy field measurements, using CropSpec. *Int. Agrophysics* **2018**, *32*, 183–191, doi:10.1515/intag-2017-0009.
7. Putra, W.B.T.; Soni, P. Enhanced broadband greenness in assessing Chlorophyll a and b, Carotenoid, and Nitrogen in Robusta coffee plantations using a digital camera. *Precis. Agric.* **2018**, *19*, 238–256, doi:10.1007/s11119-017-9513-x.
8. Putra, B.T.W.; Soni, P. Improving nitrogen assessment with an RGB camera across uncertain natural light from above-canopy measurements. *Precis. Agric.* **2020**, *21*, 147–159, doi:10.1007/s11119-019-09656-8.
9. Lima, L.M.; Pozza, E.A.; Torres, H.N.; Pozza, A.A.A.; Salgado, M.; Pfenning, L.H. Relação nitrogênio/potássio com mancha de Phoma e nutrição de mudas de cafeeiro em solução nutritiva. *Trop. Plant Pathol.* **2010**, *35*, 223–228, doi:10.1590/S1982-56762010000400003.
10. Pérez, C.D.P.; Pozza, E.A.; Pozza, A.A.A.; Freitas, A.S.; Da Silva, M.G. Nitrogênio e potássio na intensidade da mancha aureolada do cafeeiro em solução nutritiva. *Coffee Sci.* **2017**, *12*, 60–68, doi:10.25186/cs.v12i1.1210.

11. Martinez, H.E.P.; de Souza, B.P.; Caixeta, E.T.; de Carvalho, F.P.; Clemente, J.M. Water deficit changes nitrate uptake and expression of some nitrogen related genes in coffee-plants (*Coffea arabica* L.). *Sci. Hortic.* **2020**, *267*, 109254, doi:10.1016/j.scienta.2020.109254.
12. DaMatta, F.M.; Loos, R.A.; Silva, E.A.; Loureiro, M.E. Limitations to photosynthesis in *Coffea canephora* as a result of nitrogen and water availability. *J. Plant Physiol.* **2002**, *159*, 975–981, doi:10.1078/0176-1617-00807.
13. Feng, D.; Xu, W.; He, Z.; Zhao, W.; Yang, M. Advances in plant nutrition diagnosis based on remote sensing and computer application. *Neural Comput. Appl.* **2019**, 1–10, doi:10.1007/s00521-018-3932-0.
14. Ye, X.; Abe, S.; Zhang, S. Estimation and mapping of nitrogen content in apple trees at leaf and canopy levels using hyper-spectral imaging. *Precis. Agric.* **2020**, *21*, 198–225, doi:10.1007/s11119-019-09661-x.
15. Mahajan, G.R.; Pandey, R.N.; Sahoo, R.N.; Gupta, V.K.; Datta, S.C.; Kumar, D. Monitoring nitrogen, phosphorus and sulphur in hybrid rice (*Oryza sativa* L.) using hyperspectral remote sensing. *Precis. Agric.* **2017**, *18*, 736–761, doi:10.1007/s11119-016-9485-2.
16. Fitzgerald, G.; Rodriguez, D.; O’Leary, G. Measuring and predicting canopy nitrogen nutrition in wheat using a spectral index-The canopy chlorophyll content index (CCCI). *F. Crop. Res.* **2010**, *116*, 318–324, doi:10.1016/j.fcr.2010.01.010.
17. Santos, L.M.; Ferraz, G.A.E.S.; Barbosa, B.D.S.; Andrade, A.D. Use of remotely piloted aircraft in precision agriculture: A review. *DYNA* **2019**, *86*, 284–291, doi:10.15446/dyna.v86n210.74701.
18. Yang, G.; Liu, J.; Zhao, C.; Li, Z.; Huang, Y.; Yu, H.; Xu, B.; Yang, X.; Zhu, D.; Zhang, X.; et al. Unmanned aerial vehicle remote sensing for field-based crop phenotyping: Current status and perspectives. *Front. Plant Sci.* **2017**, *8*, doi:10.3389/fpls.2017.01111.
19. Buchailot, M.L.; Gracia-Romero, A.; Vergara-Diaz, O.; Zaman-Allah, M.A.; Tarekegne, A.; Cairns, J.E.; Prasanna, B.M.; Araus, J.L.; Kefauver, S.C. Evaluating maize genotype performance under low nitrogen conditions using RGB UAV phenotyping techniques. *Sensors* **2019**, *19*, doi:10.3390/s19081815.
20. Wang, H.; Mortensen, A.K.; Mao, P.; Boelt, B.; Gislum, R. Estimating the nitrogen nutrition index in grass seed crops using a UAV-mounted multispectral camera. *Int. J. Remote Sens.* **2019**, *40*, 2467–2482, doi:10.1080/01431161.2019.1569783.
21. Hunt, E.R.; Horneck, D.A.; Spinelli, C.B.; Turner, R.W.; Bruce, A.E.; Gadler, D.J.;

- Brungardt, J.J.; Hamm, P.B. Monitoring nitrogen status of potatoes using small unmanned aerial vehicles. *Precis. Agric.* **2018**, *19*, 314–333, doi:10.1007/s11119-017-9518-5.
22. Zheng, H.; Cheng, T.; Li, D.; Zhou, X.; Yao, X.; Tian, Y.; Cao, W.; Zhu, Y. Evaluation of RGB, color-infrared and multispectral images acquired from unmanned aerial systems for the estimation of nitrogen accumulation in rice. *Remote Sens.* **2018**, *10*, doi:10.3390/rs10060824.
23. Osco, L.P.; Paula, A.; Ramos, M.; Pereira, D.R.; Akemi, É.; Moriya, S.; Imai, N.N.; Matsubara, E.T. Predicting Canopy Nitrogen Content in Citrus-Trees Using Random Forest Algorithm Associated to Spectral Vegetation Indices from UAV-Imagery. *Remote Sens.* **2019**, *11*, 1–17, doi:10.3390/rs11242925.
24. Chlingaryan, A.; Sukkarieh, S.; Whelan, B. Machine learning approaches for crop yield prediction and nitrogen status estimation in precision agriculture: A review. *Comput. Electron. Agric.* **2018**, *151*, 61–69, doi:10.1016/j.compag.2018.05.012.
25. Liakos, K.G.; Busato, P.; Moshou, D.; Pearson, S.; Bochtis, D. Machine learning in agriculture: A review. *Sensors* **2018**, *18*, 1–29, doi:10.3390/s18082674.
26. Ali, I.; Greifeneder, F.; Stamenkovic, J.; Neumann, M.; Notarnicola, C. Review of machine learning approaches for biomass and soil moisture retrievals from remote sensing data. *Remote Sens.* **2015**, *7*, 16398–16421, doi:10.3390/rs71215841.
27. Qiu, J.; Wu, Q.; Ding, G.; Xu, Y.; Feng, S. A survey of machine learning for big data processing. *EURASIP J. Adv. Signal Process.* **2016**, *67*, 1–16, doi:10.1186/s13634-016-0355-x.
28. Osco, L.P.; Junior, J.M.; Ramos, A.P.M.; Furuya, D.E.G.; Santana, D.C.; Teodoro, L.P.R.; Gonçalves, W.N.; Baio, F.H.R.; Pistori, H.; Junior, C.A.D.S.; et al. Leaf nitrogen concentration and plant height prediction for maize using UAV-based multispectral imagery and machine learning techniques. *Remote Sens.* **2020**, *12*, 1–17, doi:10.3390/rs12193237.
29. Zha, H.; Miao, Y.; Wang, T.; Li, Y.; Zhang, J.; Sun, W.; Feng, Z.; Kusnierek, K. Improving Unmanned Aerial Vehicle Remote Sensing-Based Rice Nitrogen Nutrition Index Prediction with Machine Learning. *Remote Sens.* **2020**, *12*, 1–22, doi:10.3390/rs12020215.
30. Zheng, H.; Li, W.; Jiang, J.; Liu, Y.; Cheng, T.; Tian, Y.; Zhu, Y.; Cao, W.; Zhang, Y.; Yao, X. A comparative assessment of different modeling algorithms for estimating leaf nitrogen content in winter wheat using multispectral images from an un-manned aerial vehicle. *Remote Sens.* **2018**, *10*, 2026, doi:10.3390/rs10122026.

31. Parreiras, T.C.; Lense, G.H.E.; Moreira, R.S.; Santana, D.B.; Mincato, R.L. Using unmanned aerial vehicle and machine learning algorithm to monitor leaf nitrogen in coffee. *Coffee Sci.* **2020**, *15*, 1–9, doi:10.25186/v15i.1736.
32. De Freitas, A.F.; Nadaleti, D.H.S.; Silveira, H.R.D.O.; Carvalho, G.R.; Venturin, R.P.; Silva, V.A. Productivity and beverage sensory quality of arabica coffee intercropped with timber species. *Pesqui. Agropecuária Bras.* **2020**, *55*, doi:10.1590/s1678-3921.pab2020.v55.02240.
33. National Aeronautics and Space Administration—NASA. Power Data. Available online: <https://power.larc.nasa.gov/data-access-viewer/> (accessed on 29 March 2021).
34. Martinez, H.E.P.; Neves, J.C.L.; Shuler, J. Mineral Nutrition and Fertilization. In *Coffee: Production, Quality and Chemistry*; Farah, A., Ed.; Royal Society of Chemistry: London, UK, 2019, pp. 163–201.
35. Gitelson, A.A.; Kaufman, Y.J.; Merzlyak, M.N. Use of a green channel in remote sensing of global vegetation from EOS-MODIS. *Remote Sens. Environ.* **1996**, *58*, 289–298, doi:10.1016/S0034-4257(96)00072-7.
36. Rondeaux, G.; Steven, M.; Baret, F. Optimization of soil-adjusted vegetation indices. *Remote Sens. Environ.* **1996**, *55*, 95–107, doi:10.1016/0034-4257(95)00186-7.
37. Rouse, J.W.; Haas, R.H.; Deering, D.W.; Schell, J.A.; Harlan, J.C. *Monitoring the Vernal Advancement and Retrogradation (Green Wave Effect) of Natural Vegetation*; Type III, Final Report; NASA/GSFC: Greenbelt, MD, USA, 1974.
38. Huete, A.R. A soil-adjusted vegetation index (SAVI). *Remote Sens. Environ.* **1988**, *25*, 295–309, doi:10.1016/0034-4257(88)90106-X.
39. Dash, J.; Curran, P.J. The MERIS terrestrial chlorophyll index. *Int. J. Remote Sens.* **2004**, *25*, 5403–5413, doi:10.1080/0143116042000274015.
40. Gitelson, A.; Merzlyak, M.N. Quantitative estimation of chlorophyll-a using reflectance spectra: Experiments with autumn chestnut and maple leaves. *J. Photochem. Photobiol. B Biol.* **1994**, *22*, 247–252, doi:10.1016/1011-1344(93)06963-4.
41. Meyer, G.E.; Hindman, T.W.; Lakshmi, K. Machine Vision Detection Parameters for Plant Species Identification. In Proceedings of the Precision Agriculture and Biological Quality, Bellingham, DC, USA, 14 January 1998; pp. 327–335, doi:10.1117/12.336896.
42. Yang, Z.; Willis, P.; Mueller, R. Impact of band-ratio enhanced AWIFS image to crop classification accuracy. In Proceedings of the 17th William Pecora Memorial Remote Sensing Symposium, Denver, CO, USA, 18–20 November 2008.
43. Gamon, J.A.; Surfus, J.S. Assessing leaf pigment content and activity with reflectometer.

- New Phytol.* **1999**, 143, 105–117, doi:10.1046/j.1469-8137.1999.00424.x.
44. Mao, W.; Wang, Y.; Wang, Y. Real-time detection of between-row weeds using machine vision. In Proceedings of the ASAE Annual Meeting, Las Vegas, NV, USA, 27–30 July 2003; pp. 1–9, doi:10.13031/2013.15381.
  45. R Core Team. R: A Language and Environment for Statistical Computing, Vienna, Austria, 2013. Available online: <http://www.R-project.org/> (accessed on 10 July 2020).
  46. Liaw, A.; Wiener, M.; Breiman, L.; Cutler, A. Package “randomForest”, 2018. Available online: <https://cran.r-project.org/web/packages/randomForest/randomForest.pdf> (accessed on 10 July 2020).
  47. Breiman, L. Random Forests. *Mach. Learn.* **2001**, 45, 5–32.
  48. Son, N.T.; Chen, C.F.; Chen, C.R.; Minh, V.Q. Assessment of Sentinel-1A data for rice crop classification using random forests and support vector machines. *Geocarto Int.* **2018**, 33, 587–601, doi:10.1080/10106049.2017.1289555.
  49. Oliveira, S.; Oehler, F.; San-Miguel-Ayanz, J.; Camia, A.; Pereira, J.M.C. Modeling spatial patterns of fire occurrence in Med-iterranean Europe using Multiple Regression and Random Forest. *For. Ecol. Manage.* **2012**, 275, 117–129, doi:10.1016/j.foreco.2012.03.003.
  50. Rodriguez-Galiano, V.F.; Chica-Olmo, M.; Abarca-Hernandez, F.; Atkinson, P.M.; Jeganathan, C. Random Forest classification of Mediterranean land cover using multi-seasonal imagery and multi-seasonal texture. *Remote Sens. Environ.* **2012**, 121, 93–107, doi:10.1016/j.rse.2011.12.003.
  51. Kohavi, R. A Study of Cross-Validation and Bootstrap for Accuracy Estimation and Model Selection. *Int. Jt. Conf. Artif. Intell.* **1995**, 2, 1137–1143.
  52. Foody, G.M. Status of land cover classification accuracy assessment. *Remote Sens. Environ.* **2002**, 80, 185–201, doi:10.1016/S0034-4257(01)00295-4.
  53. Hand, D.J.; Till, R.J. A Simple Generalisation of the Area Under the ROC Curve for Multiple Class Classification Problems. *Mach. Learn.* **2001**, 45, 171–186, doi:10.1023/A:1010920819831.
  54. Hunt, E.R.; Doraiswamy, P.C.; McMurtrey, J.E.; Daughtry, C.S.T.; Perry, E.M.; Akhmedov, B. A visible band index for remote sensing leaf chlorophyll content at the Canopy scale. *Int. J. Appl. Earth Obs. Geoinf.* **2013**, 21, 103–112, doi:10.1016/j.jag.2012.07.020.
  55. Hunt, E.R.; Daughtry, C.S.T.; Eitel, J.U.H.; Long, D.S. Remote sensing leaf chlorophyll content using a visible band index. *Agron. J.* **2011**, 103, 1090–1099,



- doi:10.2134/agronj2010.0395.
56. Gitelson, A.A.; Viña, A.; Ciganda, V.; Rundquist, D.C.; Arkebauer, T.J. Remote estimation of canopy chlorophyll content in crops. *Geophys. Res. Lett.* **2005**, *32*, 1–4, doi:10.1029/2005GL022688.
  57. Nigon, T.J.; Mulla, D.J.; Rosen, C.J.; Cohen, Y.; Alchanatis, V.; Rud, R. Evaluation of the nitrogen sufficiency index for use with high resolution, broadband aerial imagery in a commercial potato field. *Precis. Agric.* **2014**, *15*, 202–226, doi:10.1007/s11119-013-9333-6.
  58. Bendig, J.; Yu, K.; Aasen, H.; Bolten, A.; Bennertz, S.; Broscheit, J.; Gnyp, M.L.; Bareth, G. Combining UAV-based plant height from crop surface models, visible, and near infrared vegetation indices for biomass monitoring in barley. *Int. J. Appl. Earth Obs. Geoinf.* **2015**, *39*, 79–87, doi:10.1016/j.jag.2015.02.012.
  59. Fernández, P.D.M.; Peña, F.A.G.; Ren, T.I.; Leandro, J.J.G. Fast and robust multiple ColorChecker detection using deep convolutional neural networks. *Image Vis. Comput.* **2018**, *81*, 15–24, doi:10.1016/j.imavis.2018.11.001.
  60. Prati, R.C.; Batista, G.E.D.A.P.A.; Monard, M.C. Evaluating Classifiers Using ROC Curves. *IEEE Lat. Am. Trans.* **2008**, *6*, 215–222, doi:10.1109/TLA.2008.4609920.
  61. Fawcett, T. An introduction to ROC analysis. *Pattern Recognit. Lett.* **2006**, *27*, 861–874, doi:10.1016/j.patrec.2005.10.010.
  62. Park, S.H.; Goo, J.M.; Jo, C.H. Receiver operating characteristic (ROC) curve: Practical review for radiologists. *Korean J. Radiol.* **2004**, *5*, 11–18, doi:10.3348/kjr.2004.5.1.11.
  63. Fageria, N.K.; Baligar, V.C.; Li, Y.C. The role of nutrient efficient plants in improving crop yields in the twenty first century. *J. Plant Nutr.* **2008**, *31*, 1121–1157, doi:10.1080/01904160802116068.

## CHAPTER IV: DETECTING COFFEE LEAF RUST WITH UAV-BASED VEGETATION INDICES AND DECISION TREE MACHINE LEARNING MODELS

### This chapter is based on:

Article submitted in the journal “*Computers and Electronics in Agriculture*” on November 13, 2020.

(PRELIMINARY VERSION)

**Abstract:** Coffee leaf rust (CLR) is one of the most devastating leaf diseases in coffee plantations. By knowing the symptoms, severity, and spatial distribution of CLR, farmers can improve disease management procedures and reduce losses associated with it. Recently, Unmanned Aerial Vehicles (UAVs)-based images, in conjunction with machine learning (ML) techniques, helped solve multiple agriculture-related problems. In this sense, vegetation indices processed with ML algorithms are a promising strategy. It is still a challenge to map severity levels of CLR using remote sensing data and an ML approach. Here we propose a framework to detect CLR severity with only spectral indices extracted from UAV-imagery. For that, we based our approach on decision tree models, as they demonstrated important results in related works. We evaluated a coffee field with different infestation classes of CLR: class 1 (from 2% to 5% rust); class 2 (from 5% to 10% rust); class 3 (from 10% to 20% rust), and; class 4 (from 20% to 40% rust). We acquired data with a Sequoia camera, producing images with a spatial resolution of 10.6 cm, in four spectral bands: green (530–570 nm), red (640–680 nm), red-edge (730–740 nm), and near-infrared (770–810 nm). A total of 63 vegetation indices was extracted from the images, and the following learners were evaluated in a cross-validation method with 10 folders: Logistic Model Tree (LMT); J48; ExtraTree; REPTree; Functional Trees (FT); Random Tree (RT), and; Random Forest (RF). The results indicated that the LMT method contributed the most to the accurate prediction of early and several infestation classes. For these classes, LMT returned F-measure values of 0.915 and 0.875, thus being a good indicator of early CLR (2 to 5% of rust) and later stages of CLR (20 to 40% of rust). We demonstrated a valid approach to model rust in coffee plants using only vegetation indices and ML algorithms, specifically for the disease's early and later stages. We concluded that the proposed framework allows inferring the predicted classes in remaining plants within the sampled area, thus helping the identification of potential CLR in non-sampled plants. We corroborate that the decision

tree-based model may assist in precision agriculture practices, including mapping rust in coffee plantations, providing both an efficient non-invasive and spatially continuous monitoring of the disease.

**Keywords:** multispectral imagery; precision agriculture; plant disease; logistic model tree.

## 1. Introduction

Coffee leaf rust (CLR), caused by the fungus *Hemileia vastatrix*, consists of one of the most devastating leaf diseases (Suresh et al. 2012) and a severe threat to coffee production (Cressey, 2013; Cristancho et al. 2012). In the absence of early detection and proper management, CLR can result in up to 50% loss of leaves and a reduction of 70% in coffee production due to premature leaf fall, the death of primary branches, and the weakening of the plant itself (Silva et al. 2006; Pozza, 2010). Knowing the symptoms, the severity, and the spatial distribution of CLR in the field is essential to guide disease management procedures and reduce losses associated with it. Therefore, possible crop protection methods' success depends heavily on the early detection of the CLR disease (Chemura et al. 2018).

Remote sensing systems provide farmers with accurate, updated, and rapid information on crops' conditions, reducing cultivars' protection costs, as disease control can be done early and in a more targeted manner (Barbedo 2013). Remote sensing of plant diseases can be seen as one type of a "radio-diagnosis" approach to monitor plants, being capable of providing efficient, non-invasive, and spatially continuous monitoring of diseases and pests (Zhang et al. 2019). Plants infected by diseases and pests show differences in their spectral reflectance response compared to healthy plants (Marin et al. 2019). The physiological reaction of a diseased plant will result in the change in reflectance pattern in the spectral ranges of the visible, near, and medium infrared regions, mainly because of the decrease in the chlorophyll content and changes in the internal structures of the leaves (Martinelli et al. 2015).

Recently, remote sensing systems have already been used to evaluate CLR in coffee plantations. It is possible to find studies that used data from orbital and terrestrial platforms and some applied machine learning methods to this data. For example, Pires et al. (2020) used satellites images from the Landsat-7 / ETM + and Landsat-8 / OLI-TIRS to assess the CLR epidemic in different irrigation management systems, and they reported a Pearson correlation up to -0.61 between the average reflectance of the NIR and the incidence of CLR. Chemura et

al. (2017; 2018) conducted a study in a greenhouse to evaluate the Sentinel-2 orbital images' potential for discriminating CLR infection levels using machine learning methods. For that, the reflectance measurements of the Apogee VIS-NIR handheld radio spectrum were resampled to simulate the MSI sensors' spectral bands. Chemura et al. (2017; 2018) argued that Sentinel-2 has a high potential to discriminate the levels of CLR infection, however, they recommended that further studies under field conditions should be carried out to consolidate their methodology. Although these studies have shown promising results, it should be noted that the application of orbital remote sensing in field conditions, especially for small farms, is generally limited due to mainly the low spatial resolution, clouds interference, and high cost of operation compared to Unmanned Aerial Vehicles-embedded sensors (Zhang et al. 2016; Zhou et al. 2016). Sub-orbital remote sensing systems like UAVs have high flexibility, as the altitude can be adjusted based on spatial requirements depending on the task of interest (Lan et al. 2020). In this sense, they can be used in small areas (Santos et al. 2019), with a low-cost advantage (Zhou et al. 2016).

In recent years, UAV images combined with machine learning (ML) techniques have brought up a new manner to examine datasets, attending different areas like precision agriculture (Calou et al. 2020). The UAV technologies are able to acquire datasets with a high spatial-temporal resolution, and machine learning offers favorable computational and analytical solutions for the integrated study of different types of datasets (Honkavaara et al. 2013; Priya and Ramesh, 2020). Machine learning methods can solve nonlinear problems using data sets from various sources (Liakos et al. 2018; Ali et al. 2015) and discover information hidden in the given data (Qiu et al. 2016). These methods' main ability is to generalize patterns from the available data, allowing them to develop robust and flexible forecasting models (Priya and Ramesh, 2020). One type of ML approach that has been gaining attention in remote sensing agriculture-related issues refers to decision tree models (Misha et al. 2016; Priya and Ramesh, 2020). These methods have been applied to predictions including nitrogen content and plant height (Osco et al., 2019; Osco et al. 2020a), macro and micronutrients content in leaves (Amirruddin et al. 2020; Osco et al., 2020b), grain-yield quantities (Marques Ramos et al., 2020), among others.

In this regard, the combined potential of UAVs with ML was already established to assess different diseases in plants in multiple cultures, such as citrus (DadrasJavan et al. 2019), tomato (Abdulridha et al. 2020), chestnut trees (Pádua et al. 2020), banana (Selvaraj et al. 2020), and others. However, for coffee cultures, up until now, no study has been found that assesses the potential of this method into predicting different stages of the CLR disease. Since ML models

can extract information obtained directly from UAV images' spectral indices, this study hypothesizes that this combined information can be an interesting tool for the evaluation of the CLR disease severity in commercial plantations. As the identification of different CLR stages, specifically in early phases of rust, is an important aspect in both correction and management of the crop conditions, our study proposes an easily reproducible framework to detect rust symptoms in leaves with only spectral indices from UAV-based remote systems. Here we based our approach on multiple decision tree models. Additionally, an inference mapping method considering the area evaluated is also proposed by the end of our framework.

## **2. Materials and Method**

### **2.1. Data Collection**

The study was carried out on a commercial farm on the Salto das Três Barras, located in the municipality of Nepomuceno, Minas Gerais, Brazil, with 892 m of average altitude (Figure 1). The region's climate, according to the Köppen climate classification, is Cwa (wet temperate), with hot summers and dry winters, with an average annual temperature of 19.4 °C and total annual precipitation of approximately 1,530 mm. The area has an approximate total of 9 ha, cultivated with coffee trees (*Coffea arabica* L.), of the cultivar Catuai 99, with 5 years since initial planting, with a spacing of 3.5 m between rows and 0.7 m between plants, totaling 4081 plants ha<sup>-1</sup> (Figure 1). In the field, 20 sample points were randomly demarcated. Each sampling point was composed of 5 plants, 1 central plant, and 2 plants in the east-west direction of the central plant. For the analysis of CLR, 4 leaves from the third and fourth pairs of leaves were collected in each of the five plants from the sampling points, counted from the end of the plagiotropic branch. This totalized 20 leaves per sampling point, and 400 leaves samples for the whole area, covering 100 coffee plants in total.

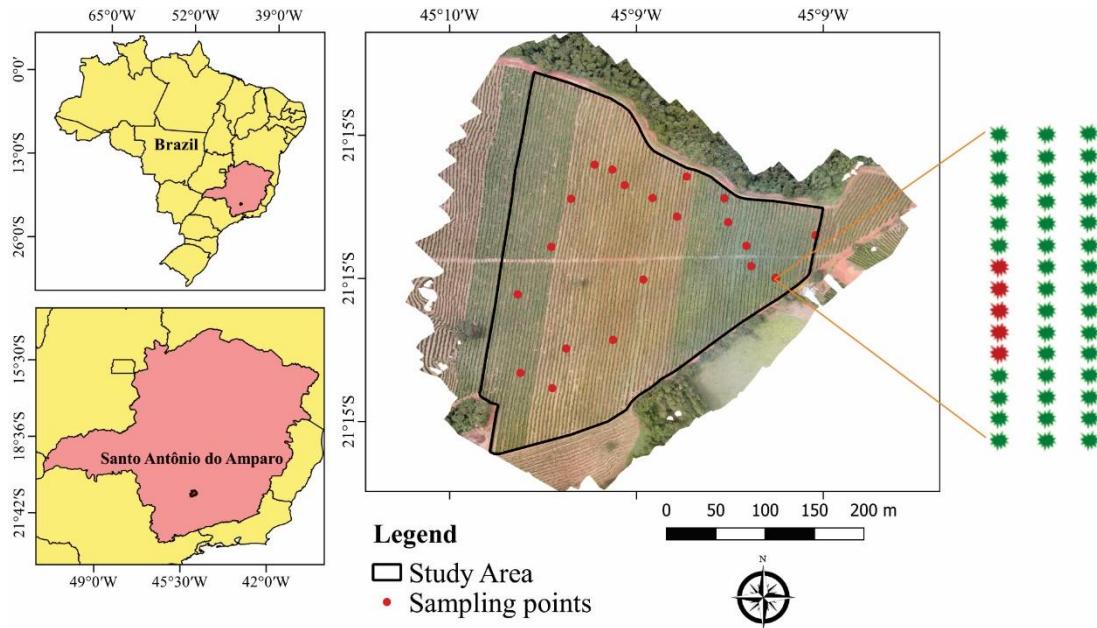


**Figure 1.** The geographic location of the studied area and illustration of the defined sampling points.

## 2.2 Coffee Leaf Rust (CLR) Analysis

The rust severity assessments were carried out by agricultural technicians, specialists in coffee diseases, observing the symptoms of the disease in the leaves of the plants. For this, 4 classes were defined according to the percentage of leaf area with symptoms of the disease, being: class 1 (from 2% to 5% rust); class 2 (from 5% to 10% rust); class 3 (from 10% to 20% rust), and; class 4 (from 20% to 40% rust). This approach was based on Capucho et al. (2011), with modifications, to estimate severities of CLR with an area-diagram based method. It was also conducted with the help of specialists in the field. As each sample point received 20 evaluations notes, the criterion used to determine the severity value was the highest frequency of the evaluation note at the sample point.

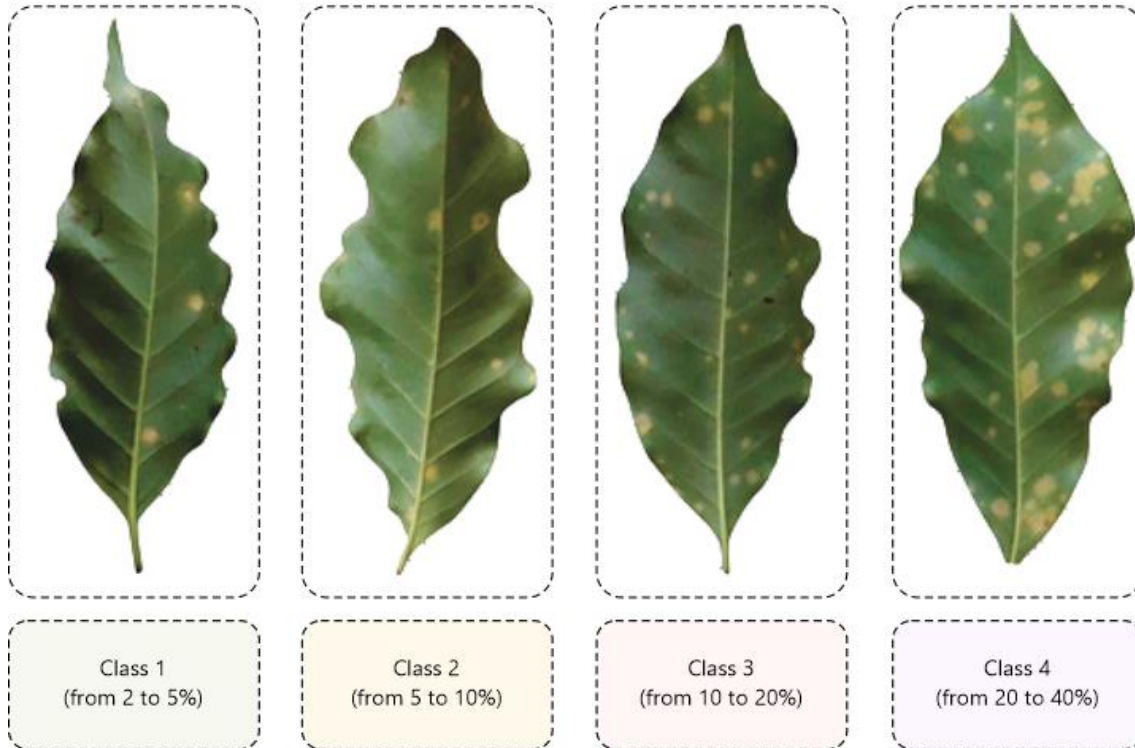


**Figure 2.** Examples of collected coffee leaves with different degrees of CLR disease severity.

### 2.3. UAV Image Acquisition and Preprocessing

The images were acquired between 12:00 and 14:00 (local time) on a non-cloudy day with low wind speed, using a commercial 3DR Solo UAV (3D Robotics, Berkeley, CA, United States) with a rotary-wing and four engines (quadcopter), equipped with the Parrot Sequoia multispectral camera. This camera has four sensors with a resolution of 1.5 megapixels (1280 x 960) in the spectral regions of green (530–570 nm), red (640–680 nm), red-edge (730–740 nm), and near-infrared (770–810 nm). In addition to it, the camera has an up-facing “sunshine sensor”, which allows radiometric calibration of these 4 multispectral bands during image collection (Sequoia User Guide, 2017). The flight missions were performed autonomously using the Mission Planner software (Osborne, 2018), executed on a portable computer. The flight altitude was fixed at 60 m above ground level, and the average speed was  $3 \text{ m}\cdot\text{s}^{-1}$ . The images were captured every 1 second and with 80% longitudinal and lateral overlap, resulting in a total of 448 scenes and an orthomosaic with 10.6 cm spatial resolution.

Image processing was performed using the Pix4Dmapper software, version 4.4.12 (Pix4D, Lausanne, Switzerland). Pix4Dmapper's standard "Ag Multispectral" model was used to generate the orthomosaics of the individual spectral bands (green, red, red-edge, and near-infrared), and the 20 control points were used to georeference the image. To identify the

sampling points in the orthomosaic, control points, visible from the image, were positioned next to the central plant of each sampling point and recorded with a GNSS. After the generation of the orthomosaics, a total of 63 vegetation indices (Table 1) were calculated in Pix4D and exported for further analysis. For this purpose, the average value of the pixels within a radius of 0.20 m was extracted from the center of each sampled plant. This radius was adopted since it covered the majority of pixels from the plant, thus removing any ground-related interference. These values were organized, and their respective class of CLR was added as ground-truth.

## **2.4 Vegetation indices**

We selected 63 vegetation indices (Table 1) based on the Index database (2019). For this, we considered the vegetation indices only associated with the spectral bands of the Parrot Sequoia camera alongside ideal intervals to identify the CLR.



**Table 1** Vegetation indices of multispectral images obtained using UAV.

(Continua)

Index	Equation
Green Ratio Vegetation Index (GRVI)	$NIR/G$
Green Difference Vegetation Index (GDVI)	$NRI - G$
Green Normalized Difference Vegetation Index (GNDVI)	$(NRI - G)/(NRI + G)$
Green Wide Dynamic Range Vegetation Index (GWDRVI)	$\frac{(a * NRI - G)}{(a * NRI + G)}$ (a = 0.12)
Green Chlorophyll Index (CIg)	$NIR/G - 1$
Modified Green Simple Ratio (MSR_G)	$(NIR/G - 1)/\sqrt{(NIR/G + 1)}$
Green Soil Adjusted Vegetation Index (GSAVI)	$1.5 * \left[ \frac{(NIR - G)}{(NIR + G + 0.5)} \right]$
Modified Soil Adjusted Vegetation Index (MSAVI)	$0.5 * [2 * NIR + 1 - \sqrt{(2 * NIR + 1)^2 - 8 * (NIR - G)}]$
Green Optimal Soil Adjusted Vegetation Index (GOSAVI)	$(1 + 0.16)(NIR - G)/(NIR + G + 0.16)$
Green Re-normalized Different Vegetation Index (GRDVI)	$\frac{(NIR - G)}{\sqrt{NIR + G}}$
Normalized Green Index (NGI)	$G/(NIR + RE + G)$
Normalized Red Edge Index (NREI)	$RE/(NIR + RE + G)$
Normalized Red Index (NRI)	$R/(NIR + RE + R)$
Normalized NIR Index (NNIR)	$NIR/(NIR + RE + G)$
Modified Double Difference Index (MDD)	$(NIR - RE) - (RE - G)$
Modified Normalized Difference Index (MNDI)	$\frac{(NIR - RE)}{(NIR - G)}$
Modified Enhanced Vegetation Index (MEVI)	$\frac{2.5 * (NIR - RE)}{(NIR + 6 * RE - 7.5 * G + 1)}$
Modified Normalized Difference Red Edge (MNDRE)	$\frac{[NIR - (RE - 2 * G)]}{[NIR + (RE - 2 * G)]}$
Modified Chlorophyll Absorption In Reflectance Index1 (MCARI1)	$\frac{[(NIR - RE) - 0.2(NIR - R)] \left( \frac{NIR}{RE} \right)}{1.5[2.5(NIR - R) - 1.3(NIR - RE)]}$
Modified Chlorophyll Absorption In Reflectance Index 2 (MCARI2)	$\frac{1.5[2.5(NIR - R) - 1.3(NIR - RE)]}{\sqrt{(2 * NIR + 1)^2 - (6 * NIR - 5\sqrt{R}) - 0.5}}$
Normalized Difference Vegetation Index (NDVI)	$\frac{(NIR - R)}{(NIR + R)}$
Ratio Vegetation Index (RVI)	$NIR/R$
Difference Vegetation Index (DVI)	$NIR - R$
Renormalized Difference Vegetation Index (RDVI)	$\frac{(NIR - R)}{\sqrt{(NIR + R)}}$
Wide Dynamic Range Vegetation Index (WDRVI)	$\frac{(a * NIR - R)}{(a * NIR + R)}$ (a = 0.12)
Soil-Adjusted Vegetation Index (SAVI)	$\frac{1.5 * (NIR - R)}{(NIR + R + 0.5)}$
Optimized SAVI (OSAVI)	$\frac{(1 + 0.16) * (NIR - R)}{(NIR + R + 0.16)}$
Modified Soil-adjusted Vegetation Index (MSAVI)	$0.5 * [2 * NIR + 1 - \sqrt{(2 * NIR + 1)^2 - 8 * (NIR - R)}]$
Transformed Normalized Vegetation Index (TNDVI)	$\sqrt{(NIR - R)/(NIR + R) + 0.5}$

**Table 1** Vegetation indices of multispectral images obtained using UAV.

(Continua)

Index	Equation
Modified Simple Ratio (MSR)	$(\text{NIR}/\text{R} - 1) / \sqrt{(\text{NIR}/\text{R} + 1)}$
Optimal Vegetation Index (VI <sub>opt</sub> )	$1.45 * ((\text{NIR}^2 + 1)/(\text{R} + 0.45))$
MERIS Terrestrial Chlorophyll Index (MTCI)	$\frac{(\text{NIR} - \text{RE})}{(\text{RE} - \text{R})}$
Nonlinear Index (NLI)	$(\text{NIR}^2 - \text{R})/(\text{RE} - \text{R})$
Modified Nonlinear Index (MNLI)	$1.5 * (\text{NIR}^2 - \text{R})/(\text{NIR}^2 + \text{R} + 0.5)$
NDVI*RV	$(\text{NIR}^2 - \text{R})/(\text{NIR} + \text{R}^2)$
SAVI*SR	$(\text{NIR}^2 - \text{R})/[(\text{NIR} + \text{R} + 0.5) * \text{R}]$
Normalized Difference Red Edge (NDRE)	$(\text{NIR} - \text{RE})/(\text{NIR} + \text{RE})$
Red Edge Ratio Vegetation Index (RERVI)	$\frac{\text{NIR}}{\text{RE}}$
Red Edge Difference Vegetation Index (REDVI)	$\text{NIR} - \text{RE}$
Red Edge Renormalized Different Vegetation Index (RERDVI)	$\frac{(\text{NIR} - \text{RE})}{\sqrt{\text{NIR} + \text{RE}}}$
Red Edge Wide Dynamic Range Vegetation Index (REWDRVI)	$\frac{(a * \text{NIR} - \text{RE})}{(a * \text{NIR} + \text{RE})}$ (a = 0.12)
Red Edge Soil Adjusted Vegetation Index (RESAVI)	$1.5 * \left[ \frac{(\text{NIR} - \text{RE})}{(\text{NIR} + \text{RE} + 0.5)} \right]$
Red Edge Optimal Soil Adjusted Vegetation Index (REOSAVI)	$(1 + 0.16)(\text{NIR} - \text{RE})/(\text{NIR} + \text{RE} + 0.16)$
Modified Red Edge Soil Adjusted Vegetation Index (MRESAVI)	$0.5 * [2 * \text{NIR} + 1 - \sqrt{(2 * \text{NIR} + 1)^2 - 8 * (\text{NIR} - \text{RE})}]$
Optimized Red Edge Vegetation Index (REVI <sub>opt</sub> )	$100 * (\ln \text{NIR} - \ln \text{RE})$
Red Edge Chlorophyll Index (CI <sub>re</sub> )	$\text{NIR}/\text{RE} - 1$
Modified Red Edge Simple Ratio (MSR <sub>RE</sub> )	$\frac{(\text{NIR}/\text{RE} - 1)}{\sqrt{(\text{NIR}/\text{RE} + 1)}}$
Red Edge Normalized Difference Vegetation Index (RENDVI)	$\frac{(\text{RE} - \text{R})}{(\text{RE} + \text{R})}$
Red Edge Simple Ratio (RESR)	$\text{RE}/\text{R}$
Modified Red Edge Difference Vegetation Index (MREDVI)	$\text{RE} - \text{R}$
MERIS Terrestrial Chlorophyll Index (MTCI)	$(\text{NIR} - \text{RE})/(\text{RE} - \text{R})$
DATT Index (DATT)	$(\text{NIR} - \text{RE})/(\text{NIR} - \text{R})$
Normalized Near Infrared Index (NNIRI)	$\text{NIR}/(\text{NIR} + \text{RE} + \text{R})$
Normalized Red Edge Index (NREI)	$\text{RE}/(\text{NIR} + \text{RE} + \text{R})$
Normalized Red Index (NRI)	$\text{R}/(\text{NIR} + \text{RE} + \text{R})$
Modified Double Difference Index (MDD)	$(\text{NIR} - \text{RE}) - (\text{RE} - \text{R})$
Modified Red Edge Simple Ratio (MRESR)	$(\text{NIR} - \text{R})/(\text{RE} - \text{R})$
Modified Normalized Difference Index (MNDI)	$(\text{NIR} - \text{RE})/(\text{NIR} + \text{RE} - 2 * \text{R})$
Modified Enhanced Vegetation Index (MEVI)	$\frac{2.5 * (\text{NIR} - \text{R})}{(\text{NIR} + 6 * \text{R} - 7.5 * \text{RE} + 1)}$
Modified Normalized Difference Red Edge (MNDRE2)	$\frac{(\text{NIR} - \text{RE} + 2 * \text{R})}{(\text{NIR} + \text{RE} - 2 * \text{R})}$
Red Edge Transformed Vegetation Index (RETVI)	$0.5 * [120 * (\text{NIR} - \text{R}) - 200 * (\text{RE} - \text{R})]$

**Table 1** Vegetation indices of multispectral images obtained using UAV.

(Conclusão)

Index	Equation
Modified Chlorophyll Absorption In Reflectance Index 3 (MCARI3)	$\frac{[(\text{NIR} - \text{RE}) - 0.2 * (\text{NIR} - \text{R})] \left(\frac{\text{NIR}}{\text{RE}}\right)}{1.5[2.5(\text{NIR} - \text{G}) - 1.3(\text{NIR} - \text{RE})]}$
Modified Chlorophyll Absorption In Reflectance Index 4 (MCARI4)	$\frac{\sqrt{(2 \text{ NIR} + 1)^2 - (6 \text{ NIR} - 5 \sqrt{\text{G}}) - 0.5}}{3 * [(\text{NIR} - \text{RE}) - 0.2 * (\text{NIR} - \text{R})] \left(\frac{\text{NIR}}{\text{RE}}\right)}$
Modified Transformed Chlorophyll Absorption In Reflectance Index (MTCARI)	$3 * [(\text{NIR} - \text{RE}) - 0.2 * (\text{NIR} - \text{R})] \left(\frac{\text{NIR}}{\text{RE}}\right)$
Modified Red Edge Transformed Vegetation Index (MRETVI)	$1.2 * [1.2 * (\text{NIR} - \text{R}) - 2.5 * (\text{RE} - \text{R})]$
Modified Canopy Chlorophyll Content Index (MCCCI)	NDRE/NDVI
MCARI1/OSAVI	MCARI1/OSAVI

## 2.5 Machine Learning Analysis

The machine learning models based on the decision and regression trees evaluated in this study were Logistic Model Tree (LMT); J48 (C4.5); ExtraTree; REPTree; Functional Trees (FT); Random Tree (RT), and; Random Forest (RF). They were implemented within the Weka 3.9.4 open-source program, integrating scikit-learn and R library of algorithms. We should point out that other state-of-the-art algorithms, aside from decision trees, like multilayers perceptron, support vector machines, linear, logistic, lazy, and bayesian models were also evaluated during an experimental phase of our study. Nonetheless, no pattern was observed in these analyses, and the majority of the results were inferior in comparison against decision tree-structured models.

Another important information to be clarified is the adoption of meta learners to improve the overall performance of the predictors and help define their hyperparameters with fine-tuning approaches. We tested different meta methods like boosting and search algorithms and, although some learners did benefit from their intervention, the gain in performance was too low (near 1%) in comparison against the baseline results. Because of that, we adopted a batch size for all decision tree models equal to 100, and the default library values were used as their hyperparameters in subsequent training and testing processes. The algorithms were evaluated in a personal computer equipped with an Intel(R) i7-8550U 1.80 GHz and 12 Gb RAM 2,333 MHz.

The LMT is composed of classification trees that use logistic regression functions within their leaves (Landwehr et al. 2005). The J48 is based on a pruned (or also unpruned) C4.5

decision tree (Quinlan, 1993). The ExtraTree uses randomized trees with independent structures in an ensemble approach (Geurts et al. 2006). The REPTree is a fast decision tree learner that constructs a decision/regression tree using information related to its gain/variance by reduced-error pruning with backfitting (Weka, 2020a). The FT functional trees with logistic regression functions at the inner nodes and/or leaves (Gama, 2004). The RT builds a non-pruning tree which considers K randomly chosen attributes at each node (Weka, 2020b). Lastly, the RF combines predictors from multiple trees where each tree depends on a random independent vector (Breiman et al., 2001).

The decision tree learners were evaluated in a cross-validation manner, using 10 folders in each run, in 10 consecutive runs. This ensured that 100 validation-sets were built and evaluated with different models from the same learner 10 times. The cross-validation method is one of the most efficient validation methods (Ramezan et al. 2019), and, in this case, it used 9 (or 90% of randomized data) from the 10 defined folders for training and 1 (or 10%) for validation. This configuration-set is repeated 10 times until every sample is used for validating the prediction of the model. Here, a total of 100 samples was used, and 10% of them were also separated for a testing phase, to ensure that all the algorithms were also evaluated in the same sample dataset. For evaluating the classification, we calculated the True-Positive (TP) and False-Positive (FP) Rates, the Receiver Operating Characteristic (ROC) curve, and the Precision, Recall, and F-measure values. A Shapiro-Wilk normality test was executed, followed by Mann-Whitneys' pairwise comparison to determine differences between the algorithms.

The described approach was able to indicate the overall best learner to model the given data to classify CLR according to its respective stages. Once this learner was defined, we implemented a ranking approach as reported in previous studies (Osco et al., 2019; Osco et al., 2020; Marques Ramos et al., 2020). Differently from Osco et al. (2019) that evaluated the contribution of individual vegetation indices with a Relief-F approach, here we implemented the ranking method based on the overall accuracy of our model. The ranking method calculates the increased or decreased difference in the performance of the algorithm against the performance of a baseline method in relation to a given input variable. As a baseline, the ZeroR algorithm was adopted since it uses the averaged value of the target variable (i.e. ground-truth) in its prediction. This returns a metric score for the individual input variables (i.e. vegetation indices in this case), thus indicating the contribution of each index into the model.

### 2.5.1 Map Inference

To perform the CLR inference in the remaining plants, we individually labelled all of the coffee plants in the area and extracted the values of the vegetation indices at the same 0.20 m radius from its center. Then, the average value of the pixels inside this radius was extracted, as in the sampling process, and organized in a similar dataset, adopting an “?” cell-value in the ground-truth column. It was necessary to ensure that the overall best learner would use the information from the input variables (vegetation indices), with the architecture predefined in the training phase, to predict the unknown values according to their respective CLR classes. Since it consists of an inference process in non-sampled data, we assume that the classification metrics results are sufficient to indicate the accuracy obtained within this process, mainly because it consists of the same sampled area and imagery.

Since we evaluated CLR severity classes from 2% to 40% rust leaf coverage, we ensured that plants that did not match the range of pixel values as in the sampled plants were excluded from the analysis. For this, we compared the interquartile values of the pixels inside the 0.20 m radius and, if the non-sampled plant returned values outside a 95% confidence interval, they were not considered. It was necessary since most of the plants in the experimental area present less than 2% of rust in their leaves. So to not wrongfully classify a health plant as a class 1 of CLR, we choose to implement this strategy. Thus, when producing the result in a cartographic product, only plants that were spectrally related to the CLR samples were represented. We choose to adopt different sizes and colors for each CLR class to improve the visualization. This approach could be useful for indicating the spatial distribution of CLR around the plantation field.

## 3. Results and discussion

Initially, we compared the training performance of the different decision tree models with multiple consecutive runs (Figure 3). The F-measure consists of a harmonic mean between Precision and Recall values (Han and Kamber, 2006), and was used to compare the overall performance of the individual models. Results state that multiple learners (LMT, RF, FT, and REPTree) presented similar performance (indicated by letter a) in the proposed task (Figure 3), according to the Mann-Whitney test with 95% of probability.

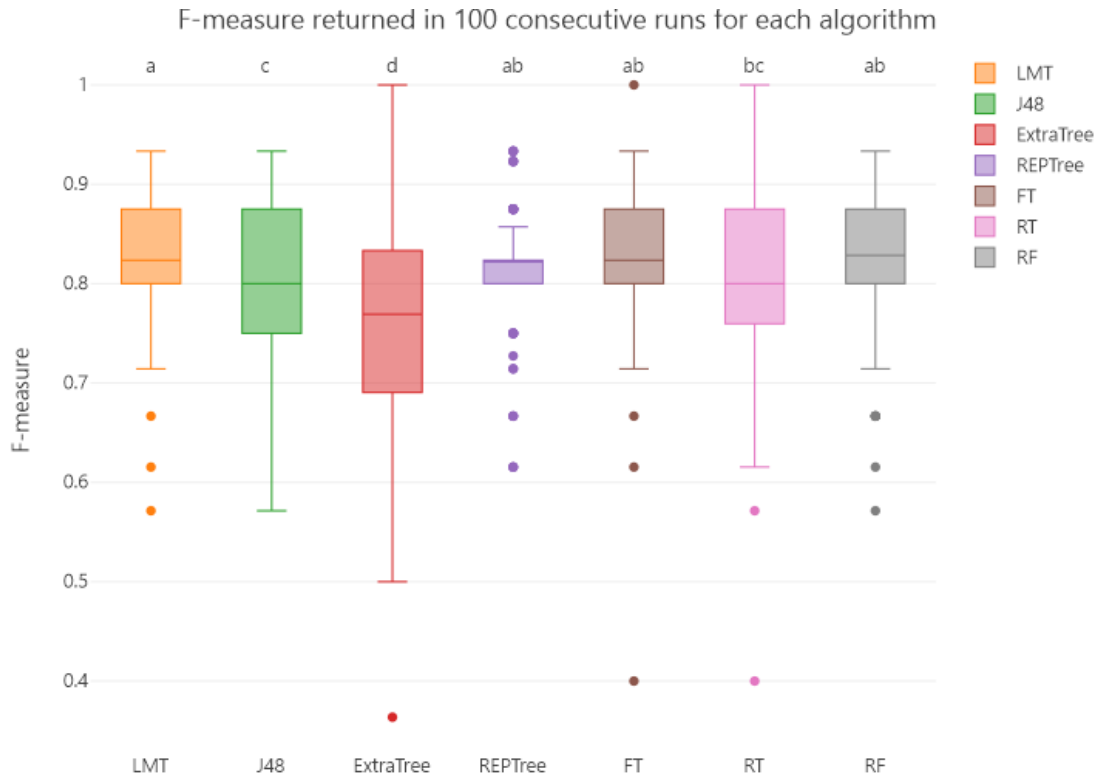


**Figure 3.** Box-plot indicating the F-measure results from the training analysis performed by 10 runs and 100 validation-sets. The same letters above the boxes indicate no statistical difference by the Mann-Whitney test at 95% probability.

The median F-measure value of LMT at training was 0.823, while RF achieved a value equal to 0.828. However, their performance significantly dropped with the testing set (Table 2), which was somewhat expected. This difference between training and testing phases was expected since the testing samples are not used during the training phase of the algorithm (Priya and Ramesh, 2020), and can be considered “never-before-seen” data, in any aspect, for the learning patterns of the algorithm. In our study case, the LMT F-measure value was superior (0.695) but was also followed by the RF value (0.677). RF, which is one of the most robust learners tested here, returned higher Precision and ROC area values, but LMT was superior overall in testing phases (Table 2). RF has been classified as an effective machine-learning method for attending to agriculture-related problems as demonstrated in recent studies (Jeong et al. 2016; Osco et al. 2020; Marques Ramos et al. 2020). Also, interestingly enough, the ExtraTree model (Table 2) returned the lowest FP Rate, but this model ROC area was not too low in comparison to the other learners.

**Table 2.** Averaged classification metrics values with the testing-set for the decision tree-based models used.

<b>Model</b>	<b>TP Rate</b>	<b>FP Rate</b>	<b>Precision</b>	<b>Recall</b>	<b>F-Measure</b>	<b>ROC Area</b>
LMT	<b>0.747</b>	0.494	<b>0.672</b>	<b>0.747</b>	<b>0.695</b>	0.734
J48	0.646	0.377	0.628	0.646	0.635	0.665
ExtraTree	0.616	<b>0.272</b>	0.654	0.616	0.628	0.672
REPTree	0.707	0.521	0.394	0.707	0.369	0.664
FT	0.737	0.494	0.660	0.737	0.676	0.713
RT	0.616	0.313	0.664	0.616	0.633	0.652
RF	0.717	0.455	<b>0.674</b>	0.717	0.677	<b>0.817</b>

To evaluate the classification results indicating the predictions according to the evaluated CLR classes, we used information extracted from their respective F-measures (for individual classes) and the relationship between TP and FP, illustrated in a ROC curve type of graphic (Figure 4). The ROC graphic and the respective F-measure class values indicated that the LMT algorithm was able to differentiate significantly the most severe CLR class (Class 4) from the others, with an F-measure equal to 0.915. This was followed by a high F-measure value for the earlier CLR class (Class 1), which is an indication of rust with a 2% to 5% leaf coverage. The remaining intermediate classes (2 and 3) returned lower values, like in Class 4, which was under 0.5 and, therefore, worse than a random-guess prediction (i.e. 50%). This confusion between the intermediate classes, however, explains the reason for LMT and other models' performance return values under an average of 0.7 in testing since they are the ones responsible for lowering this metric.

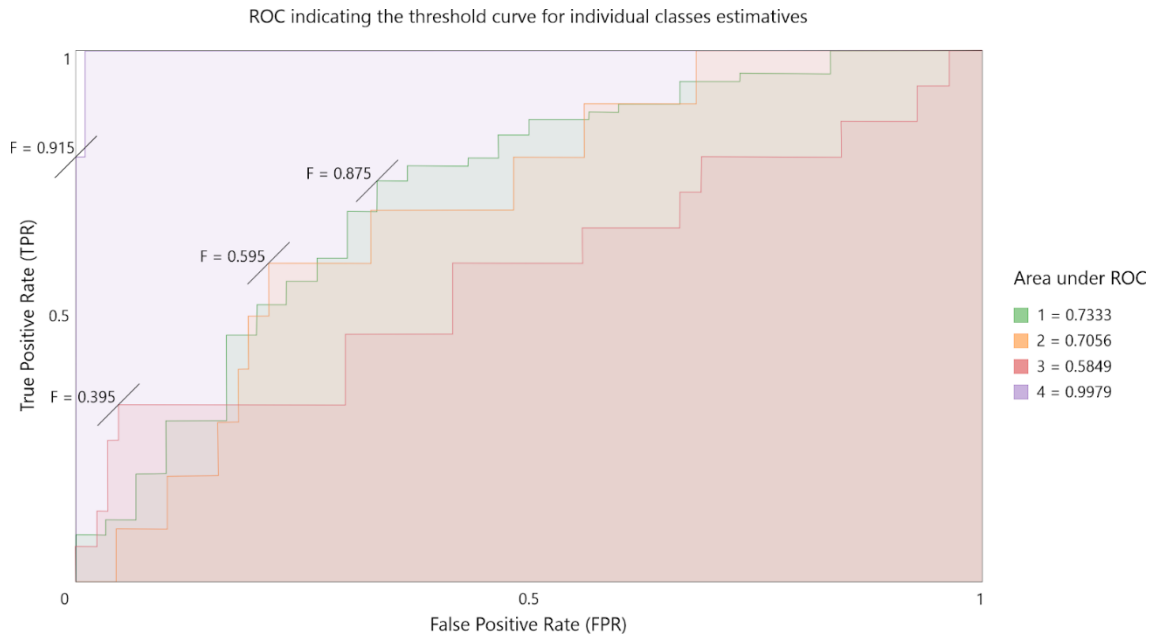


**Figure 4.** Receiver Operating Characteristic (ROC) of the prediction returned by the Logistic Model Tree (LMT) algorithm. F-measure value highlighted at the point with the best TP-FP ratio.

Although the intermediate stages of the disease are not well separated by the methods, it is important to highlight the differences in detecting early and late stages of the disease. According to Velásquez et al. (2020), coffee rust gradually progresses in the crop and reaches later stages. The initial stage of the disease, called the “slow phase” (severity  $\leq 5\%$ ), is where the first structures responsible for spore production appear, making the low levels of infection evident. In the final stage, called the maximum or terminal phase ”(severity  $> 30\%$ ), it occurs when most leaves are severely damaged and a small number of healthy leaves remain. Therefore, for the predictions of infection in the early stages, decision-making models may be able to indicate to farmers the correct time to initiate disease control measures, with applications of fungicides, for example, preventing the spread of the disease in the field. Regarding the predictions in the late stages, the models can be used to evaluate the efficiency of the control measures, as well as the need to modify these measures. Also, in the worst case, they can be used to estimate damage and productivity losses in the following years, as the high severity of the rust causes the defoliation of a large part of the plant.

To help ascertain the relationship between the adopted vegetation indices and the LMT model, we choose to plot a representation of its nodes and leaves (Figure 5). The LMT is constructed in a different manner than most regression/decision trees since it bases itself on a logistic function to determine the combined information (variable + value) of the input



vegetation indices necessary to predict each class (Landwehr et al. 2005). The LMT was already used in other remote sensing approaches non-related to agronomic variables (Colkesen and Kavzoglu, 2006). A study (Amirruddin et al. 2020) evaluating hyperspectral spectroscopy data implemented the LMT algorithm with an imbalance approach and a boosting method for classifying some nutrients in oil palm-trees, achieving satisfactory performances, with averaged accuracies between 0.760 and 1.000. Regarding plant monitoring, one research (Pham et al. 2018) used the ALOS PALSAR data to map the spatial distribution of mangrove species, resulting in an overall accuracy of 0.838. From the best of our knowledge, our study case appears to be the first conducted approach related to plant diseases that returned important estimations with the LMT algorithm.

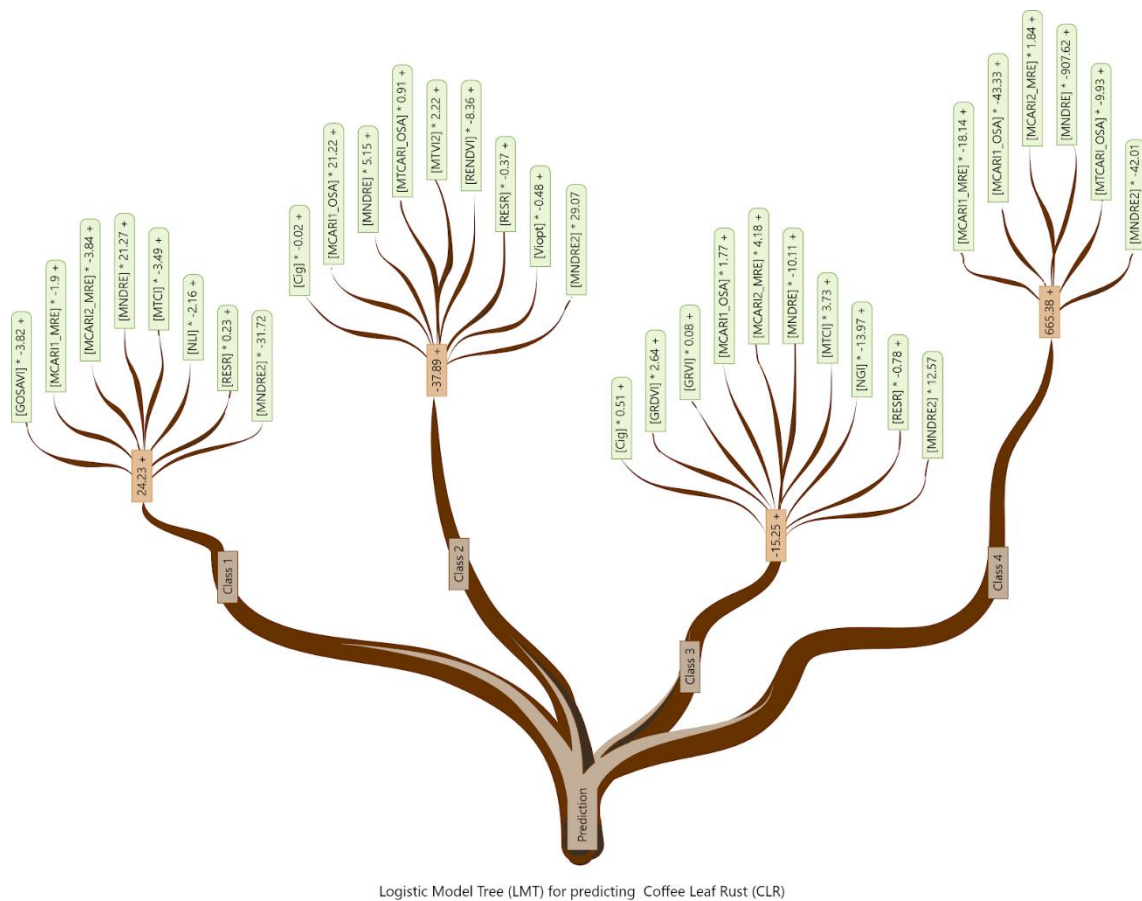


**Figure 5.** Logistic Model Tree (LMT) representation with the vegetation indices formula for each class prediction.

The ranking approach was performed to determine the individual contribution of the vegetation indices to the LMT model. The vegetation indices indicated by this approach differentiate themselves from the indices used by the LMT learner. It happens mainly because

machine learning algorithms, in a general sense, perform multiple combinations and calculations between the input variables (Priya and Ramesh, 2020). In this aspect, probably, the LMT model did not build its tree under the individual performance of the vegetation indices. Regardless, the ranking method, in this case, could offer some potential since it helps to reduce the number of variables (in this case, indices) evaluated by the algorithm. To ascertain this information, we calculated the Metric score of the individual spectral indices concerning a baseline learner ZeroR, and we choose to plot their increase in performance (Figure 6) while highlighting the spectral indices used by the LMT algorithm in its final prediction tree (Figure 5).

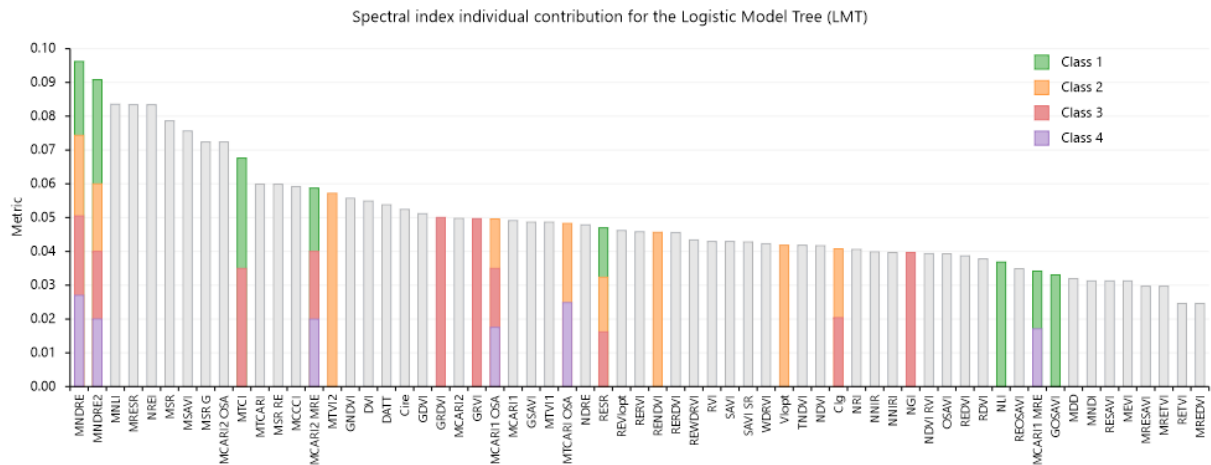


**Figure 6.** The individual contribution of the vegetation indices for the Logistic Model Tree (LMT).

The ranking approach was evaluated in previous studies related to agronomic variables that also adopted machine learning algorithms in their evaluation (Osco et al. 2020; Marques Ramos et al. 2020). This approach is interesting as it, as mentioned, reduces the number of input variables, returning the highest individually contributive ones in a rank, offering potential performance while decreasing the required computational cost. To test this method in the CLR prediction, we evaluated the LMT performances at an interval of 10 input variables decreasing, from the total 63 to only the top 3 spectral indices (Table 3).

**Table 3.** Averaged performance of the LMT learner when reducing the number of vegetation indices as input variables.

<b>Vegetation Indices (n)</b>	<b>Precision</b>	<b>Recall</b>	<b>F-Measure</b>	<b>ROC Area</b>
<b>63</b>	<b>0.672</b>	<b>0.747</b>	<b>0.695</b>	<b>0.734</b>
53	0.637	0.727	0.655	0.726
43	0.578	0.737	0.657	0.661
33	0.563	0.727	0.645	0.710
<b>23</b>	<b>0.666</b>	<b>0.737</b>	<b>0.685</b>	<b>0.724</b>
13	0.565	0.707	0.636	0.673
03	0.546	0.707	0.626	0.658

As expected, the accuracy variation occurred at each interval evaluated. It should be emphasized that decision trees benefit themselves from a higher input number of variables since their predictions are based on the combined accuracies of multiple decision nodes. However, at the 5th interval (Table 3), i.e., considering only 23 vegetation indices, the LMT model could return relative accuracy values from the total dataset (63 indices). This is important since decreasing the number of variables by 40, it helps to consider less computational costs for low-budget computers. As novel methods in remote sensing approaches are currently being proposed for both in-field and real-time evaluations (Benincasa et al. 2017; Marino et al. 2020), the amount of processed data was also considered.

To produce a graphic representation of the proposed approach, we estimated the CLR severity infection in the non-sampled portion of the experimental area and plot in a quantitative map (Figure 7). The cartographic product was composed of different size symbols according to the severity of the disease. Although most coffee plants (Figure 7) were classified in the less severity class (early stages of rust infestation by 2% to 5%), it is interesting to notice some patterns in the evaluated area. The most severely damaged plants were situated at the north portion of the plantation, while some intermediated classes (2 and 3) were present at the south portion. According to the results, we verified that the intermediate classes presented some degree of confusion between themselves, explaining the overall accuracy achieved by all tested machine learning models.

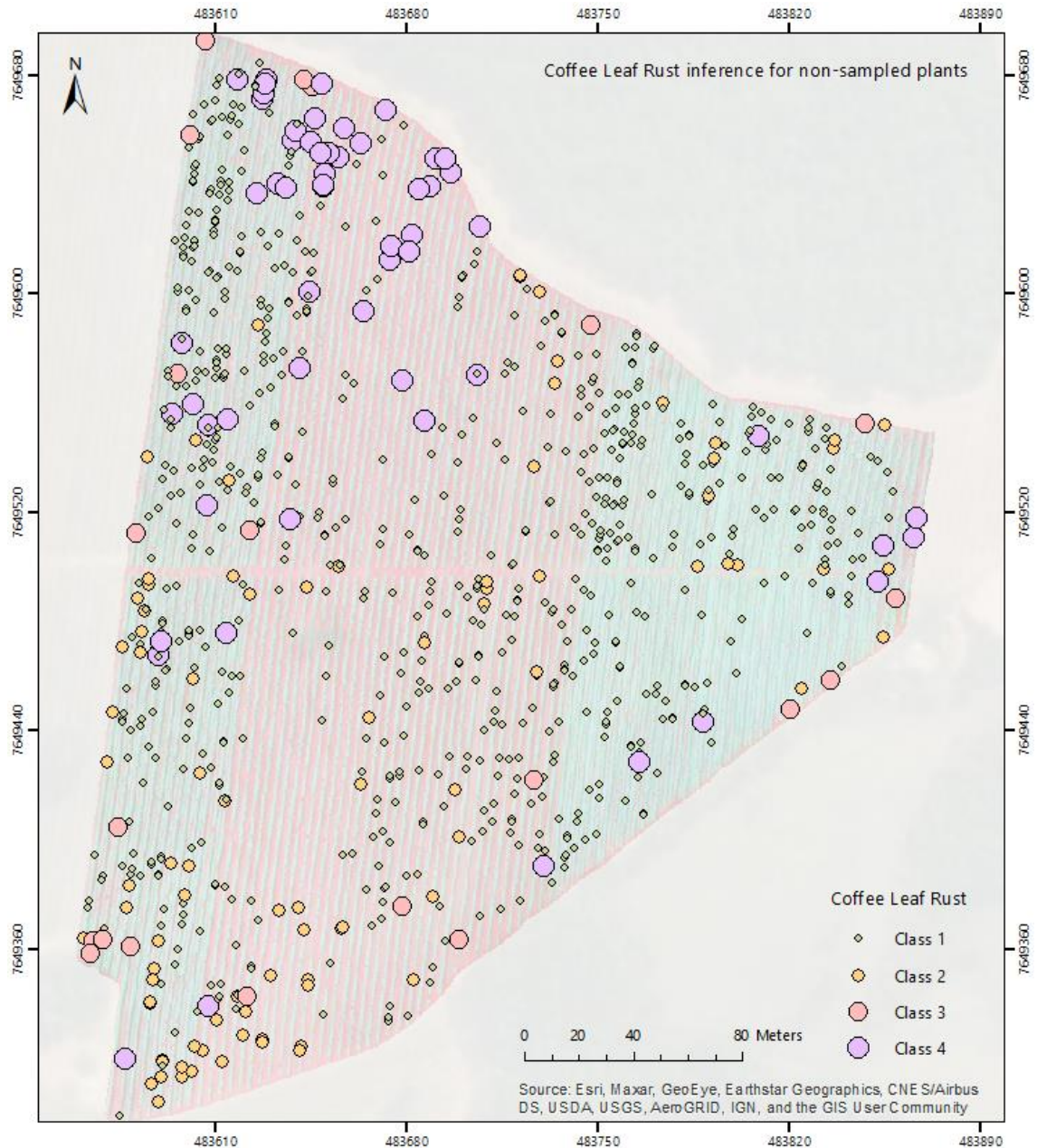


**Figure 7.** Predicted map of Coffee Leaf Rust (CLR) for the non-sampled portion of the area. The remaining plants were considered healthy since they were not classified in any of the predicted classes.

Regardless, LMT can be considered a valid approach to accurately detect the early stages (class 1) and the later stages (class 4) of the CLR disease. Knowing the spatial distribution of the severity of rust in the crop may indicate regions most susceptible to the disease. In this way, the producer can apply differentiated and targeted control measures to plants in early and later stages, reducing control costs and environmental contamination associated with excessive fungicide applications, as well as preventing the disease from spreading to healthy plants.

Besides, the CLR inference for non-sampled plants can produce a quick and accurate result of the disease severity across the crop, assisting the producer in the correct management. And, perhaps, most importantly, it can assist the current methods of assessing the disease, which in addition to being costly, demand excessive time that can hamper decision-making and quick response in controlling the disease.

#### **4. Conclusion**

In this study, we proposed a framework to detect Coffee Leaf Rust (CLR) using only vegetation indices extracted from UAV-based imagery. For that, we based our approach on decision tree models, as they are known to produce satisfactory predictions in related research. We found out that, although most of the evaluated machine learning models returned similar performance, the LMT method contributed the most to the accurate prediction of CLR disease. It achieved an overall Precision, Recall, and F-measures of 0.672, 0.747, and 0.695, respectively. Nonetheless, for classes 1 and 4, it returned F-measure values of 0.915 and 0.875, thus being a good indicator of early CLR (between 2 and 5%) and of later stages of CLR (between 20 and 40%).

We conclude that vegetation indices from UAV combined with ML algorithms based on decision trees are a valid approach to model rust in coffee plants, specifically in the early and later stages. Additionally, the rank approach allowed us to reduce by 63% the number of vegetation indices used in the LMT model without a large decrease in accuracy values in the prediction of CLR's stages. We also conclude that the framework to infer the predicted classes in the remaining plants within the sampled area is an interesting strategy to identify potential CLR. This model could assist in precision agriculture practices as it provides efficient non-invasive and spatially continuous monitoring of the disease.

#### **Acknowledgments**

This work was supported by the National Council for Scientific and Technological Development (CNPq), the Coordination for the Improvement of Higher Education Personnel (CAPES), the Federal University of Lavras (UFLA) and Empresa de Assistência Técnica e Extensão Rural do Estado de Minas Gerais (EMATER).

## References

- Abdulridha, J., Ampatzidis, Y., Qureshi, J., Roberts, P., 2020. Laboratory and UAV-based identification and classification of tomato yellow leaf curl, bacterial spot, and target spot diseases in tomato utilizing hyperspectral imaging and machine learning. *Remote Sens.* 12, 1–17. <https://doi.org/10.3390/RS12172732>
- Ali, I., Greifeneder, F., Stamenkovic, J., Neumann, M., Notarnicola, C., 2015. Review of machine learning approaches for biomass and soil moisture retrievals from remote sensing data. *Remote Sens.* 7, 16398–16421. <https://doi.org/10.3390/rs71215841>
- Amirruddin, A.D., Muharam, F.M., Ismail, M.H., Tan, N.P., Ismail, M.F., 2020. Hyperspectral spectroscopy and imbalance data approaches for classification of oil palm's macronutrients observed from frond 9 and 17. *Comput. Electron. Agric.* 178, 105768. <https://doi.org/10.1016/j.compag.2020.105768>
- Avelino, J., Willocquet, L., Savary, S., 2004. Effects of crop management patterns on coffee rust epidemics. *Plant Pathol.* 53, 541–547. <https://doi.org/10.1111/j.1365-3059.2004.01067.x>
- Barbedo J.G.A., 2013. Digital image processing techniques for detecting, quantifying and classifying plant diseases. *SpringerPlus* 2, 1–12. <https://doi.org/10.1186/2193-1801-2-660>
- Breiman, L., 2001. Random Forests. *Machine Learning* 45, 5–32.
- Benincasa, P., Antognelli, S., Brunetti, L., Fabbri, C.A., Natale, A., Sartoretti, V., Modeo, G., Guiducci, M., Tei, F., Vizzari, M., 2018. Reliability of ndvi derived by high resolution satellite and uav compared to in-field methods for the evaluation of early crop n status and grain yield in Wheat. *Exp. Agric.* 54, 604–622. <https://doi.org/10.1017/S0014479717000278>
- Calou, V.B.C., Teixeira, A. dos S., Moreira, L.C.J., Lima, C.S., de Oliveira, J.B., de Oliveira, M.R.R., 2020. The use of UAVs in monitoring yellow sigatoka in banana. *Biosyst. Eng.* 193, 115–125. <https://doi.org/10.1016/j.biosystemseng.2020.02.016>
- Chemura, A., Mutanga, O., Dube, T., 2017. Separability of coffee leaf rust infection levels with machine learning methods at Sentinel-2 MSI spectral resolutions. *Precis. Agric.* 18, 859–881. <https://doi.org/10.1007/s11119-016-9495-0>
- Chemura, A., Mutanga, O., Sibanda, M., Chidoko, P., 2018. Machine learning prediction of coffee rust severity on leaves using spectroradiometer data. *Trop. Plant Pathol.* 43, 117–127. <https://doi.org/10.1007/s40858-017-0187-8>
- Colkesen, I., Kavzoglu, T., 2017. The use of logistic model tree (LMT) for pixel- and object-

- based classifications using high-resolution WorldView-2 imagery. *Geocarto Int.* 32, 71–86. <https://doi.org/10.1080/10106049.2015.1128486>
- Cressey, D., 2013. Coffee rust regains foothold. Researchers marshal technology in bid to thwart fungal outbreak in Central America. *Nature* 493, 587.
- Cristancho, M., Rozo, Y., Escobar, C., Rivillas, C., Gaitán, A., 2012. Outbreak of coffee leaf rust (*Hemileia vastatrix*) in Colombia. *New Disease Reports* 25, 19. <https://doi.org/10.5197/j.2044-0588.2012.025.019>
- DadrasJavan, F., Samadzadegan, F., Seyed Pourazar, S.H., Fazeli, H., 2019. UAV-based multispectral imagery for fast Citrus Greening detection. *J. Plant Dis. Prot.* 126, 307–318. <https://doi.org/10.1007/s41348-019-00234-8>
- Gama, J., 2004. Functional Trees. *Machine Learning* 55, 219–250.
- Garçon, C.L.P., Zambolim, L., Mizubuti, E.S.G., Vale, F.X.R. do, Costa, H., 2004. Coffee leaf rust control based on rust severity values. *Fitopatol. Bras.* 29, 486–491. <https://doi.org/10.1590/s0100-41582004000500003>
- Ghini, R., Bettioli, W., Hamada, E., 2011. Diseases in tropical and plantation crops as affected by climate changes: Current knowledge and perspectives. *Plant Pathol.* 60, 122–132. <https://doi.org/10.1111/j.1365-3059.2010.02403.x>
- Han, J. D., Kamber, M., 2006. *Data Mining Concept and Tehniques*. Morgan Kauffman, San Fransisco.
- Honkavaara, E., Saari, H., Kaivosoja, J., Pölönen, I., Hakala, T., Litkey, P., Mäkyänen, J., Pesonen, L., 2013. Processing and assessment of spectrometric, stereoscopic imagery collected using a lightweight UAV spectral camera for precision agriculture. *Remote Sens.* 5, 5006–5039. <https://doi.org/10.3390/rs5105006>
- Index DataBase. A Database for Remote Sensing Indices. The IDB Project, 2011–2019. Available from <https://www.indexdatabase.de>.
- Jeong, J.H., Resop, J.P., Mueller, N.D., Fleisher, D.H., Yun, K., Butler, E.E., Timlin, D.J., Shim, K.M., Gerber, J.S., Reddy, V.R., Kim, S.H., 2016. Random forests for global and regional crop yield predictions. *PLoS One* 11, 1–15. <https://doi.org/10.1371/journal.pone.0156571>
- Lan, Y., Huang, Z., Deng, X., Zhu, Z., Huang, H., Zheng, Z., Lian, B., Zeng, G., Tong, Z., 2020. Comparison of machine learning methods for citrus greening detection on UAV multispectral images. *Comput. Electron. Agric.* 171, 105234. <https://doi.org/10.1016/j.compag.2020.105234>
- Landwehr, N., Hall, M., Frank, E., 2005. Logistic model trees. *Mach. Learn.* 59, 161–205.

- <https://doi.org/10.1007/s10994-005-0466-3>
- Liakos, K.G., Busato, P., Moshou, D., Pearson, S., Bochtis, D., 2018. Machine learning in agriculture: A review. *Sensors (Switzerland)* 18, 1–29.  
<https://doi.org/10.3390/s18082674>
- Marin, D.B., de Carvalho Alves, M., Pozza, E.A., Belan, L.L., de Oliveira Freitas, M.L., 2019. Multispectral radiometric monitoring of bacterial blight of coffee. *Precis. Agric.* 20. <https://doi.org/10.1007/s11119-018-09623-9>
- Marino, E., Yebra, M., Guillén-Climent, M., Algeet, N., Tomé, J.L., Madrigal, J., Guijarro, M., Hernando, C., 2020. Investigating live fuel moisture content estimation in fire-prone shrubland from remote sensing using empirical modelling and RTM simulations. *Remote Sens.* 12. <https://doi.org/10.3390/rs12142251>
- Marques Ramos, A.P., Prado Osco, L., Elis Garcia Furuya, D., Nunes Gonçalves, W., Cordeiro Santana, D., Pereira Ribeiro Teodoro, L., Antonio da Silva Junior, C., Fernando Capristo-Silva, G., Li, J., Henrique Rojo Baio, F., Marcato Junior, J., Eduardo Teodoro, P., Pistori, H., 2020. A random forest ranking approach to predict yield in maize with uav-based vegetation spectral indices. *Comput. Electron. Agric.* 178, 105791.  
<https://doi.org/10.1016/j.compag.2020.105791>
- Martinelli, F., Scalenghe, R., Davino, S., Panno, S., Scuderi, G., Ruisi, P., Villa, P., Stroppiana, D., Boschetti, M., Goulart, L.R., Davis, C.E., Dandekar, A.M., 2015. Advanced methods of plant disease detection. A review. *Agron. Sustain. Dev.* 35, 1–25.  
<https://doi.org/10.1007/s13593-014-0246-1>
- Melo, G.A., Shimizu, M.M., Mazzafera, P., 2006. Polyphenoloxidase activity in coffee leaves and its role in resistance against the coffee leaf miner and coffee leaf rust. *Phytochemistry* 67, 277–285. <https://doi.org/10.1016/j.phytochem.2005.11.003>
- Mishra, S., Mishra, D., Santra, G.H., 2016. Applications of machine learning techniques in agricultural crop production: A review paper. *Indian J. Sci. Technol.* 9.  
<https://doi.org/10.17485/ijst/2016/v9i38/95032>
- Osco, L.P., Junior, J.M., Ramos, A.P.M., Furuya, D.E.G., Santana, D.C., Teodoro, L.P.R., Gonçalves, W.N., Baio, F.H.R., Pistori, H., Junior, C.A. da S., Teodoro, P.E., 2020. Leaf Nitrogen Concentration and Plant Height Prediction for Maize Using UAV-Based Multispectral Imagery and Machine Learning Techniques. *Remote Sens.* 12, 3237.  
<https://doi.org/10.3390/rs12193237>
- Osco, L.P., Paula, A., Ramos, M., Pereira, D.R., Akemi, É., Moriya, S., Imai, N.N., Matsubara, E.T., 2019. Predicting Canopy Nitrogen Content in Citrus-Trees Using



- Random Forest Algorithm Associated to Spectral Vegetation Indices from UAV-Imagery. *Remote Sens.* 1–17.
- Pádua, L., Marques, P., Martins, L., Sousa, A., Peres, E., Sousa, J.J., 2020. Monitoring of chestnut trees using machine learning techniques applied to UAV-based multispectral data. *Remote Sens.* 12. <https://doi.org/10.3390/RS12183032>
- Pham, T.D., Bui, D.T., Yoshino, K., Le, N.N., 2018. Optimized rule-based logistic model tree algorithm for mapping mangrove species using ALOS PALSAR imagery and GIS in the tropical region. *Environ. Earth Sci.* 77. <https://doi.org/10.1007/s12665-018-7373-y>
- Pires, M.S.O., de Carvalho Alves, M., Pozza, E.A., 2020. Multispectral radiometric characterization of coffee rust epidemic in different irrigation management systems. *Int. J. Appl. Earth Obs. Geoinf.* 86, 102016. <https://doi.org/10.1016/j.jag.2019.102016>
- Pozza, E. A., Carvalho, V. L., Chalfoun, S. M., 2010. Sintomas de injurias causadas por doenças do cafeeiro. In: Guimarães, R. J., Mendes, A. N. G., Baliza, D. P. (Eds.), *Semiologia do Cafeeiro*. Editora UFLA, Lavras, pp. 67-106).
- Priya, R., Ramesh, D., 2020. ML based sustainable precision agriculture: A future generation perspective. *Sustain. Comput. Informatics Syst.* 28, 100439. <https://doi.org/10.1016/j.suscom.2020.100439>
- Ramezan, C.A., Warner, T.A., Maxwell, A.E., 2019. Evaluation of sampling and cross-validation tuning strategies for regional-scale machine learning classification. *Remote Sens.* 11. <https://doi.org/10.3390/rs11020185>
- Quinlan, R., 1993. *C4.5: Programs for Machine Learning*. Morgan Kaufmann, San Mateo.
- Qiu, J., Wu, Q., Ding, G., Xu, Y., Feng, S., 2016. A survey of machine learning for big data processing. *EURASIP J. Adv. Signal Process.* 2016. <https://doi.org/10.1186/s13634-016-0355-x>
- Santos, L.M.D., Ferraz, G.A.S., Andrade, M.T., Santana, L.S., Barbosa, B.D.S., Maciel, D.T., Rossi, G., 2019. Analysis of flight parameters and georeferencing of images with different control points obtained by RPA. *Agron. Res.* 17, 2054–2063. <https://doi.org/10.15159/AR.19.173>
- Silva, M.C., Várzea, V., Guerra-Guimarães, L., Azinheira, H.G., Fernandez, D., Petitot, A.-S., Bertrand, B., Lashermes, P., Nicole, M., 2006. Coffee resistance to the main diseases: leaf rust and coffee berry disease. *Brazilian J. Plant Physiol.* 18, 119–147.
- Gomez Selvaraj, M., Vergara, A., Montenegro, F., Alonso Ruiz, H., Safari, N., Raymaekers, D., Ocimati, W., Ntamwira, J., Tits, L., Omondi, A.B., Blomme, G., 2020. Detection of banana plants and their major diseases through aerial images and machine learning

- methods: A case study in DR Congo and Republic of Benin. *ISPRS J. Photogramm. Remote Sens.* 169, 110–124. <https://doi.org/10.1016/j.isprsjprs.2020.08.025>
- Suresh, N., Ram, S.A., Shivanna, M.B., 2012. Coffee Leaf Rust (CLR) and Disease Triangle : a Case Study. *Int. J. Food, Agric. Vet. Sci.* 2, 50–55.
- Velásquez, D., Sánchez, A., Sarmiento, S., Toro, M., Maiza, M., Sierra, B., 2020. A method for detecting coffee leaf rust through wireless sensor networks, remote sensing, and deep learning: Case study of the Caturra variety in Colombia. *Appl. Sci.* 10, 1–27. <https://doi.org/10.3390/app10020697>
- WEKA., 2020a. Random Tree. `weka.classifiers.trees.RandomTree`. Available from <https://weka.sourceforge.io/doc.dev/weka/classifiers/trees/RandomTree.html>.
- WEKA., 2020b. REPTree. `weka.classifiers.trees.REPTree`. Available from <https://weka.sourceforge.io/doc.dev/weka/classifiers/trees/REPTree.html>.
- Zhang, J., Hu, J., Lian, J., Fan, Z., Ouyang, X., Ye, W., 2016. Seeing the forest from drones: Testing the potential of lightweight drones as a tool for long-term forest monitoring. *Biol. Conserv.* 198, 60–69. <https://doi.org/10.1016/j.biocon.2016.03.027>
- Zhou, J., Pavek, M.J., Shelton, S.C., Holden, Z.J., Sankaran, S., 2016. Aerial multispectral imaging for crop hail damage assessment in potato. *Comput. Electron. Agric.* 127, 406–412. <https://doi.org/10.1016/j.compag.2016.06.019>

## CHAPTER V: FINAL CONSIDERATIONS

The general objective of this study was to develop a methodology to assess and monitor the spatial variability of biotic and abiotic stressors in coffee (*Coffea arabica* L.), using multispectral remote sensing data collected by Remotely Piloted Aircraft (RPA). Based on the results, it can be considered that:

The multispectral images obtained via RPA can help producers to identify frost damage in coffee crops, as well as assessing the frost related physiological response.

The Random Forest machine learning method, applied to vegetation indices, offers a very promising approach to map and quantify nitrogen status in coffee trees, contributing therefore, to rational management of N in crops.

Vegetation indices combined with machine learning algorithms based on decision trees is a valid approach to model leaf rust in coffee, specifically in early and late stages of the disease.

Although this study has presented efficient and conclusive results, further research is required to understand the relationship between coffee trees reflectance and stress condition caused by biotic and abiotic factors. For instance, the use of thermal and hyperspectral sensors, herewith continuous assessments during different phenological cycles of coffee trees, considering other cultivars and climatic conditions.